北海道大学
HOKKAIDO UNIVERSITY

Study on dual-phase oxygen separation membrane with percolation structures of oxide ionic and electronic conductors

酸化物イオン・電子伝導体のパーコレーション構造を持つ二相酸素分離膜に関する研究

Aunsaya Eksatit

March 2023

Materials Chemistry and Engineering Course

Graduate School of Chemical Sciences and Engineering

Hokkaido University

Contents

Chapter 1 | Introduction

1.1 Application of oxygen gas

Oxygen gas (O_2) is the most abundant element on earth. It is a chemically reactive gas and a strong oxidant, which means that it is nonflammable, but can significantly accelerate the rate of combustion [1, 2]. There are a variety of industrial applications for oxygen. Oxygen gas is used to enrich air and increase combustion temperatures for cutting, welding, heating, and melting processes in the metal industry. The conversion of combustion systems from air fuel to oxy-fuel resulted in the reduction of particulate and greenhouse gas emissions which were developed for use in the manufacturing of glass and ceramics [3, 4]. Oxygen is utilized in the chemical industry for both heating applications and chemical synthesis. In addition, home medical care has grown in popularity in recent years, resulting in a high demand for oxygen gas generator equipment for home oxygen therapy [5].

1.2 Oxygen separation technologies

The production of oxygen gas is necessary because there is a high demand for its industrial applications. Typically, oxygen gas can be produced by separating

air [6, 7]. The air in the earth's atmosphere is composed of a mixture of 79% nitrogen, 21% oxygen, 1% argon and other gases. There are mainly three methods for separating oxygen gas from air; i.e., cryogenic, pressure swing adsorption, and oxygen separation membrane [8].

1.2.1 Cryogenic air separation

Cryogenic air separation is currently the most efficient method to produce large quantities of oxygen, nitrogen, and argon gases. The cryogenic air separation technique utilizes the difference in boiling points of the gases to separate each high-purity gas from air. This method is temperature and assisted pressure dependent. Cryogenic separation is currently commercially available for oxygen gas separation due to its ability to produce large quantities of gas with a purity of 99 %. However, large-scale production requires very large facilities and a significant amount of energy to run the process [9, 10].

1.2.2 Pressure swing adsorption

Pressure swing adsorption (PSA) is a cyclic separation process in which oxygen gas is separated from air using microporous-mesoporous adsorbents, such

as a zeolite, activated carbon, molecular sieves, etc., under the pressure of the feeding air. During pressurization, the process of adsorption occurs. There is a difference in the attraction between the absorbent material and absorbed gases [11, 12]. By passing other gases through an absorbent medium, the most strongly attracted gases are drawn to the solid surface. The operation then shifts to low pressure to remove the adsorbed gas after separation. This method is appropriate for small to medium scale oxygen production [13]. The pressure swing technique is widely employed in the air-drying sector, for the purification of hydrogen, and for the generation of approximately 95% purity oxygen gas [14]. It has been determined to be more cost-effective than the cryogenic approach since it functions at temperatures close to those of the surrounding environment, whereas the cryogenic process requires high temperatures. In addition, it is simple to operate and has a long operational lifetime. However, this approach is not suitable for the production of high-purity oxygen, as it was developed to obtain oxygen with a low purity [15, 16].

1.2.3 Membrane separation

Membrane separation technology is one of the promising methods for separating a selective substance from mixtures utilizing membrane materials with a physical or chemical interaction [17]. High efficiency, simple operation, and low cost has made the gas separation membrane attract attention. The mechanism for separation depends on the differential permeability of materials and substances. Differences in the pressure, concentration, and electric potential provide the driving force for the separation. The pressure differential across the membrane is the driving force behind the gas separation process, which separates one gas from a mixture of gases. There are several advantages to using a membrane separation procedure for separating gases. The concept of operation and employed method are both simple and easy to perform; no chemical additives or phase transformation processes are required. In addition, the equipment can be reduced in size to meet the current requirement for a home gas generator [18, 19].

1.3 Gas separation membrane classification

The gas separation membrane can be categorized by barrier selection, membrane shape and morphology, and membrane material as shown in Figure 1-1.

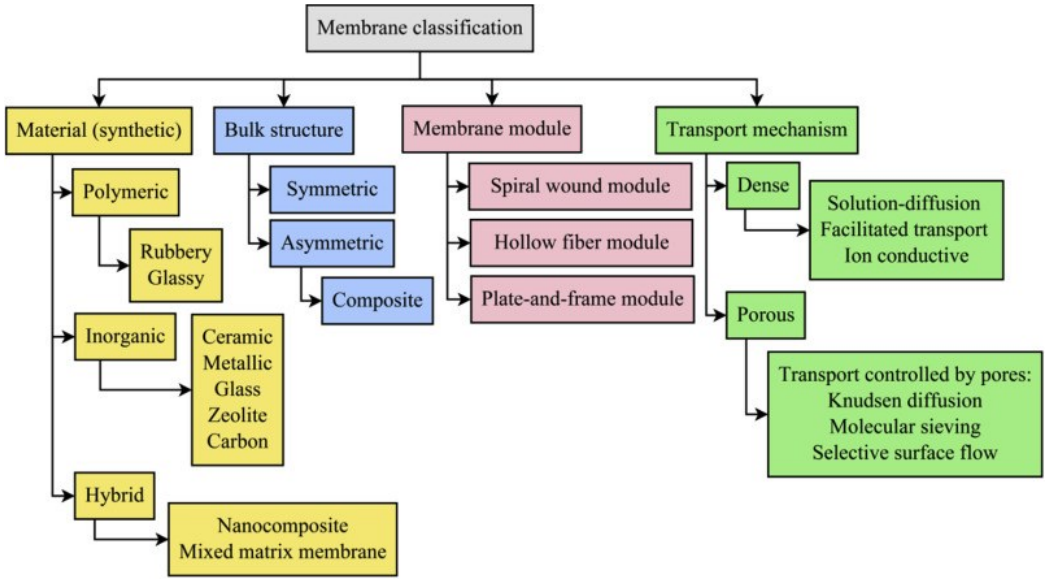

Fig. 1-1 Membrane classification[20].

1.3.1 Gas separation membrane based on selective barrier

The gas separation membrane can be categorized into two groups; i.e., porous and nonporous, depending on the selective barrier they employ. Transport over a porous membrane is accomplished by the diffusion or flow of a viscous substance. The basis of this selection is size selection. A nonporous membrane

facilitates molecular transport via a solution-diffusion process, in which separation is achieved by differences in the solubility and/or diffusivity of the solutes. Measuring porosity has no relation to the characterization of this type of membrane, which is determined by its physical and chemical properties [21, 22].

1.3.2 Gas separation membrane based on membrane structure

Membrane morphology can be divided into two types; i.e., isotropic or symmetric membrane and anisotropic or asymmetric membrane, as shown in Figure 1-2. The symmetric membrane is a dense or microporous membrane with a uniform structure over its entirety. The structure of the symmetric membrane is nearly consistent across the membrane's depth. This enables the membrane to function as a selective barrier against the transport of particles or molecules. Flow can continue in either direction across the symmetric membrane. In addition, the symmetric membrane tends to retain particles that are nearly the same size as the membrane's pores. Because of this, the membrane serves as both a depth filter and a surface filter. The separation efficiency of the symmetric membrane may gradually decrease as the membrane becomes permanently obstructed. To describe an asymmetric membrane, a selective thin layer was

formed on the top surface of the porous support layer. Dense membranes were enhanced in their mechanical qualities by attaching to a thick, porous support material whose porosity and pore size varied throughout the cross section of the membrane. To separate substances, a thin dense layer is utilized as a selective layer. The separated fluxes depend on the substantial thickness of the selective layer [23].

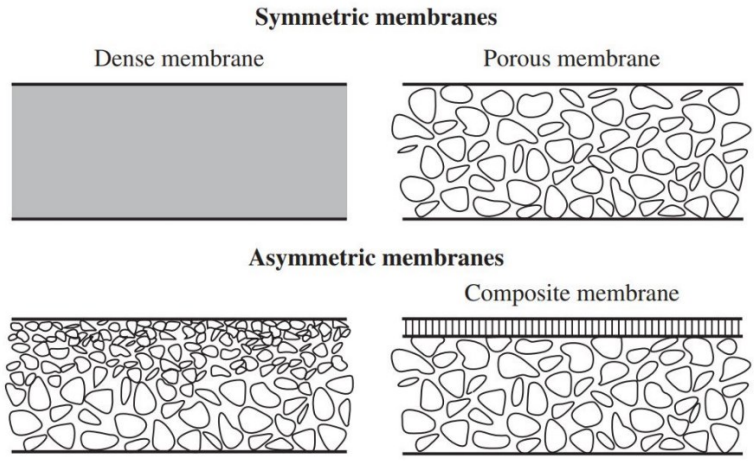

Fig. 1-2 Classification of membrane based on membrane morphology [24].

1.3.3 Gas separation membrane based on membrane materials

Based on the membrane materials, the separation membrane can be characterized as an organic membrane or an inorganic membrane. A membrane composed of polymers such as cellulose acetate, polytetrafluoroethylene,

polyvinylidene fluoride, polyamide, etc., is an organic membrane. Currently, the polymer membrane is utilized in the production of natural gas. This type of membrane is very selective, inexpensive, and easy to process. However, the operating temperature and pressure are limited, and it is chemically unstable and has a limited life [25]. Therefore, an inorganic membrane with increased chemical and thermal stability and resistance to severe atmospheres are actively being developed [6, 26].

1.3.3.1 Mixed ionic-electronic conductor

The mixed ionic–electronic conductor (MIEC) membrane is a type of dense ceramic membrane that separates oxygen gas from air by the transport of oxide ions through the ceramic crystal structure [27, 28]. As shown in Figure 1-3(a), the crystal structure of mixed conductor materials is typically a perovskite structure. The perovskite material is derived from the mineral perovskite ($CaTiO_3$). ABO_3 is the general chemical formula used to designate perovskite substances [27, 29]. The ideal perovskite structure is a simple cubic. A framework structure constructed of the BO_6 octahedra with A cations located in 12-coordinated interstices, where the A cation is a larger ion, such as a rare earth, and

the B cation is generally a smaller ion and often a transition metal. The unique characteristics of perovskite materials that are required for the oxygen separation property are the crystal structure's stability when it becomes nonstoichiometric [30-32]. Two cation sites in the perovskite oxides make it possible to substitute lower valence cations, thus expanding the class of materials that may conduct oxide ions or mixed ions and electrons (Figures 1-3(b)). In general, the conduction mechanism occurs when oxide ions pass through vacant or interstitial sites, which is assisted by the structure disorder [33].

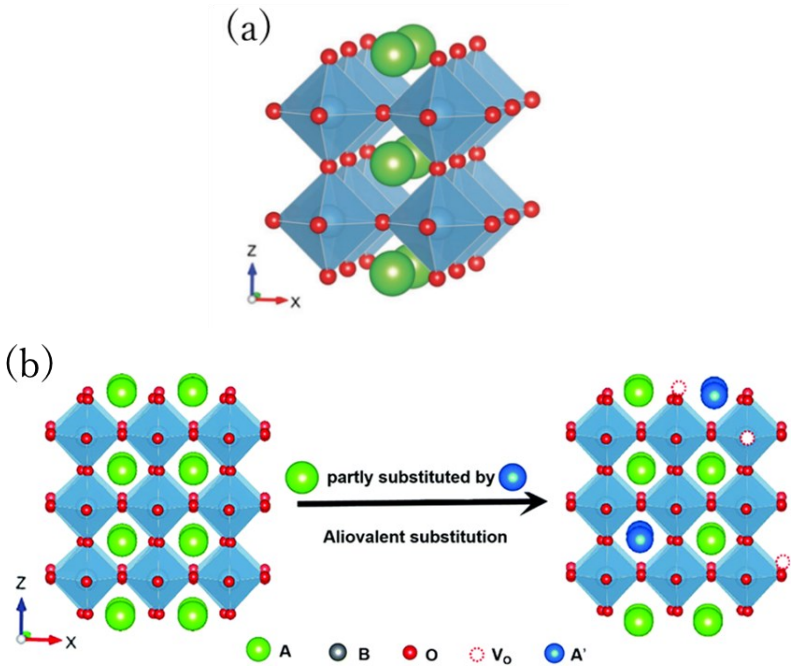

Fig. 1-3 (a) Crystal structure of perovskite oxide (b) Schematic representation of the formation of oxygen vacancies [34].

1.3.3.2 Oxide ionic conductor

An oxide ionic conductor is a material whose oxide ionic conductivity is two orders of magnitude higher than its electronic conductivity, and which is classified as a pure oxide ionic conductor. Figure 1-4 show the example of the materials that have oxide ion conductivity. The most common oxide ionic conducting materials are the fluorite-type oxides [35, 36]. The crystal structure of fluorite is a face-centered cubic arrangement of cubic cations with anions occupying the entire tetrahedral site. Fluorite oxide has the general formula AO_2, where A represents a large tetravalent cation. To generate an oxide ion conductivity, it is necessary to provide oxygen vacancies by substituting a cation with a lower valence element, which has the additional effect of introducing oxygen vacancies to maintain charge neutrality. These oxygen vacancies provide the corresponding site for oxide ion migration, resulting in an oxide ionic conductivity [37]. The zirconia-based oxide is the most used fluorite oxide for oxygen separation at temperatures between 500 and 1000 °C. The zirconia based oxide known as yttria-stabilized zirconia (YSZ) is commonly used [38]. It is highly stable in oxidizing and reducing environments and has an excellent oxygen diffusivity in addition to its excellent mechanical properties. Figure 1-5 show the

crystal structure of YSZ. Normally, ZrO_2 has a monoclinic structure at room temperature, however, a phase transition occurs at 1170 ºC to a tetragonal structure and a cubic structure at 2370 ºC, accompanied by a large volume change. To avoid the volume change caused by the pure zirconia phase transitions, doping with yttria can prevent the phase transform, resulting in a stable cubic structure at room temperature. Furthermore, the substitution of Y^{3+} also introduced oxygen vacancies, leading to a high ionic conductivity. In Kröger–Vink notation, the defect equation for the dissolution of yttria into the fluorite phase of ZrO_2 is as follows:

$$\frac{1}{2}Y_2O_3 \xrightarrow{ZrO_2} Y'_{Zr} + \frac{1}{2}V_O^{\cdot\cdot} + \frac{3}{2}O_O^{\times} \qquad (1\text{-}1)$$

At a dopant concentration of 8 mol% Y_2O_3, the oxide ion conductivity of YSZ reaches its maximum value; below this concentration, the conductivity generally increases. However, based on the mol percent of Y_2O_3, substituting higher than 8 mol%, the defect interaction takes over as the primary contributor to lowering the conductivity due to the reduced mobility of the oxide ions [39, 40].

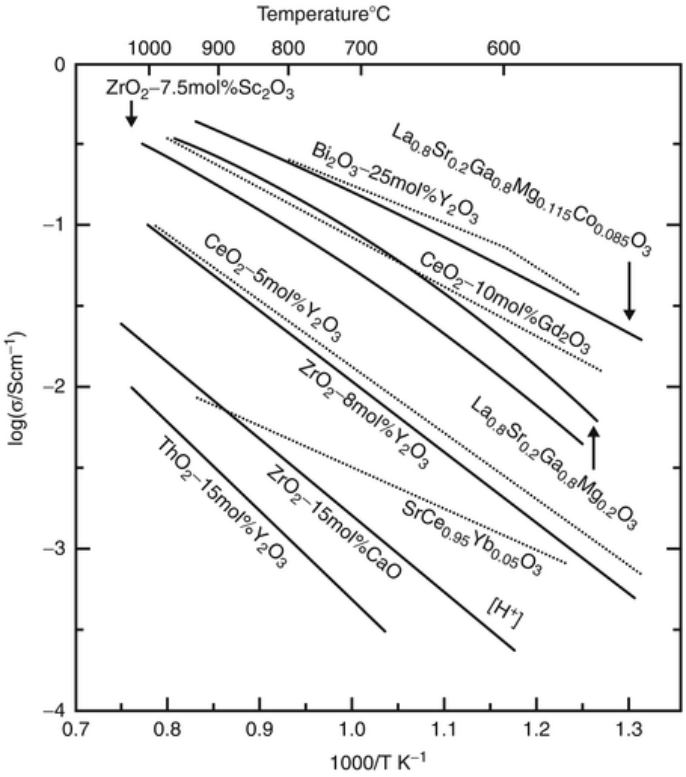

Fig. 1-4 Comparison of oxide ion conductivity in typical materials [41].

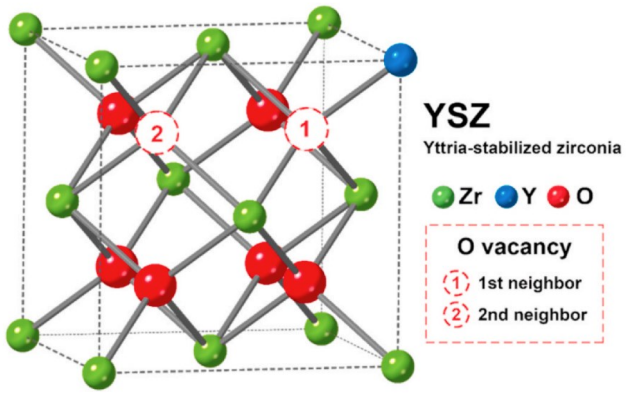

Fig. 1-5 The crystal structure of Yttria-stabilized zirconia [40].

1.4 Principle of oxygen permeation

The theoretical oxygen permeation mechanism in single-phase MIEC membranes is illustrated in Figure 1-6. The MIEC membrane allowed oxygen gas to dissociate and associate from the feed side to the permeate side on the membrane surfaces [42, 43]. On the side with a high oxygen partial pressure, the vacancies are filled by oxide ions created by the ionization and dissociation of oxygen molecules in the gas phase. Oxide ions in the air move through the vacancies in the membrane lattice, and oxygen is neutrally released into the gas phase on the side with a low partial pressure. At elevated temperatures, the process is driven by the oxygen partial pressure difference across the membrane. When a partial pressure gradient is present, oxide ion diffusion results in hopping from the high-pressure side to the low-pressure side. Kröger–Vink notation is used to describe the reaction of the oxide ion transport, which is the reaction between the gaseous oxygen and the oxide lattice:

$$O_2 + 2V_O^{\cdot\cdot} + 4e' \leftrightarrow 2O_O^{\times} \tag{1-2}$$

The expression for the reaction between the electrons and holes is

$$null \leftrightarrow e' + h^{\cdot} \tag{1-3}$$

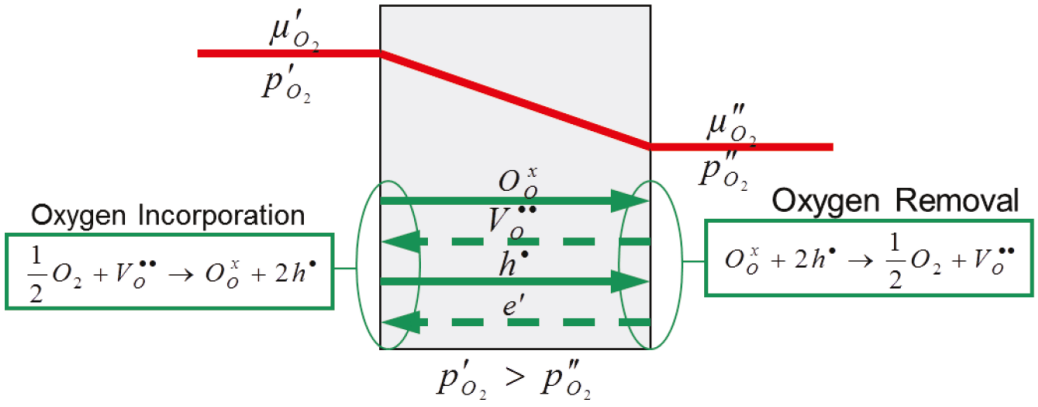

Fig. 1-6 Oxygen separation mechanism of the oxygen separation membrane [44]

1.4.1 Factor controlling the oxygen permeation

The permeation rate across a dense oxygen-permeable membrane is primarily determined by two factors; i.e., the rate of solid-state diffusion within the membrane material and the rate of interfacial oxygen exchange on both sides of the membrane. As shown in Figure 1-7, a membrane is separated into a central bulk diffusion-controlled zone and nearby interfacial zones. The bulk diffusion rate depends on the thickness (L_C) of the membrane, which changes based on the material and the environment [45]. To improve the oxygen permeability, the membrane thickness should be reduced. Due to the rate control of the surface exchange kinetics and bulk diffusion, when this thickness is decreased, the oxygen flux limitation due to the surface exchange kinetics at the interface becomes

dominant. Oxygen penetration through the membrane will be controlled by surface reactions with regard to L_C [46].

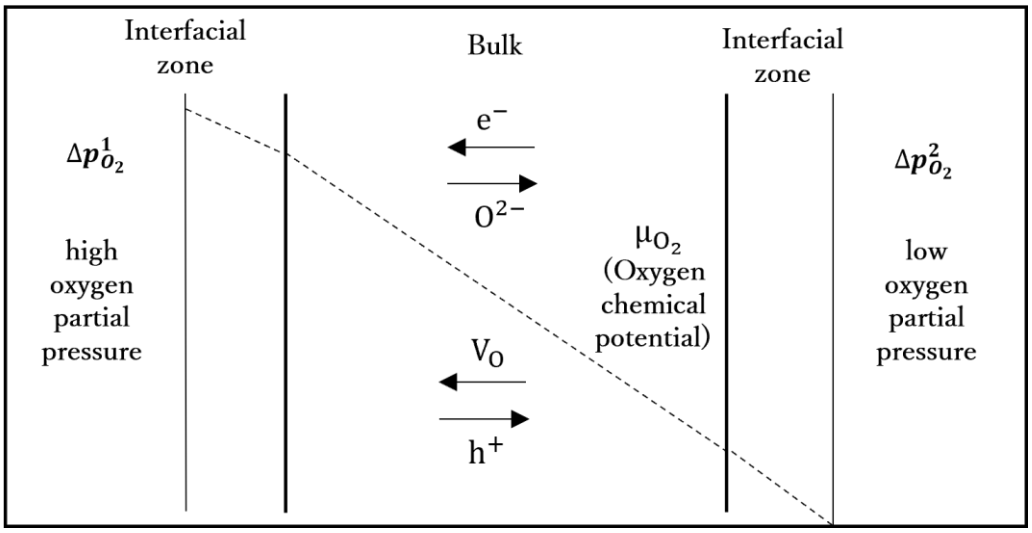

Fig. 1-7 Diagram representing the chemical potential of MIEC membrane.

1.4.2 Bulk transport

According to the bulk transport theory, the rate-limiting steps in oxygen moving through the bulk oxide are thought to be the diffusion of oxygen anions or the transport of electrons and holes. The oxygen permeation flux, j_{O2} (mol· cm^{-2}· s^{-1}), through a solid crystal can be described by the Wagner equation:

$$jO_2 = -\frac{RT}{16F^2L}\int_{lnP'_{O_2}}^{lnP''_{O_2}} \frac{\sigma_i\sigma_e}{\sigma_i+\sigma_e} dlnP(O_2) \qquad (1\text{-}4)$$

where R is the gas constant (8.314 J/mol·K), T is the temperature (K), F is the Faraday constant (96485 C/mol), L is the membrane thickness (cm), and P'_{O2} and P''_{O2} represent the oxygen partial pressure on the high and low oxygen pressure sides of the membrane, respectively. σ_e is the electronic conductivity, σ_i is the oxide ion conductivity (S/cm), and $P(O_2)$ the oxygen partial pressure [47].

1.4.3 Surface exchange kinetic

There are multiple reaction steps in the oxygen exchange reaction between the membrane surfaces and the gas phase, and each step can determine the overall reaction rate. Oxygen molecules first adsorb onto the membrane surface, where they then dissociate, transfer charges, undergo surface diffusion of the intermediate species, and finally integrate into the lattice structure in the near-surface layer. In most cases, it is assumed that the association of oxide ions follows the same processes in the reverse direction. For oxygen transport across a membrane, Wagner's equation is valid only if the bulk transport is the rate-determining step. When the thickness of the membrane decreased, the surface exchange reactions became the rate-determining step. The kinetics of the oxygen permeation were determined using the characteristic thickness (Lc) to define

whether bulk diffusion or surface exchange was the controlling mechanism [47-49]. Lc is determined by the ratio between the oxygen self-diffusion coefficient (D_S) and the oxygen surface exchange coefficient (k_S):

$$L_C = \frac{D_S}{k_S} \tag{1-5}$$

In general, Lc is not a material property, it depends on the temperature, oxygen partial pressure, surface roughness, etc. In consideration of the bulk diffusion and surface exchange kinetics limitations, the Wagner's equation can be rewritten as follows:

$$jO_2 = \frac{RT}{16F^2}\frac{1}{L + 2L_C}\int_{lnP'_{O_2}}^{lnP''_{O_2}} \frac{\sigma_i\sigma_e}{\sigma_i + \sigma_e} dlnP(O_2) \tag{1-6}$$

1.5 The limitation of the MIEC

Generally, the thermodynamic and kinetic stabilities of single-phase perovskite oxides (ABO_3) contribute to their overall stability. The average bond energy (ABE) of the A- and B-site ions with oxygen is a major factor in determining the thermodynamic stability. Although an increased stability is observed at the higher ABE levels, the oxide ion mobility inside the lattice is hindered. The kinetic stability of a single-phase membrane is dependent on the

metal cation self-diffusion coefficients. When the oxygen partial pressure on opposite sides of a membrane is different, both oxide ions and metal cations are transported across the membrane. This kinetic reaction is dependent on changes in the temperature, atmospheric conditions, membrane microstructure, the oxygen pressure gradient across the membrane, and oxygen exchange rates at the surfaces. Besides a single-phase membrane, a dual-phase membrane could be developed by the combination of oxide ionic conducting materials and electronic conducting materials. Generally, it is challenging to obtain a membrane with both a great permeability and stability. Dual-phase membranes provide several advantages over a single-phase mixed ionic-electronic conductor membrane, including a greater chemical stability, compatibility in interaction with the other membrane components, mechanical stability, and easiness to be tailored for a particular application. For these reasons, a dual-phase membrane attracts attention to overcome the obstacle that a single-phase membrane could not by selecting the optimal oxide ion conductor and electronic conductor [47, 50, 51].

1.6 Dual-phase membrane

The dual-phase oxygen separation membrane is a composite membrane composed of oxide ionic conductors and electronic conductors or a mixed oxide ionic and electronic conductor, in which the diffusion path of oxide ions and the transport path of electrons are separated in the membrane bulk. By constructing a dual-phase membrane, it is possible to get both a high oxygen permeability and stability [52-56]. Thus, by using a dual-phase membrane, it is possible to overcome the limitations of a single-phase membrane, such as its inferior oxide ion diffusion rate, lack of stability under harsh conditions, and limited oxygen permeability. In general, the microstructure of a dual-phase membrane has a significant influence on performance. First, the oxygen-permeable dual-phase membrane requires a good percolation of both the ionic and electronic conducting phases. Typically, the conductivity of an electronic conductor is significantly higher than that of an oxide ion conductor. Therefore, the lowest volume fraction of the electrical conducting phase would result in a high-performance dual-phase membrane. Consequently, even with comparable volume fractions, the performance of a particular material combination can be significantly dependent on the processing. In addition, the microstructure of the phase mixture defines

the triple phase boundaries, which are necessary for oxygen surface exchange reactions.

There are important criteria for selecting the oxide-ionic and electronic conductors in a dual-phase membrane since the various interactions between the two phases, including chemical, thermal, and mechanical, among others, introduce further complications compared to the single-phase membrane [27, 40, 57]. Normally, the oxygen separation membrane is operated at high temperatures (500-900 ºC), the feed side of the membrane is exposed to an oxidizing atmosphere, while the permeate side is exposed to a strongly reducing atmosphere containing oxygen and a sweep gas. As a result, membrane materials must maintain their crystal structure in both the oxidizing and reducing environments. Moreover, the other criterion for the selection of the ionic conducting phase is chemical compatibility with the electronic conducting phase. The sintering process can lead to the formation of a secondary phase at the interface of the two phases, which negatively affects the membrane's performance, so the selected composite should have a good chemical compatibility that has no reaction under the sintering and working conditions. Furthermore, not only the above requirements but also the thermal stress and microstructure of both selected

materials should be considered [58-62]. Generally, the dual-phase membrane can be mainly classified into two groups based on the selection of an electronic conductor; i.e., (i) pure electronic conductors, and (ii) mixed conductors, as shown in Figure 1-8 [42, 63].

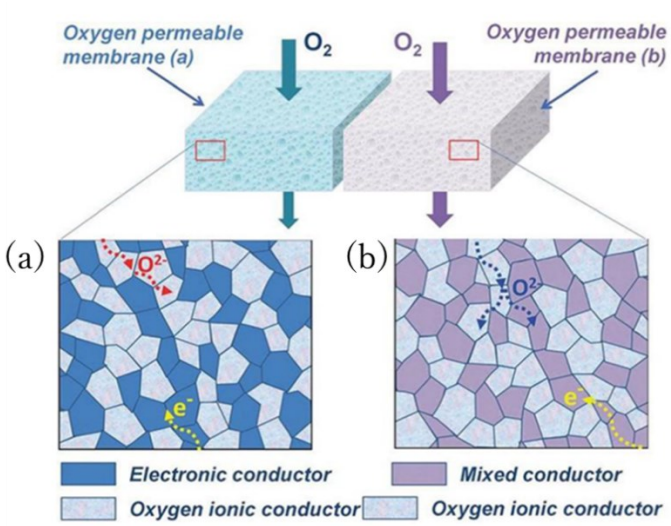

Fig. 1-8 Schematic illustration of (a) oxide ion-pure electronic conductor dual-phase membrane and (b) oxide ion-mixed oxide ion and electronic conductor dual-phase membrane [44].

1.6.1 Types of dual-phase membrane

1.6.1.1 Metal-ceramic dual-phase membrane

The dual-phase metal-ceramic membrane consists of a metal phase as the

electronic conducting component and a ceramic phase as the oxide ionic conducting component. R. Kiebach et al. report that the initial study about the dual-phase membrane started with the dual-phase membrane made of noble metals (for example, Au, Pd, Pt, Ag, etc.) and oxide ionic ceramic conductors [47]. Due to the high cost of noble metals, using noble metals as an electronic conducting phase is not suitable for industrial applications [64]. To reduce the material costs of a dual-phase membrane, electronic conducting oxides or alloys have been proposed as noble metal replacements [65].

1.6.1.2 Ceramic-ceramic dual-phase membrane

Combining the oxide ion conducting phase with another ceramic phase that can conduct electrons, such as perovskites and spinel materials, is another approach for enhancing the electronic conductivity without increasing the price as much as noble metals. In the case of ceramic-ceramic systems, the stability of both phases and the thermal-chemical expansion must be carefully considered. Perovskite and spinel structures exhibit a higher electronic conductivity than other ceramic materials, so they are typically employed as the electronic phase, whereas structures of the fluorite type are typically utilized as the oxide ion

conducting phase [66].

1.7 The Fabrication of dual-Phase Membrane

1.7.1 Preparation method of dual-phase membrane powders

The efficiency of a dual-phase membrane is directly related to the raw material powder. The microstructure of the two phases in the dual-phase membrane is significantly affected by the powder properties, such as surface area, particle size distribution, and homogeneity of the two powder phases, combined with the sintering process. Porosity, the percolation of oxide ionic or electronic pathways, or the contact area between both phases are all aspects of the microstructure that have a significant influence on the membrane performance. For example, to fabricate a thin membrane layer and achieve full densification, the powder from the two phases must have a small particle size. Generally, the characterization of a powder mostly depends on the fabrication process. Powder manufacturing techniques can be mainly categorized into two types; i.e., solid state reaction method and wet chemical procedures (such as co-precipitation, sol-gel, hydrothermal, and spray techniques)[67].

1.7.1.1 Solid state reaction

The common method for producing a ceramic powder is the solid-state reaction technique, often known as the mixed powder technique [68]. This fabrication method is widely employed to produce a dual-phase ceramic membrane. Due to its low cost, ease of use, and reliance on readily available precursors and industrial equipment, this technique has the potential to be utilized on an industrial scale. Usually, the membranes derived using this method have a higher oxygen permeability than those derived from a liquid phase synthesis. The main reason is that the oxide ionic conductivity and oxygen exchange are improved by the defects present in the membrane. However, a large particle size, limited surface area, poor chemical homogeneity, and the development of undesirable phases are some of the problems that occur due to the high sintering temperature [69, 70].

1.7.1.2 Wet chemical method

Wet synthesis is an alternative to using only solid precursors. The one-pot method is an attractive wet chemical route for the synthesis of dual-phase powders because it allows the two compositions to be synthesized in a single step using

conventional solution fabrication techniques for ceramics, such as sol-gel, co-precipitation, hydrothermal synthesis, or spray pyrolysis. All these processes utilize a precursor solution, although the crystallites or powders are produced in different ways. The main advantages relative to this technique are the smaller particle size, higher purity, and homogeneity of the powder, which is an improvement over the mixed powder method because of the substantially lower calcination temperatures required to achieve the necessary oxide phases. However, it is difficult to minimize the phase volume because the minor phase might not percolate, which will decrease the conductivity and reduce the oxygen flux [47, 71].

1.7.2 Preparation method of dual-phase membrane green compact

1.7.2.1 Pressing

In dry pressing, powders are generally compacted in the uniaxial direction between two punches in hardened metal molds. The compact membrane of millimeter thickness could be obtained by these methods. The compact membrane is then sintered in the furnace to obtain a self-standing planar dual-phase membrane [72]. This strategy is based on the simplicity of the fabrication method,

which enables the rapid preparation of small samples with a simple geometry.

1.7.2.2 Tape casting

Tape casting is a cost-effective method for producing an ultrathin planar ceramic membrane. A ceramic powder is dispersed in a slurry consisting of a solvent, surfactants, binder, and plasticizers to create a green tape, i.e., a sheet that is flexible and mechanically stable. The slurry is cast onto a flat surface using a doctor blade process followed by slow drying in a drying chamber with a well-controlled atmosphere [73-76].

1.7.2.3 Screen printing

Screen printing provides an economical method of applying films on an industrial scale. Ceramic ink is pressed into the empty spaces in a mesh aperture. For the fabrication of a dual-phase membrane, to minimize the shrinking of the layer during sintering on a pre-sintered membrane and maximize the density of the dual-phase membrane layer, it is preferable that the inks used in the dual-phase membrane must have a high solids loading [54].

1.7.2.4 Radio Frequency (RF) Sputtering

RF sputtering is an efficient technique for uniformly producing a large thin film from 50 nm to 5 μ m in thickness. Applying an energetic wave to an inert gas (such as argon) in a vacuum chamber causes the gas to become ionized. By hitting a target with high-energy ions (Ar^+), a plasma is created. This plasma contains positively-charged atoms that accumulate on the substrate face of the target [47].

1.7.3 Membrane sintering process

Sintering dual-phase membrane presents several difficulties, including those related to achieving a uniform density throughout the material and preventing the reactions or evaporation of the dual-phase components at elevated temperatures. A dual-phase membrane is a composite of two or more phases which is necessary that these phases should be dense and have a close contact between the grains to prevent any leaking behavior. However, it might be challenging to sinter such compacts because the optimal sintering conditions vary depending on each phase.

1.7.3.1 Conventional sintering processes

Conventional sintering procedures involve the uniaxial or isostatic pressing of the green disks, followed by several hours of sintering at a high temperature. Densification at high temperatures is always associated with grain growth and consequent grain boundary and interfacial issues. Therefore, various techniques have been developed to lower the sintering temperature.

1.7.3.2 Hot pressing

Hot pressing is a powder process that uses high pressure and a low strain rate to produce a compacted powder at a temperature high enough to induce sintering and creep. The process of applying heat and pressure at the same time accomplishes this. Generally, the loose powder or pre-compacted part is placed in a graphite mold that allows induction or resistance heating up to high temperatures under the application of pressure [77].

1.7.3.3 Spark plasma sintering process

Spark Plasma Sintering (SPS) is an advanced sintering technique that permits grain development and densification to independently occur. Figure 1-9

shows a schematic of the SPS. During sintering, an external pressure and high current amplitude pulse are applied via the conductive die and the sample, internally heating the sample using the "Joule heating mechanism" as opposed to using an external heating source to improve the densification of the powder compacts as shown in Figure 1-10. Since the sample can self-heat from both the interior and exterior, it offers substantial advantages over conventional hot pressing and hot isostatic pressing sintering. In addition, both the heating rate and mass transfer speed are rapid and confined, so the sintering process is often quite rapid. Thus, in contrast to conventional sintering methods, which require a high sintering temperature and a long sintering time to achieve complete densification [78-82], the SPS process can produce dense ceramics in a very short sintering time and at relatively low temperatures allowing for microstructure control [83-89]. This approach is especially effective for producing composite materials with a uniform microstructure. Since grain growth and coarsening are slowed by the high heating rate, extremely high relative densities are achieved. In addition, the rapid heating rate in SPS suppresses unfavorable reactions and prevents the development of undesirable phases and byproducts [89-91].

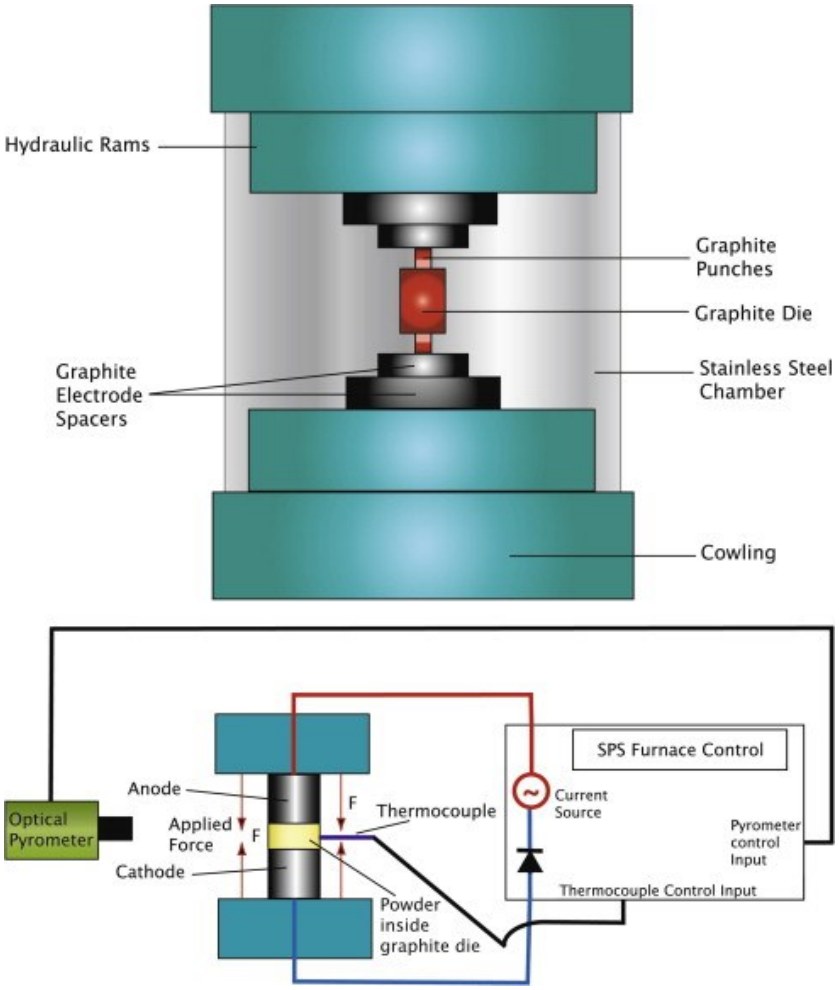

Fig. 1-9 SPS process schematic representation [92].

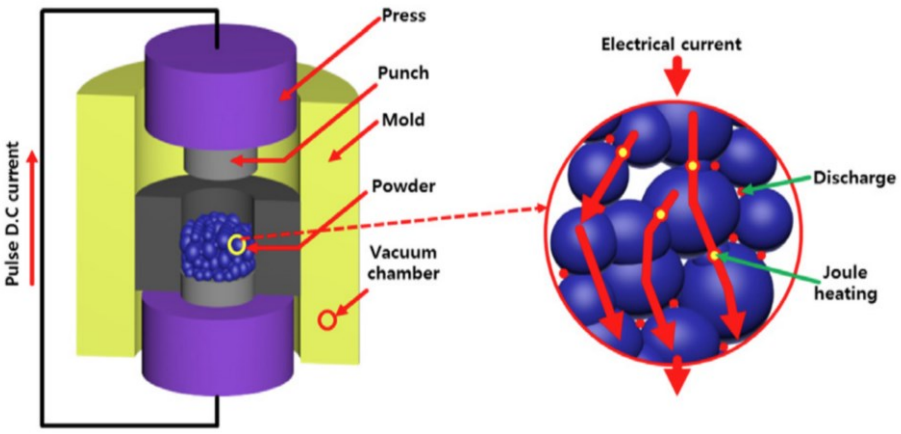

Fig. 1-10 Schematic diagram of Spark Plasma Sintering process [93].

There are generally four steps involved in the spark plasma sintering process. Gases must first be evacuated by generating a vacuum. The second stage involves applying pressure, followed by resistance heating in the third stage and cooling in the final stage. During the initial stage, the packing and necking of particles occur. During the intermediate stage, the compact shrinks and the densification is achieved. During this stage, volume densification and grain boundary diffusion are occurring. Finally, the isolation of pores takes place in the last stage [93, 94].

The densification mechanism by the spark plasma sintering process is based on the spark plasma effect, which supposedly consists of (i) spark discharges, (ii) plasma formation, (iii) surface oxide removal, (iv) electromigration, (v) thermomigration, (vi) an increased defect concentration, (vii) enhanced defect mobility, and (viii) local overheating up to melting of the contacts between the powder particles [95]. Figure 1-11 illustrates the fundamental mechanism of neck generation by spark plasma in which the pulsed current propagates across particle surfaces. The local heat generated in the discharge column results in a temporary increase in temperature when the spark generates in empty spaces or at contact points of the powder particles. This high

temperature causes the evaporation of impurities as well as the evaporation and melting on the surface of the powder particles, finally producing the necks between the powder particles. The compressive stress applied during SPS results in a better contact between the powder particles, changes the amount of those contacts, and promotes the densification mechanisms [96].

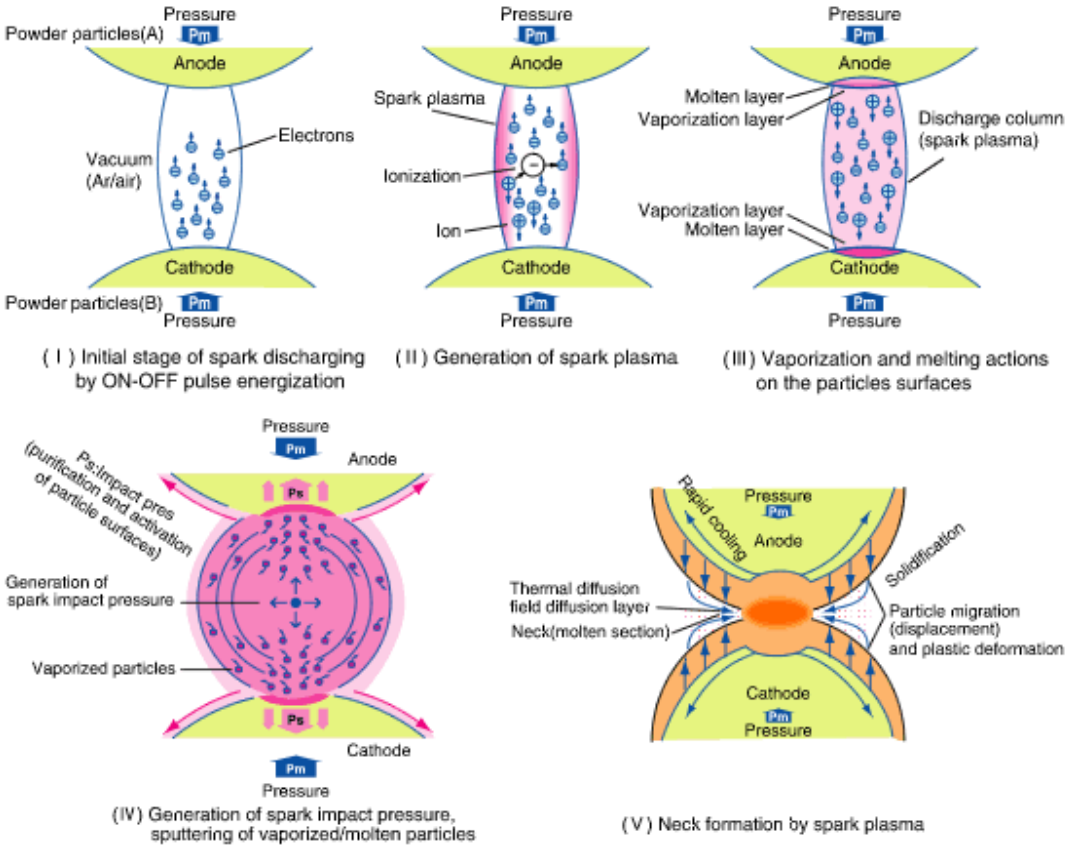

Fig. 1-11 Mechanism of neck formation by spark plasma [97].

1.8 Purpose of this study

The oxygen separation membrane is a device that electrochemically separates oxygen gas from air. It has attracted attention for use as a small-scale oxygen gas generator with a high-purity oxygen production, simple operation, and a low investment cost. MIEC materials are the most popular materials used in the oxygen separation membrane which demonstrate a high oxygen selectivity and high permeability. To improve the oxygen permeation performance, both the bulk diffusion rate and surface exchange reactions dominate the oxygen diffusion kinetics of the membrane. MIEC material development is currently limited due to the difficulty in improving the oxide diffusion rate in single-phase materials. The dual-phase membrane of an oxide ion conductive phase and an electronic conductive phase was attempted to be fabricated in order to combine the good properties including high oxide ion and electron diffusion, high mechanical properties, and high stabilities. Based on the sintering process, the conventional sintering technique is commonly used to fabricate a membrane. However, to achieve a high densification of the membrane materials, a high sintering temperature and time are required, which can result in an inter-phase reaction. As already mentioned, the spark plasma sintering (SPS) technique, which is a high

pulse direct current and pressure-assisted sintering process, has attracted attention. The advantage of SPS is that this sintering technique can lower the densification temperature of the membrane material by applying high pulses of direct current and pressure during the sintering process within a short sintering time. There are a few studies that have applied SPS to the fabricated dual-phase membrane. In this research study, the SPS process was investigated to achieve a dual-phase membrane with a percolation structure to obtain oxygen dissociation and associated exchange activities. Variations of the material combination, fabrication process, and modification were studied to improve the oxygen separation performance of the dual-phase membrane.

References

1. Ahmad F.I., Kailash C.K., and Takeshi M., Gas separation membrane: Springer International, (2015).
2. Zhu X. and Yang W., Microstructural and Interfacial Designs of Oxygen-Permeable Membranes for Oxygen Separation and Reaction–Separation Coupling. Advanced Materials, 31(2019) 1902547.
3. Chorowski M. and Gizicki W., Technical and economic aspects of oxygen separation for oxy-fuel purposes. Archives of Thermodynamics, 36(2015) 157-170.
4. Chen W., Chen C., Bouwmeester H.J.M., Nijmeijer A., and Winnubst L., Oxygen-selective membranes integrated with oxy-fuel combustion. Journal of Membrane Science, 463(2014) 166-172.
5. Ackley M.W., Medical oxygen concentrators: a review of progress in air separation technology. Adsorption, 25(2019) 1437-1474.
6. Pandey P. and Chauhan R.S., Membranes for gas separation. Progress in Polymer Science, 26(2001) 853-893.
7. Smith A.R. and Klosek K., A review of air separation technologies and their integration with energy convesion processes. Fuel Processing Technology,

70(2000) 115-134.

8. Hashim S.S., Mohamed A.R., and Bhatia S., Oxygen separation from air using ceramic-based membrane technology for sustainable fuel production and power generation. Renewable and Sustainable Energy Reviews, 15(2011) 1284-1293.

9. Zhu Y., Legg S., and Laird C.D., Optimal design of cryogenic air separation columns under uncertainty. Computers & Chemical Engineering, 34(2010) 1377-1384.

10. Cornelissen R.L. and Hirs G.G., Exergy analysis of cryogenic air separation. Energy Conversion and Management, 39(1998) 1821-1826.

11. Jee J.G., Kim M.B., and Lee C.H., Pressure swing adsorption processes to purify oxygen using a carbon molecular sieve. Chemical Engineering Science, 60(2005) 869-882.

12. Gomes V.G. and Yee K.W.K., Pressure swing adsorption for carbon dioxide sequestration from exhaust gases. Separation and Purification Technology, 28(2002) 161-171.

13. Grande C.A. and Rodrigues A.E., Biogas to Fuel by Vacuum Pressure Swing Adsorption I. Behavior of Equilibrium and Kinetic-Based

Adsorbents. Industrial & Engineering Chemistry Research, 46(2007) 4595-4605.

14. Santos J.C., Cruz P., Regala T., Magalhães F.D., and Mendes A., High-Purity Oxygen Production by Pressure Swing Adsorption. Industrial & Engineering Chemistry Research, 46(2007) 591-599.

15. Sircar S., Pressure Swing Adsorption. Industrial & Engineering Chemistry Research, 41(2002) 1389-1392.

16. Smith O.J. and Westerberg A.W., The optimal design of pressure swing adsorption systems. Chemical Engineering Science, 46(1991) 2967-2976.

17. Kujawski W., Application of pervaporation and vapor permeation in environmental protection. Polish Journal of Environmental Studies, 9(2000) 13-26.

18. Smart S., Lin C., Ding L., Thambimuthu K., and Da Costa J.C.D., Ceramic membranes for gas processing in coal gasification. Energy & Environmental Science, 3(2010) 268-278.

19. Adhikari B., Orme C.J., Klaehn J.R., and Stewart F.F., Technoeconomic analysis of oxygen-nitrogen separation for oxygen enrichment using membranes. Separation and Purification Technology, 268(2021) 118703.

20. Dalane K., Dai Z., Mogseth G., Hillestad M., and Deng L., Potential applications of membrane separation for subsea natural gas processing: A review. Journal of Natural Gas Science and Engineering, 39(2017) 101-117.

21. Ravanchi M., Kaghazchi T., and Kargari A., Application of membrane separation processes in petrochemical industry: a review. Desalination, 235(2009) 199-244.

22. Scott K., Membrane Materials, Preparation And Characterisetion, in Handbook of Industrial Membranes, Scott K., Editor, Amsterdam: Elsevier, (1995) 187-269.

23. Abdullah N., Rahman M.A., Dzarfan Othman M.H., Jaafar J., and Ismail A.F., Chapter 2 - Membranes and Membrane Processes: Fundamentals, in Current Trends and Future Developments on (Bio-) Membranes, Basile A., Mozia S., and Molinari R., Editors: Elsevier, (2018) 45-70.

24. Mahenthiran A.V. and Jawad Z.A., A Prospective Concept on the Fabrication of Blend PES/PEG/DMF/NMP Mixed Matrix Membranes with Functionalised Carbon Nanotubes for CO_2/N_2 Separation. Membranes, 7(2021) 519.

25. Robeson L.M., Burgoyne W.F., Langsam M., Savoca A.C., and Tien C.F., High performance polymers for membrane separation. Polymer, 35(1994) 4970-4978.

26. Amin S.K., Hassan M., El-Sherbiny S., and Abdallah H., An Overview of Production and Development of Ceramic Membranes. International Journal of Applied Engineering Research, 11(2016) 7708-7721.

27. Sunarso J., Baumann S., Serra J.M., Meulenberg W.A., Liu S., Lin Y.S., and Diniz da Costa J.C., Mixed ionic–electronic conducting (MIEC) ceramic-based membranes for oxygen separation. Journal of Membrane Science, 320(2008) 13-41.

28. Chen D.J., Chen C., Zhang Z.B., Baiyee Z.M., and Ciucci F., Compositional Engineering of Perovskite Oxides for Highly Efficient Oxygen Reduction Reactions. ACS Applied Materials & Interfaces, 7(2015) 8562-8571.

29. Ezbiri M., Allen K.M., Galvez M.E., Michalsky R., and Steinfeld A., Design Principles of Perovskites for Thermochemical Oxygen Separation. ChemSusChem, 8(2015) 1966-1971.

30. Kharton V.V. and Marques F.M.B., Mixed ionic–electronic conductors:

effects of ceramic microstructure on transport properties. Current Opinion in Solid State and Materials Science, 6(2002) 261-269.

31. Teraoka Y., Zhang H.M., Okamoto K., and Yamazoe N., Mixed ionic-electronic conductivity of $La_{1-x}Sr_xCo_{1-y}Fe_yO_{3-\delta}$ perovskite-type oxides. Materials Research Bulletin, 23(1988) 51-58.

32. Brisotto M., Cernuschi F., Drago F., Lenardi C., Rosa P., Meneghini C., Merlini M., and Rinaldi C., High temperature stability of $Ba_{0.5}Sr_{0.5}Co_{0.8}Fe_{0.2}O_{3-\delta}$ and $La_{0.6}Sr_{0.4}Co_{1-y}Fe_yO_{3-\delta}$ oxygen separation perovskite membranes. Journal of the European Ceramic Society, 36(2016) 1679-1690.

33. Tuller H.L., Oxygen ion conduction and structural disorder in conductive oxides. Journal of Physics and Chemistry of Solids, 55(1994) 1393-1404.

34. Ji Q., Bi L., Zhang J., Cao H., and Zhao X.S., The role of oxygen vacancies of ABO_3 perovskite oxides in the oxygen reduction reaction. Energy & Environmental Science, 13(2020) 1408-1428.

35. Hohnke D.K., Ionic conduction in doped oxides with the fluorite structure. Solid State Ionics, 5(1981) 531-534.

36. Mogensen M., Lybye D., Bonanos N., Hendriksen P., and Poulsen F.,

Factors controlling the oxide ion conductivity of fluorite and perovskite structured oxides. Solid State Ionics, 174(2004) 279-286.

37. Chatzichristodoulou C., Norby P., Hendriksen P.V., and Mogensen M.B., Size of oxide vacancies in fluorite and perovskite structured oxides. Journal of Electroceramics, 34(2014) 100-107.

38. Manning P.S., Sirman J.D., and Kilner J.A., Oxygen self-diffusion and surface exchange studies of oxide electrolytes having the fluorite structure. Solid State Ionics, 93(1996) 125-132.

39. Wachsman E.D., Effect of oxygen sublattice order on conductivity in highly defective fluorite oxides. Journal of the European Ceramic Society, 24(2004) 1281-1285.

40. Shi H., Su C., Ran R., Cao J., and Shao Z., Electrolyte materials for intermediate-temperature solid oxide fuel cells. Progress in Natural Science: Materials International, 30(2020) 764-774.

41. Ishihara T., Oxide Ion Conductor, in Encyclopedia of Applied Electrochemistry, Kreysa G., Ota K.i., and Savinell R.F., Editors, New York: Springer, (2014) 1453-1458.

42. Zhu X. and Yang W., Microstructural and Interfacial Designs of Oxygen-

Permeable Membranes for Oxygen Separation and Reaction-Separation Coupling. Advanced Materials, 31(2019) 1902547.

43. Gupta S., Mahapatra M.K., and Singh P., Lanthanum chromite based perovskites for oxygen transport membrane. Materials Science and Engineering: R: Reports, 90(2015) 1-36.

44. Ramasamy M., Dual Phase Oxygen Transport Membrane for Efficient Oxyfuel Combustion. Reihe Energie & Umwelt / Energy & Environment, 351(2016).

45. Hong W.K. and Choi G.M., Oxygen permeation of BSCF membrane with varying thickness and surface coating. Journal of Membrane Science, 346(2010) 353-360.

46. Bouwmeester H., Kruidhof H., and Burggraaf A., Importance of the surface exchange kinetics as rate limiting step in oxygen permeation through mixed-conducting oxides. Solid state ionics, 72(1994) 185-194.

47. Kiebach R., Pirou S., Martinez Aguilera L., Haugen A.B., Kaiser A., Hendriksen P.V., Balaguer M., García-Fayos J., Serra J.M., Schulze-Küppers F., Christie M., Fischer L., Meulenberg W.A., and Baumann S., A review on dual-phase oxygen transport membranes: from fundamentals to

commercial deployment. Journal of Materials Chemistry A, 10(2022) 2152-2195.

48. Na B.T., Park J.H., Park J.H., Yu J.H., and Joo J.H., Elucidation of the Oxygen Surface Kinetics in a Coated Dual-Phase Membrane for Enhancing Oxygen Permeation Flux. ACS Applied Materials & Interfaces, 9(2017) 19917-19924.

49. Hunt A., Dimitrakopoulos G., and Ghoniem A.F., Surface oxygen vacancy and oxygen permeation flux limits of perovskite ion transport membranes. Journal of Membrane Science, 489(2015) 248-257.

50. Hendriksen P.V., Larsen P.H., Mogensen M., Poulsen F.W., and Wiik K., Prospects and problems of dense oxygen permeable membranes. Catalysis Today, 56(2000) 283-295.

51. Wang H., Yang W.S., Cong Y., Zhu X., and Lin Y.S., Structure and oxygen permeability of a dual-phase membrane. Journal of Membrane Science, 224(2003) 107-115.

52. Yun K.S., Yoo C.Y., Yoon S.G., Yu J.H., and Joo J.H., Chemically and thermo-mechanically stable LSM–YSZ segmented oxygen permeable ceramic membrane. Journal of Membrane Science, 486(2015) 222-228.

53. Marinha D. and Belmonte M., Mixed-ionic and electronic conduction and stability of YSZ-graphene composites. Journal of the European Ceramic Society, 39(2019) 389-395.

54. Gaudillere C., Garcia-Fayos J., Balaguer M., and Serra J.M., Enhanced oxygen separation through robust freeze-cast bilayered dual-phase membranes. ChemSusChem, 7(2014) 2554-2561.

55. Cao Z., Zhu X., Li W., Xu B., Yang L., and Yang W., Asymmetric dual-phase membranes prepared via tape-casting and co-lamination for oxygen permeation. Materials Letters, 147(2015) 88-91.

56. Jinsoo Kim Y.S.L., Synthesis and oxygen permeation properties of ceramic metal dual phase membrane. Journal of Membrane Science, (2000) 123-133.

57. Ai N., Jiang S.P., Lü Z., Chen K., and Su W., Nanostructured (Ba, Sr) (Co, Fe)$O_{3-\delta}$ Impregnate (La, Sr)MnO_3 Cathode for Intermediate-Temperature Solid Oxide Fuel Cells. Journal of The Electrochemical Society, 157(2010) B1033.

58. Tok A.I.Y., Luo L.H., Boey F.Y.C., and Woodhead J.L., Consolidation and properties of Gd0.1Ce0.9O1.95 nanoparticles for solid-oxide fuel cell

electrolytes. Journal of Materials Research, 21(2006) 119-124.

59. Santos T.H., Grilo J.P.F., Loureiro F.J.A., Fagg D.P., Fonseca F.C., and Macedo D.A., Structure, densification and electrical properties of Gd^{3+} and Cu^{2+} co-doped ceria solid electrolytes for SOFC applications: Effects of Gd_2O_3 content. Ceramics International, 44(2018) 2745-2751.

60. Zeng F., Malzbender J., Baumann S., Nijmeijer A., Winnubst L., Ziegner M., Guillon O., Schwaiger R., and Meulenberg W.A., Optimization of sintering conditions for improved microstructural and mechanical properties of dense $Ce_{0.8}Gd_{0.2}O_2$-$FeCo_2O_4$ oxygen transport membranes. Journal of the European Ceramic Society, 41(2021) 509-516.

61. Guo T., Zhang L., Song X., Dong X., Shirolkar M.M., Wang M., Li M., and Wang H., Influences of $Gd_2Ti_2O_7$ sintering aid on the densification, ionic conductivity and thermal expansion of $Gd_{0.1}Ce_{0.9}O_{1.95}$ electrolyte for solid oxide fuel cells. Journal of Power Sources, 262(2014) 239-244.

62. Kwon Y., Park J.H., Kang S.M., Nam G.D., Lee J.W., Kim J.H., Kim D., Jeong S.M., Yu J.H., and Joo J.H., Novel strategy for improving the oxygen permeability of zirconia-based dual-phase membranes. Energy & Environmental Science, 12(2019) 1358-1368.

63. Kim J. and Lin Y.S., Synthesis and oxygen permeation properties of ceramic-metal dual-phase membranes. Journal of Membrane Science, 167(2000) 123-133.

64. Luo H., Jiang H., Klande T., Cao Z., Liang F., Wang H., and Caro J., Novel Cobalt-Free, Noble Metal-Free Oxygen-Permeable $40Pr_{0.6}Sr_{0.4}FeO_{3-\delta}$–$60Ce_{0.9}Pr_{0.1}O_{2-\delta}$ Dual-Phase Membrane. Chemistry of Materials, 24(2012) 2148-2154.

65. Badwal S.P.S. and Ciacchi F.T., Ceramic Membrane Technologies for Oxygen Separation. Advanced Materials, 13(2001) 993-996.

66. Arratibel P.A., Cruellas L.A., Liu Y., Badiola P.N., Pacheco T.D.A., Sint A.M.V., and Gallucci F., Mixed Ionic-Electronic Conducting Membranes (MIEC) for Their Application in Membrane Reactors: A Review. Processes, 7(2019) 128.

67. Will J., Mitterdorfer A., Kleinlogel C., Perednis D., and Gauckler L., Fabrication of thin electrolytes for second-generation solid oxide fuel cells. Solid State Ionics, 131(2000) 79-96.

68. Segal D., Chemical synthesis of ceramic materials. Journal of Materials Chemistry, 7(1997) 1297-1305.

69. Zhu X. and Yang W., eds. Chapter 12 - Critical Factors Affecting Oxygen Permeation Through Dual-phase Membranes. Membrane Science and Technology, ed. Oyama S.T. and Stagg-Williams S.M.: Elsevier, (2011) 275-293.

70. Zhang Z., Zhou W., Chen Y., Chen D., Chen J., Liu S., Jin W., and Shao Z., Novel Approach for Developing Dual-Phase Ceramic Membranes for Oxygen Separation through Beneficial Phase Reaction. ACS Applied Materials & Interfaces, 7(2015) 22918-22926.

71. Balaguer M., García-Fayos J., Solís C., and Serra J.M., Fast Oxygen Separation Through SO_{2-} and CO_{2-}Stable Dual-Phase Membrane Based on $NiFe_2O_4$–$Ce_{0.8}Tb_{0.2}O_{2-\delta}$. Chemistry of Materials, 25(2013) 4986-4993.

72. Drago F., Fedeli P., Cavaliere A., Cammi A., Passoni S., Mereu R., De La Pierre S., Smeacetto F., and Ferraris M., Development of a Membrane Module Prototype for Oxygen Separation in Industrial Applications. Membranes, 12(2022) 167.

73. Fernández-González R., Molina T., Savvin S., Moreno R., Makradi A., and Núñez P., Fabrication and electrical characterization of several YSZ tapes for SOFC applications. Ceramics International, 40(2014) 14253-14259.

74. Kwon Y.i., Park J.H., Kang S.M., Nam G.D., Lee J.W., Kim J.H., Kim D., Jeong S.M., Yu J.H., and Joo J.H., Novel strategy for improving the oxygen permeability of zirconia-based dual-phase membranes. Energy & Environmental Science, 12(2019) 1358-1368.

75. Michálek M., Blugan G., Graule T., and Kuebler J., Comparison of aqueous and non-aqueous tape casting of fully stabilized ZrO_2 suspensions. Powder Technology, 274(2015) 276-283.

76. Huang H., Cheng S., Gao J., Chen C., and Yi J., Phase-inversion tape-casting preparation and significant performance enhancement of $Ce_{0.9}Gd_{0.1}O_{1.95}$–$La_{0.6}Sr_{0.4}Co_{0.2}Fe_{0.8}O_{3-\delta}$ dual-phase asymmetric membrane for oxygen separation. Materials Letters, 137(2014) 245-248.

77. Atkinson H. and Davies S., Fundamental aspects of hot isostatic pressing: an overview. Metallurgical and Materials Transactions A, 31(2000) 2981-3000.

78. Zhang H.B., Kim B.N., Morita K., Yoshida H., Lim J.H., and Hiraga K., Optimization of high-pressure sintering of transparent zirconia with nano-sized grains. Journal of Alloys and Compounds, 508(2010) 196-199.

79. Mosadeghkhah A., Alaee M.A., and Mohammadi T., Effect of sintering

temperature and dwell time and pressing pressure on $Ba_{0.5}Sr_{0.5}Co_{0.8}Fe_{0.2}O_{3-\delta}$ perovskite-type membranes. Materials & Design, 28(2007) 1699-1706.

80. Zhang H., Kim B.N., Morita K., Keijiro Hiraga H.Y., and Sakka Y., Effect of sintering temperature on optical properties and microstructure of translucent zirconia prepared by high-pressure spark plasma sintering. Science and Technology of Advanced Materials, 12(2011) 055003.

81. Mishra T.P., Laptev A.M., Ziegner M., Sistla S.K., Kaletsch A., Broeckmann C., Guillon O., and Bram M., Field-Assisted Sintering/Spark Plasma Sintering of Gadolinium-Doped Ceria with Controlled Re-oxidation for Crack Prevention. Materials, 13(2020) 3184.

82. Dudina D.V., Bokhonov B.B., and Olevsky E.A., Fabrication of porous materials by spark plasma sintering: A review. Materials, 12(2019) 541.

83. Grasso S., Saunders T., Porwal H., Milsom B., Tudball A., Reece M., and Chen I.W., Flash Spark Plasma Sintering (FSPS) of α and β SiC. Journal of the American Ceramic Society, 99(2016) 1534-1543.

84. Vasylkiv O., Borodianska H., Sakka Y., and Demirskyi D., Flash spark plasma sintering of ultrafine yttria-stabilized zirconia ceramics. Scripta

Materialia, 121(2016) 32-36.

85. Anselmi-Tamburini U., Garay J.E., Munir Z.A., Tacca A., Maglia F., Chiodelli G., and Spinolo G., Spark plasma sintering and characterization of bulk nanostructured fully stabilized zirconia: Part II. Characterization studies. Journal of Materials Research, 19(2004) 3263-3269.

86. Chang S.Y., Oh S.-T., Suk M.-J., and Hong C.S., Spark Plasma Sintering of Stainless Steel Powders Fabricated by High Energy Ball Milling. Journal of Korean Powder Metallurgy Institute, 21(2014) 97-101.

87. Wang S., Liu Y., He J., Chen F., and Brinkman K.S., Spark-plasma-sintered barium zirconate based proton conductors for solid oxide fuel cell and hydrogen separation applications. International Journal of Hydrogen Energy, 40(2015) 5707-5714.

88. Flaureau A., Weibel A., Chevallier G., and Estournès C., Study of the densification and grain growth mechanisms occurring during spark plasma sintering of different submicronic yttria-stabilized zirconia powders. Journal of the European Ceramic Society, 41(2021) 3581-3594.

89. Fish J.S., Ricote S., Lenrick F., Wallenberg L.R., Holgate T.C., O'Hayre R., and Bonanos N., Synthesis by spark plasma sintering of a novel

protonic/electronic conductor composite: $BaCe_{0.2}Zr_{0.7}Y_{0.1}O_{3-\delta}$ /$Sr_{0.95}Ti_{0.9}Nb_{0.1}O_{3-\delta}$ (BCZY27/STN95). Journal of Materials Science, 48(2013) 6177-6185.

90. Jiang Q.H., Shen Z.J., Zhou J.P., Shi Z., and Nan C.W., Magnetoelectric composites of nickel ferrite and lead zirconnate titanate prepared by spark plasma sintering. Journal of the European Ceramic Society, 27(2007) 279-284.

91. Mahmud N.N., Vajpai S.K., and Ameyama K., Fabrication of Yttria Stabilized Zirconia-Silicon Carbide Composites with High Strength and High Toughness by Spark Plasma Sintering of Mechanically Milled Powders. Materials Transactions, 55(2014) 1827-1833.

92. O'Brien R., Ambrosi R., Bannister N., Howe S., and Atkinson H., Spark Plasma Sintering of simulated radioisotope materials within tungsten cermets. Journal of Nuclear Materials, 393(2009) 108-113.

93. Lee S., Spark Plasma Sintering Technique and Application for All-Solid-State Batteries. Ceramist, 22(2019) 170-181.

94. Cavaliere P., Sadeghi B., and Shabani A., Spark Plasma Sintering: Process Fundamentals, in Spark Plasma Sintering of Materials: Advances in

Processing and Applications, Cavaliere P., Editor, Cham: Springer International Publishing, (2019) 3-20.

95. Trapp J., Semenov A., Eberhardt O., Nöthe M., Wallmersperger T., and Kieback B., Fundamental principles of spark plasma sintering of metals: part II – about the existence or non-existence of the 'spark plasma effect'. Powder Metallurgy, 63(2020) 312-328.

96. Grasso S., Sakka Y., and Maizza G., Pressure Effects on Temperature Distribution during Spark Plasma Sintering with Graphite Sample. Materials Transactions, 50(2009) 2111-2114.

97. Suárez M., Fernández A., Menéndez J., Torrecillas R., Kessel H., Hennicke J., Kirchner R., and Kessel T., Challenges and opportunities for spark plasma sintering: a key technology for a new generation of materials. Sintering applications, 13(2013) 319-342.

Chapter 2 | Fabrication of YSZ-carbon felt oxygen separation dual-phase membrane by vacuum filtration method.

Preface

The dual-phase membrane constructed of both an oxide ion conducting phase and an electronic conducting phase has attracted attention for oxygen separation applications, as discussed in the previous chapter. Achieving both the percolation structures of the oxide ion conduction phase and the electron conduction phase is necessary to achieve an oxygen dissociation and association reaction. In this study, a new and simple fabrication method using a vacuum infiltration and spark plasma sintering (SPS) process for a dual-phase oxygen separation membrane consisting of YSZ and carbon felt has been developed.

1. Introduction

Oxygen is one of the most important industrial gases widely used in various fields. Generally, oxygen is produced by separation from air. The methods to separate oxygen from air can be classified into three types which are cryogenic separation, adsorption separation and membrane separation. First, the cryogenic separation method, which is a method using the difference in the boiling points of

the air components, is a commercialized technology for the large-scale production of pure oxygen. Adsorption separation is the process of using an adsorbent to separate oxygen gas through adsorption and desorption cycles. The oxygen separation membrane is a method of sieving a specific gas based on differences in the material's micropore size and gas molecule size [1]. Currently, a household oxygen supplier, which is a small to medium scale oxygen separation production, has attracted attention [2]. Among these three methods, the oxygen separation membrane is suitable for small-scale production. Among the various types of separation membranes, the separation membrane using a mixed oxide ion-electron conductor (MIEC)-based membrane is a promising oxygen separation membrane that electrochemically separates oxygen gas because it can be driven only by the oxygen partial pressure difference across the membrane at high temperatures without connecting to external circuits [3, 4]. The mechanism of the oxygen separation process on the oxygen separation membrane is as follows: oxygen molecules in the air dissociate on the surface of the membrane to generate oxide ions on the high oxygen partial pressure side or feed side, then the oxide ions diffuse from the feed side through the lattice vacancies in the crystal structure to the low oxygen partial pressure side or permeation side, and recombine to form

oxygen molecules. In this process, electrons are transported in the opposite direction of the oxygen transport path to balance the charge neutrality [5]. Important requirements for the membrane material selection are a high oxide ion conductivity, chemical stability, and high mechanical strength. Oxide-ion conductors with the structure of fluorite (AO_2) and perovskite (ABO_3) meet these requirements [6, 7]. MIEC are commonly used as single-phase oxygen separation membranes [8]. $Ba_{0.5}Sr_{0.5}Co_{0.8}Fe_{0.2}O_{3-\delta}$ (BSCF), which has both a high ionic and electronic conductivity, has the highest oxygen permeability of all the MIEC ceramic materials [9, 10]. To further improve the oxygen separation properties, it is not enough to just look for new MIEC materials, as the diffusion rate of oxide ions in the MIEC-based single-phase membrane is almost at its limit.

In this study, attention is being paid to a dual-phase membrane. A dual-phase membrane is a composite material consisting of an oxide ion-conducting phase as the oxide ions transportation path and an electron-conducting phase as an electron transportation path [11, 12]. By separating the transport paths of the oxide ions and electrons, it is possible to obtain a membrane that can achieve a high conductivity for both the oxide ions and electrons. Eight mol% yttria-stabilized zirconia (8YSZ) is an excellent oxide-ion conductor with a fluorite

structure. It is suitable for use as the oxide ion conductive phase in a dual-phase membrane [13, 14]. Carbon with a high electron conductivity is suitable for the electron conduction phase [15, 16]. Most conventional methods for producing a dual-phase membrane are by a solid-phase reaction in which different types of powders are simply mixed and sintered [17, 18]. However, it is quite difficult to achieve both the percolation structures of the oxide ion conduction phase and the electron conduction phase. Therefore, a new method is necessary to realize the co-continuous structure of the two phases for improvement of the separation performance. In this study, a new and simple manufacturing process of a dual-phase membrane by filling an oxide ion conductive phase material in the pores of an electron conductive phase material with a three-dimensional network structure is presented.

2. Experimental methods

The microstructure of the carbon felt is shown in Figures 2-1. The continuous porous structure, which leads to the continuous transportation of electrons, exhibited a high electronic conductivity. TG-DSC analyses (STA 449 F3 Jupiter, NETZSCH Japan K.K., Japan) were used to measure the carbon

oxidation over the oxygen permeation temperature range of 500 to 900 ºC in an air atmosphere. Figure 2-2 show the TG and DSC profiles of the carbon felt. The mass loss rate significantly changes at the temperature around 550 ºC. Carbon felt was drastically oxidized from 550 to 680 ºC. The TG-DSC result indicated that the dual-phase membrane made of carbon felt was suitable to perform an oxygen permeation test below 550 ºC.

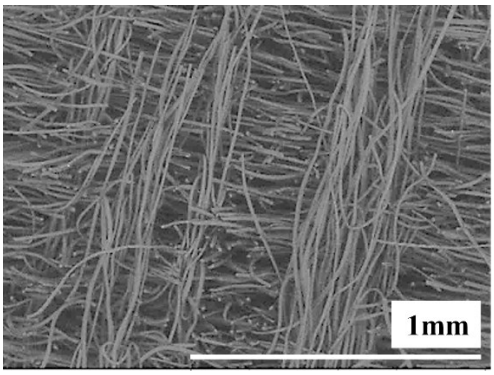

Fig. 2-1 Microstructure of carbon felt.

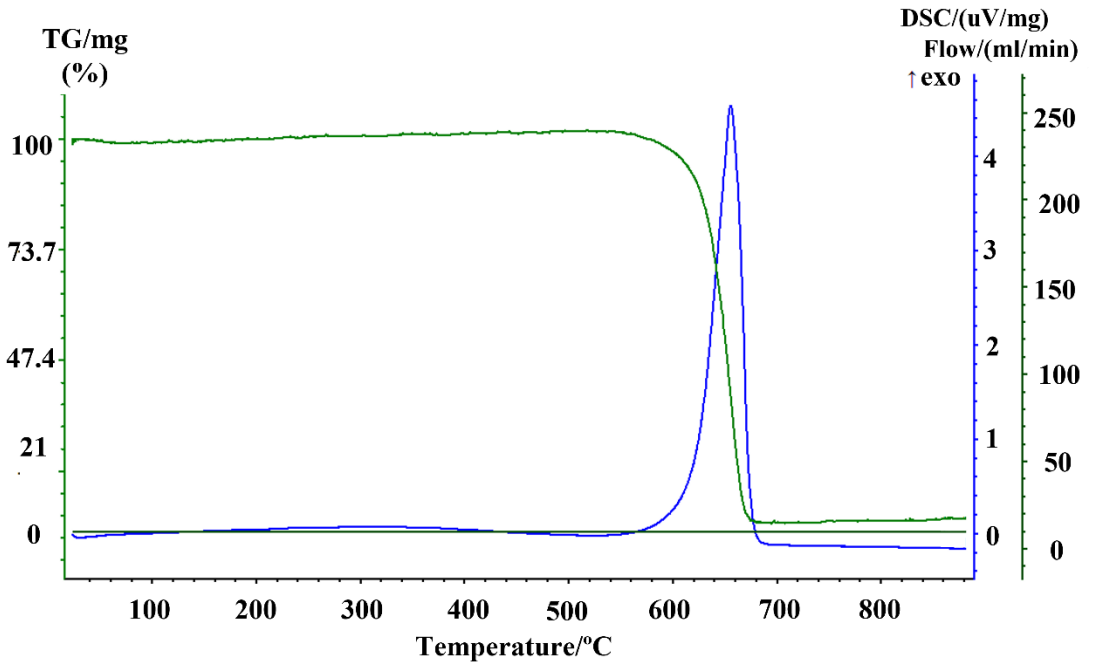

Fig. 2-2 Combined TG-DSC measurement of carbon felt.

The zeta potentials of TZ-8YS and TZ-8Y (8 mol% yttria-doped zirconia powders (TZ-8YS (D50: 0.6 μm) and TZ-8Y (D50: 0.6 μm), Tosoh Corporation, Japan)) suspensions were measured using laser doppler velocimetry (Zetasizer Nano-ZS, Malvern Panalytical Ltd., UK) as a function of the dispersant addition (ammonium polyacrylate, Alon-A6114, Toagosei Co., Ltd., Japan). The result is shown in Fig. 2-3. The zeta potentials of both TZ-8YS and TZ-8Y with the addition of 2 wt% ammonium polyacrylate exhibited high values of -54.96 and -58.96 mV, indicating their high stability in aqueous solutions. Thus, the addition of 2 wt% ammonium polyacrylate was used to stabilize both the TZ-8YS and

TZ-8Y suspensions.

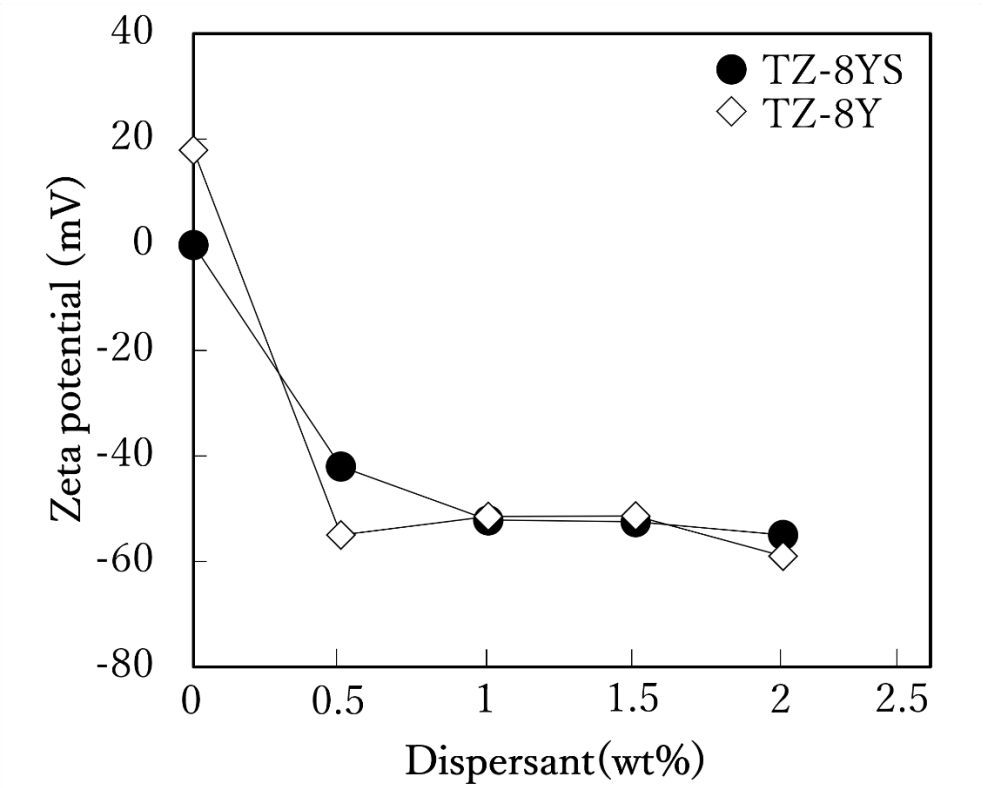

Fig.2-3 Relation of zeta potential of YSZ versus dispersant addition.

A schematic showing the preparation process of the YSZ-carbon felt dual-phase membranes is shown in Figure 2-4. To prepare the suspensions, 30 vol% TZ-8Y and 40 vol% TZ-8YS were dispersed in distilled water with 2 wt% ammonium polyacrylate as a dispersant. The carbon felt was cut into a 15-mm diameter disk with a thickness of 3 mm and placed in distilled water, followed by an evacuation for 30 minutes to remove all the gas in the porous structure. The

green composite bodies were formed by the vacuum filtration of the YSZ suspension into the carbon felt. The excess powder was removed with sandpaper before being cold isostatically pressed at 350 MPa for 10 minutes to achieve uniform packing of the YSZ particles inside the porous structure. The green samples were sintered by two types of sintering processes which are the conventional sintering process under an Ar atmosphere and the spark plasma sintering process under a vacuum atmosphere (SPS, LaboxTM-325 Sinter Land Inc., Japan). As mentioned in Chapter 1, SPS is a high-pulse direct current technique to densify the sample at a low sintering temperature and short sintering time [19]. The YSZ-carbon felt dual-phase membranes were sintered by SPS for 10 minutes at different temperatures and pressures. By using this new fabrication technique, a continuous-phase structure would be formed with a simple, low-cost, and low-energy consumption.

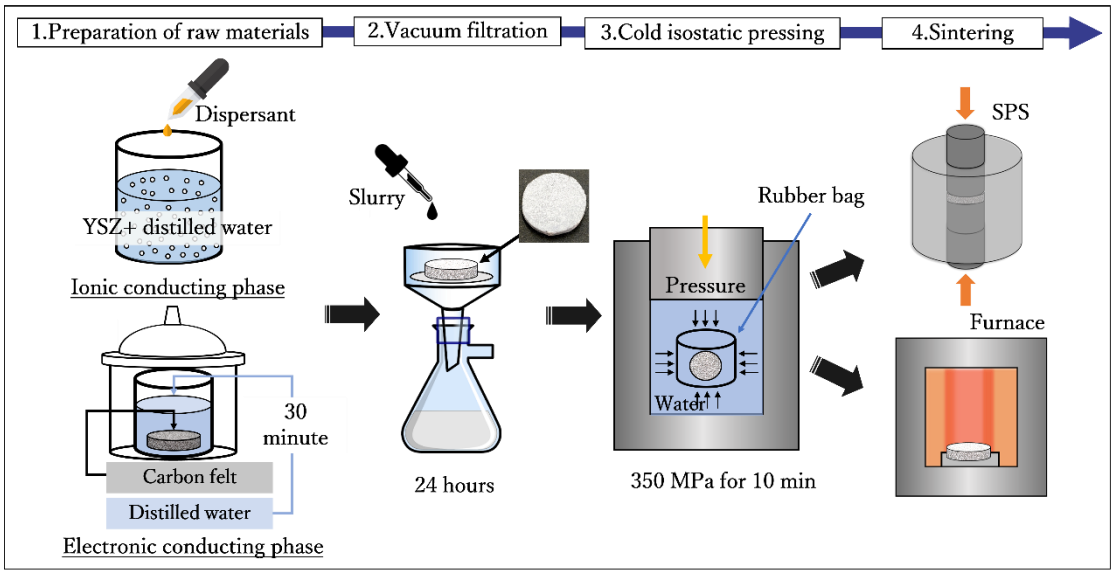

Fig. 2-4 Schematic showing the preparation process of YSZ-based dual-phase membranes.

The phase stability and chemical compatibility of the dual-phase membranes fabricated at the different sintering temperatures were investigated. The sintered samples were ground in an agate mortar and analyzed by X-ray diffraction (XRD, Miniflex 600, Rigaku Corporation, Japan). The XRD patterns were obtained with a step of 0.02 deg and a speed of 10 deg/min at 40 kV and 15 mA. The microstructure of the dual-phase membranes was observed using a scanning electron microscope (SEM, JSM-5600LV, JEOL Ltd., Japan) at a 5 kV accelerating voltage. Finally, an oxygen separation test was performed using the selected sample. Figure 2-5 is a schematic of the experimental setup for the oxygen

permeation test. The sealing of the 15-mm diameter membrane disk and the aluminum tube was performed using a silver ring at 900 ºC under the Ar atmosphere to prevent any oxidation that may occur before the measurement. After the silver ring attachment, the temperature was decreased to 550 ºC, then air was flowed on the feed side at a rate of 250 ml/min. On the other side, an Ar sweep gas was flowed at the rate of 250 ml/min on the permeation side, and the amount of oxygen in the permeate gas was monitored by an oxygen galvanic analyzer (MC-8G-L, Iijima Electronics Corporation, Japan). This experimental setup was operated at temperatures ranging from 400 to 550 ºC. A gas chromatograph (GC-8A, Shimadzu Corporation, Japan) was used to monitor the air leak behavior.

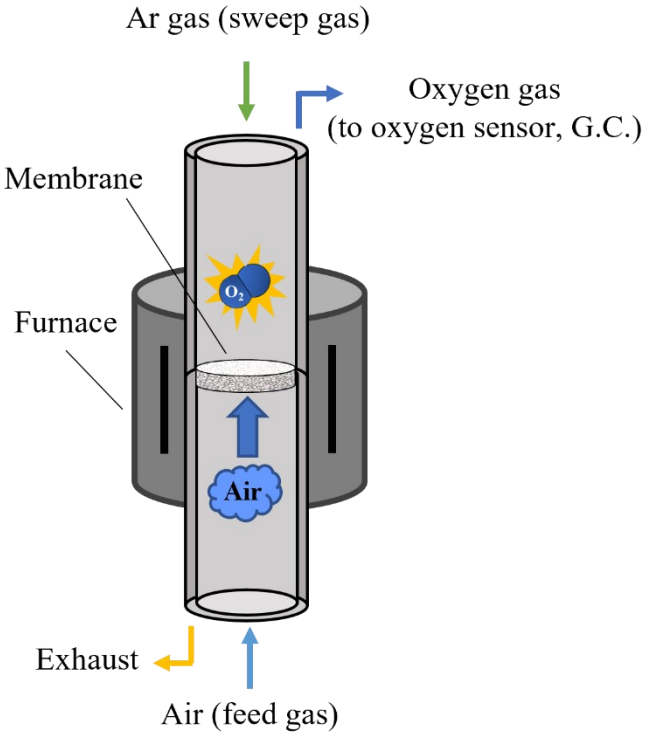

Fig. 2-5 Schematic of oxygen separation performance test.

3. Results and discussion

3.1 Comparison of sintering properties of different raw material powders

In this experiment, two types of YSZ powders (TZ-8YS and TZ-8Y) were used as mentioned in the experimental procedures. The company's catalog states that TZ-8Y has a smaller primary particle size and is easier to sinter than TZ-8YS; therefore, it was inferred that TZ-8Y could be densified at lower temperatures. However, the solid concentration of the highly-fluid suspensions was approximately 40 vol% and 30 vol% for TZ-8YS and TZ-8Y, respectively, even

when the amount of the dispersant was optimized. The specific surface areas of TZ-8YS and TZ-8Y were 7 m^2/g and 16 m^2/g, respectively. This difference is reasonable considering that TZ-8Y has more particle-to-particle interactions and is more likely to agglomerate than TZ-8YS. It was difficult to fill the voids of the carbon felt with the agglomerated powder like TS8Y, and only low-density compacts were obtained as shown in Figure 2-6, resulting in the requirement of a higher temperature for densification. Therefore, TZ-8YS was used for preparation of the membrane.

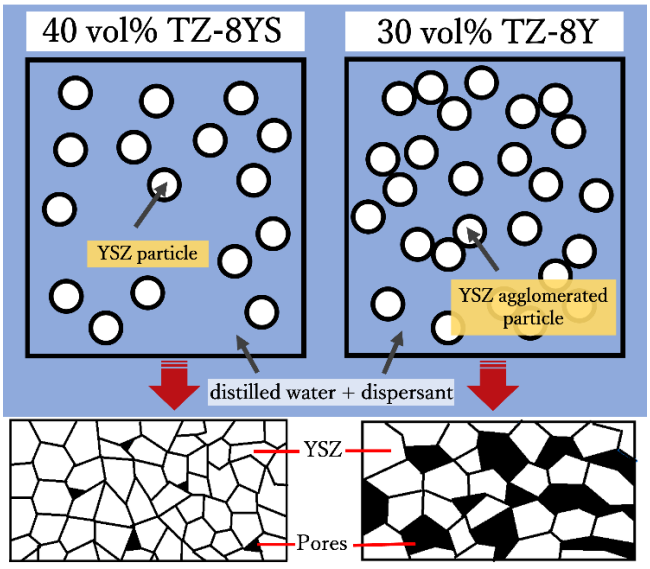

Fig. 2-6 Schematic illustration showing the relationship between the dispersion state of the two 8YSZ powders in their slurries and the microstructure of the subsequent sintered bodies.

Figure 2-7(a) shows the microstructure of the YSZ-carbon felt dual-phase membrane prepared from TZ-8YS. The sample sintered at 1600 °C has a relative density of 95%. Compared to the microstructure of the YSZ-carbon felt dual-phase membrane prepared from TZ-8Y in Figure 2-7(b), the sample sintered at the same temperature has a relative density of only 86%, and small particles can be seen around it. Based on these results, the TZ-8YS was used as the YSZ source for preparing the YSZ suspension.

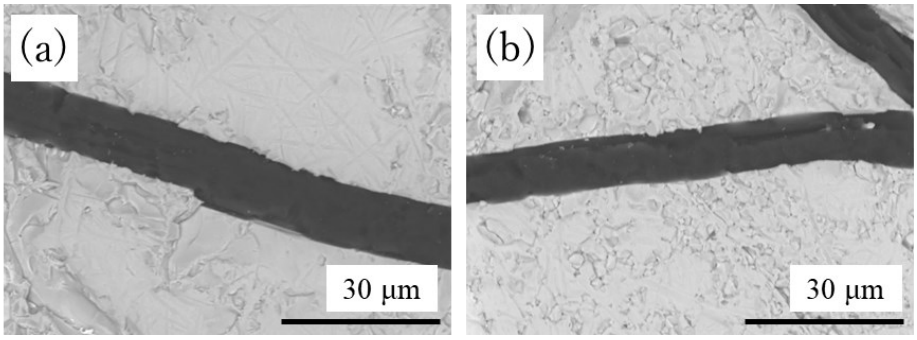

Fig. 2-7 The microstructure of (a) 40 vol% TZ8YS, and (b) 30 vol% TZ8Y of YSZ-carbon felt dual-phase membranes sintered by SPS at 1600 °C.

3.2 Comparison of sintering characteristics by different sintering methods

Achieving a gas-tight dense structure is one of the requirements for fabricating the oxygen separation membrane without leaking nitrogen gas on the

permeation side. The dense packing of the YSZ particles would increase the transportation path of the oxide ions. The YSZ sintered sample with a low packing could lead to gas leakage in addition to low oxygen transportation. To achieve a gas-tight dense membrane, the sintering process should be optimized. The effects of the sintering process on the microstructure and density of the sintered samples were characterized. The sample sintered at 1600 ºC for the YSZ-carbon felt dual-phase membrane was fabricated by SPS in a vacuum and the conventional sintering process in an argon atmosphere was investigated.

Figure 2-8 compares the microstructures of the YSZ-carbon felt dual-phase membrane sintered by SPS and the conventional sintering process. The samples sintered by SPS have a good attachment between the YSZ and carbon felt. Small, flaky YSZ crystals were observed in the samples sintered by the conventional sintering process, and the relative density decreased from the green compact density to 23.9%. As a result of the spark plasma sintering process, the densification of the YSZ-based dual-phase membrane with a high structural stability was clearly enhanced. Thus, the SPS process is a promising technique for the sintered membrane in this research study.

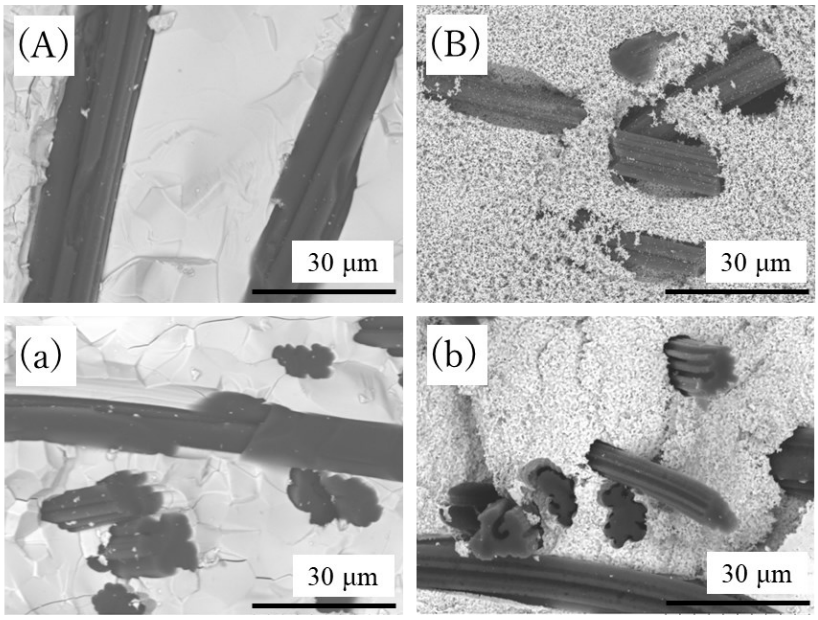

Fig. 2-8 Surface and cross section images of the microstructures of YSZ-carbon felt dual-phase membrane sintered at 1600 °C by SPS ((A), (a)) and conventional sintering((B), (b)).

3.3 Sintering parameters in spark plasma sintering

For the sintering process, it is necessary to study the sintering conditions of the SPS to successfully fabricate a gas-tight YSZ-carbon felt dual-phase membrane.

3.3.1 Applied pressure

The effect of the applied pressure on the relative density of the YSZ-carbon felt membrane sintered at 1600 °C for 10 minutes under the applied pressures of

40, 60 and 80 MPa is shown in Figure 2-9. An applied pressure increases of 40–80 MPa increases the relative density of the sintered membrane. The relative density of the YSZ-carbon felt dual-phase membrane can be achieved up to 95% at the applied pressure of 80 MPa.

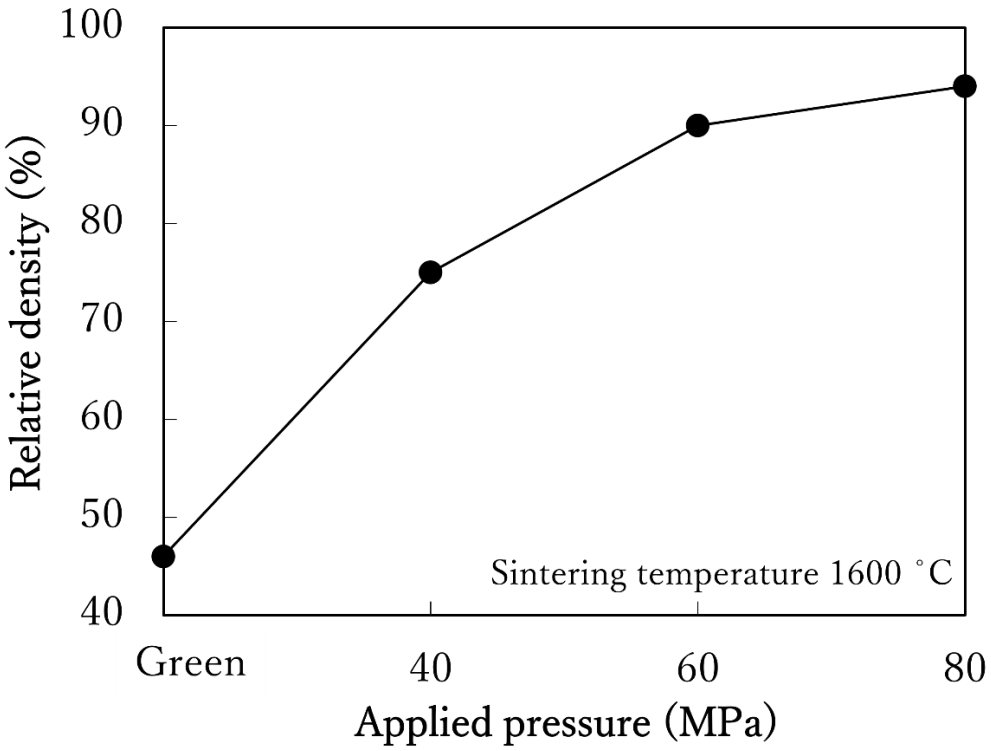

Fig. 2-9 Relative density of the YSZ-carbon felt dual-phase membranes sintered by SPS at different applied pressures.

3.3.2 Sintering temperature

Figure 2-10 depicts the relationship between sample relative density and sintering temperature. To enhance the conductivity of an oxide ion conductor, it is preferable to achieve a high level of densification. The graph reveals that acceptable dense samples for achieving a high oxide ion conductivity were produced by sintering at temperatures up to 1500 °C.

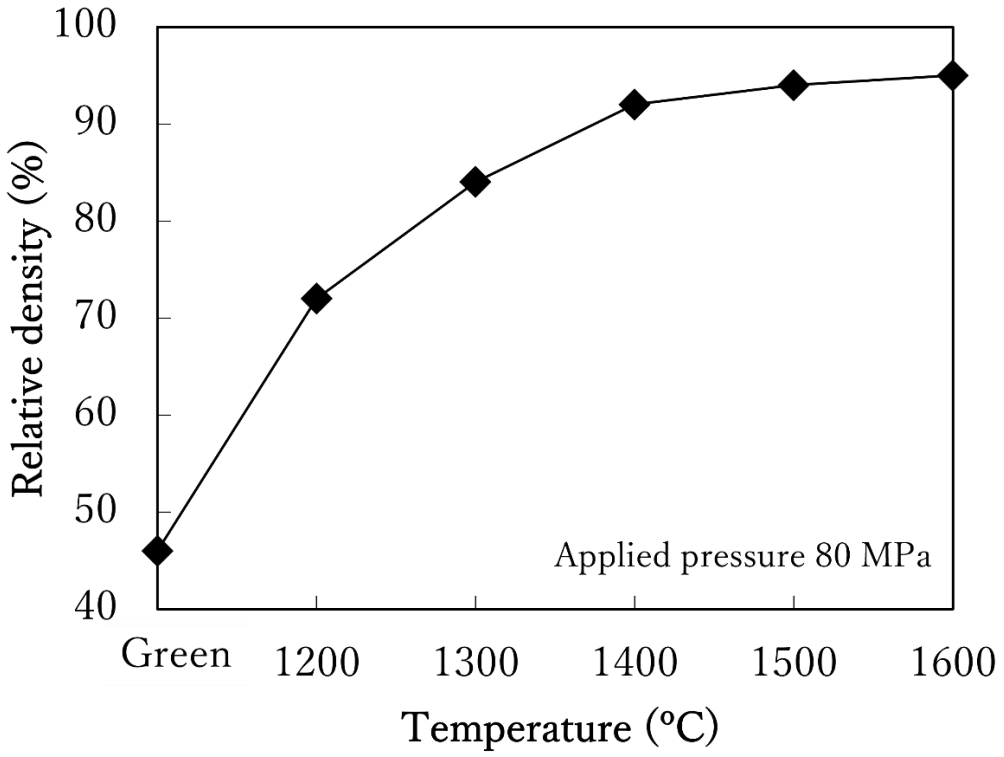

Fig. 2-10 Relative density of YSZ-carbon felt dual-phase membranes sintered by SPS at different sintering temperatures.

Figure 2-11 illustrates the XRD pattern of the YSZ-carbon felt membrane sintered using SPS. The XRD patterns of the sintered samples at 1200 and 1500 ºC indicated that the sintered sample consisted of YSZ and graphite, suggesting that there is no reaction between the YSZ and carbon felt at the sintering temperatures below 1500 ºC. When the temperature was raised to 1600 ºC, small peaks of the secondary phase zirconia carbide were observed. This secondary phase indicated the strong bond between YSZ and carbon felt sintered at high temperatures.

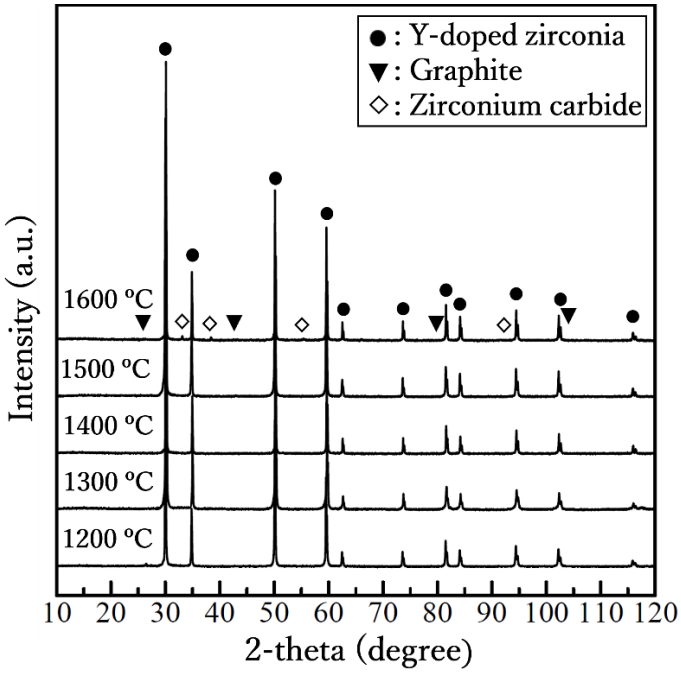

Fig. 2-11 XRD patterns of YSZ-carbon felt membrane sintered at 1200-1600 °C by SPS.

Figure 2-12 shows an SEM image of the microstructure of a YSZ-carbon felt dual-phase membrane sintered at the temperatures of 1200, 1400, and 1600 ºC. This demonstrates that the two phases in the membrane were tightly attached. Since there are no voids between the two phases, it can be assumed that there will be no gas leaks during the air separation process.

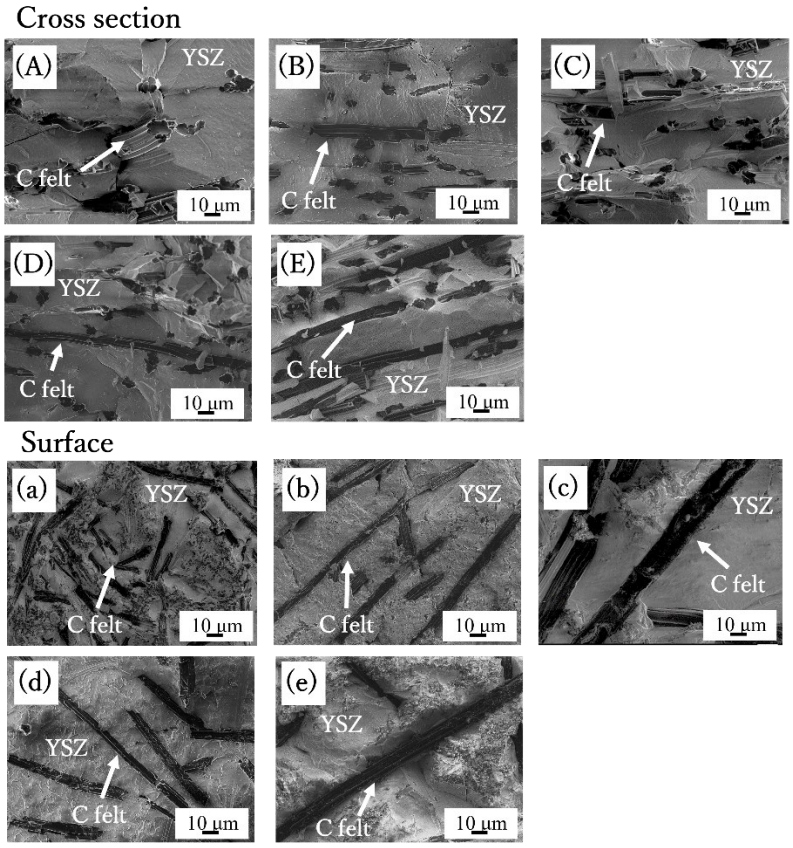

Fig. 2-12 Surface and cross section images of the microstructures of YSZ-carbon felt dual-phase membranes sintered at (A) and (a) 1200 °C, (B) and (b) 1300 °C, and (C) and (c) 1400 °C, (D) and (d) 1500 °C, (E) and (e) 1600°C.

3.4 Oxygen separation performance of the YSZ-carbon felt dual-phase membrane

As a result, a YSZ-carbon felt dual-phase membrane was selected to perform an oxygen separation performance test. Figure 2-13 shows the oxygen permittivity of the YSZ-carbon felt dual-phase membrane as a function of the temperature. The YSZ-carbon felt dual-phase membrane has the ability to separate the oxygen gas from air which exhibited the oxygen permeation flux of 0.42 ml(STP)/min·cm² at 550 ºC, suggesting that this fabrication route could be used to produce the dual-phase membrane for oxygen separation applications.

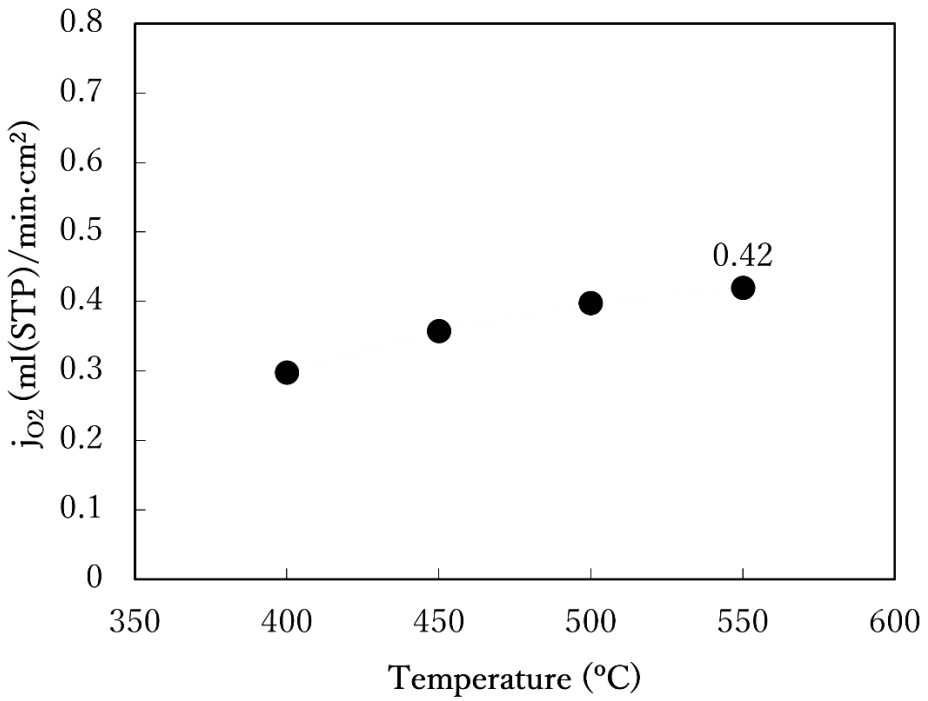

Fig. 2-13 Oxygen separation performance of the YSZ-carbon felt dual-phase membrane.

4. Conclusions

YSZ-carbon felt dual-phase membranes using TZ-8YS powder as a YSZ source were successfully fabricated by SPS with a good phase stability and high chemical compatibility. The relative density of 95% could be obtained by the YSZ-carbon felt dual-phase membrane sintered at 1600 ºC. Due to the strong attachment between the two phases in the YSZ-carbon felt dual-phase membrane, the XRD results revealed the appearance of zirconia carbide when sintered at 1600 ºC. The YSZ-carbon felt dual-phase membranes achieved a tight attachment at the performed temperatures. Finally, the YSZ-carbon felt dual-phase membrane sintered at 1500 ºC was chosen for the oxygen separation performance test. The highest oxygen permeation flux of 0.42 ml(STP)/min·cm² was obtained at 550 ºC. However, oxidation of the carbon felt is a critical problem, so further improvement of the oxygen separation performance of the YSZ-based dual-phase membrane will be described in the next chapter.

References

1. Ishii K., Matsunaga C., Kobayashi K., Stevenson A.J., Tardivat C., and Uchikoshi T., Fabrication of BSCF-based mixed ionic-electronic conducting membrane by electrophoretic deposition for oxygen separation application. Journal of the European Ceramic Society, 39(2019) 5292-5297.
2. Adhikari B., Orme C.J., Klaehn J.R., and Stewart F.F., Technoeconomic analysis of oxygen-nitrogen separation for oxygen enrichment using membranes. Separation and Purification Technology, 268(2021) 118703.
3. Riess I., Mixed ionic-electronic conductors-material properties and applications. Solid State Ionics, 157(2003) 1-17.
4. Hashim S.S., Mohamed A.R., and Bhatia S., Oxygen separation from air using ceramic-based membrane technology for sustainable fuel production and power generation. Renewable and Sustainable Energy Reviews, 15(2011) 1284-1293.
5. Badwal S.P.S. and Ciacchi F.T., Ceramic Membrane Technologies for Oxygen Separation. Advanced Materials, 13(2001) 993-996.
6. Sunarso J., Baumann S., Serra J.M., Meulenberg W.A., Liu S., Lin Y.S., and

Diniz da Costa J.C., Mixed ionic–electronic conducting (MIEC) ceramic-based membranes for oxygen separation. Journal of Membrane Science, 320(2008) 13-41.

7. Chatzichristodoulou C., Norby P., Hendriksen P.V., and Mogensen M.B., Size of oxide vacancies in fluorite and perovskite structured oxides. Journal of Electroceramics, 34(2014) 100-107.

8. Lin Y., Fang S., Su D., Brinkman K.S., and Chen F., Enhancing grain boundary ionic conductivity in mixed ionic-electronic conductors. Nature communications, 6(2015) 6824.

9. Ishii K., Matsunaga C., Kobayashi K., Stevenson A.J., Tardivat C., and Uchikoshi T., Fabrication of BSCF-based mixed oxide ionic-electronic conducting multi-layered membrane by sequential electrophoretic deposition process. Journal of the European Ceramic Society, 41(2021) 2709-2715.

10. Baumann S., Schulze-Küppers F., Roitsch S., Betz M., Zwick M., Pfaff E.M., Meulenberg W.A., Mayer J., and Stöver D., Influence of sintering conditions on microstructure and oxygen permeation of $Ba_{0.5}Sr_{0.5}Co_{0.8}Fe_{0.2}O_{3-\delta}$ (BSCF) oxygen transport membranes. Journal of

Membrane Science, 359(2010) 102-109.

11. Zhang Z., Zhou W., Chen Y., Chen D., Chen J., Liu S., Jin W., and Shao Z., Novel Approach for Developing Dual-Phase Ceramic Membranes for Oxygen Separation through Beneficial Phase Reaction. ACS Applied Materials & Interfaces, 7(2015) 22918-22926.

12. Schulze-Küppers F., Baumann S., Meulenberg W.A., Stöver D., and Buchkremer H.P., Manufacturing and performance of advanced supported $Ba_{0.5}Sr_{0.5}Co_{0.8}Fe_{0.2}O_{3-\delta}$ (BSCF) oxygen transport membranes. Journal of Membrane Science, 433(2013) 121-125.

13. Wang H., Yang W.S., Cong Y., Zhu X., and Lin Y.S., Structure and oxygen permeability of a dual-phase membrane. Journal of Membrane Science, 224(2003) 107-115.

14. Joshi A.V., Steppan J.J., Taylor D.M., and Elangovan S., Solid Electrolyte Materials, Devices, and Applications. Journal of Electroceramics, 13(2004) 619-625.

15. Huong Le T.X., Bechelany M., and Cretin M., Carbon felt based-electrodes for energy and environmental applications: A review. Carbon, 122(2017) 564-591.

16. Panthi D., Hedaya N., and Du Y., Densification behavior of yttria-stabilized zirconia powders for solid oxide fuel cell electrolytes. Journal of Advanced Ceramics, 7(2018) 325-335.

17. Chaudhari N.K., Jin H., Kim B., and Lee K., Nanostructured materials on 3D nickel foam as electrocatalysts for water splitting. Nanoscale, 9(2017) 12231-12247.

18. Zhu X., Wang H., and Yang W., Relationship between homogeneity and oxygen permeability of composite membranes. Journal of Membrane Science, 309(2008) 120-127.

19. Chen X.J., Khor K.A., Chan S.H., and Yu L.G., Overcoming the effect of contaminant in solid oxide fuel cell (SOFC) electrolyte: spark plasma sintering (SPS) of 0.5wt.% silica-doped yttria-stabilized zirconia (YSZ). Materials Science and Engineering: A, 374(2004) 64-71.

Chapter 3 | Selection of electron conductive metal foam for percolation design of dual-phase oxygen permeable membrane

Preface

In the previous chapter, YSZ-carbon felt dual-phase membranes were successfully fabricated by applying the SPS method. The oxygen diffusion rate generally increases with the temperature and an operating temperature of 500-900 ºC is required for an improved oxygen separation performance. However, an operating temperature above 550 ºC will cause oxidation of the carbon felt in air, significantly degrading the performance of the dual-phase membrane. In this chapter, several metallic materials, selected for their high melting point and oxidation resistance, were investigated for their applicability as an electronically-conductive phase alternative to carbon felt for oxygen separation applications. A commercially-available metal foam was used as the electron-conducting phase, and dual phase membranes with a structure in which 8YSZ filled the metal foam were fabricated by vacuum filtration and the subsequent spark plasma sintering process as described in Chapter 2.

1. Introduction

In a dual-phase membrane, the percolation structures of both the oxide ionic conducting phase and the electronic conducting phase are very important in achieving the oxygen separating capacity. The methods for fabricating a dual-phase membrane include the solid-state reaction process [1-4], tape casting [5, 6] and screen printing [7]. With the conventional ceramic process, the formed dual-phase membrane typically possesses a random packing structure for both the oxide ion conducting phase and the electronic conducting phase. [8]. Achieving the percolation structure [9, 10], reduction of the membrane thickness [11, 12], and optimization of both phases are necessary. For the simplicity of the percolation structure of the dual-phase membrane, the design and preparation of the dual-phase membrane with a continuous microstructure were presented. In the previous research, the YSZ-carbon felt dual-phase membrane was produced by impregnating carbon felt with the YSZ phase. The percolation structure could be automatically achieved by using electrically conductive foam as the carbon felt. Carbon felt is unsuitable as an electronic conducting phase for a dual-phase oxygen separation membrane due to the oxidation of the carbon felt during the oxygen separation process. In general, composite membrane material selection is

challenging [13]. The conductivities and reaction of the two materials must be considered [14, 15]. To achieve a high oxygen permeability, the chemical compatibility of the oxide ionic and electronic conducting phases is critical [16]. Currently, the most popular construction is an oxide ionic conductor-MIEC dual-phase membrane. Zirconia-based materials, such as YSZ, are promising oxide ion conductors, but they readily react with perovskite-type oxides, leading to the formation of a secondary phase with poor oxide ionic and electronic conductivities. As a means of preventing the formation of a secondary phase, the selection of a metal as an electronic conducting phase is gaining attention. There is a number of metals which can be used as an electronic conducting phase, and most of them have a high electrical conductivity. However, the low melting point and the oxidation resistance present a significant challenge when constructing the YSZ-based dual-phase membranes. Nickel (Ni) is a low-cost metal that exhibits an excellent electrical conductivity and a high melting point. It was chosen as a close match for the criterion. Not only can it significantly improve the electronic conductivity, but also the mechanical stability. Nickel-based alloys are also of interest, as the alloying of nickel with chromium (Ni-Cr) reduces oxidation in oxidizing environments, making them suitable for oxygen separation applications.

Silicon carbide (SiC) is a ceramic with promising physical and chemical properties, such as a high mechanical stability at high temperatures, a low thermal expansion coefficient, and high oxidation resistance. Stainless steel (SS) is a cost-effective alloy with an extremely high oxidation resistance and excellent electrical conductivity. In this study, different types of electronic conducting foams were investigated in order to select the most suitable material for use in the YSZ-based dual-phase membranes created by impregnating YSZ into the pores of an electronic conductive phase material.

2. Experimental methods

In this research, Ni foam (Sumitomo electric Toyama Co., Ltd., Japan), Ni-Cr foam (Sumitomo electric Toyama Co., Ltd., Japan), SS316L foam (Nagamine Manufacturing Co., Ltd., Japan), and SiC foam (Fushimi Pharmaceutical Co., Ltd., Japan) were selected. Figures 3-1 indicates the structures of the various metal foams.

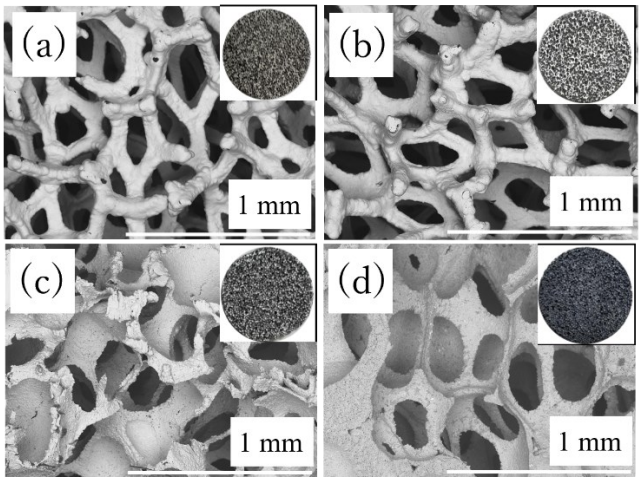

Fig. 3-1Microstructure of (a) nickel foam, (b) nickel chromium foam, (c) 316L stainless steel foam and (d) silicon carbide foam.

Figure 3-1 shows a schematic illustration of the YSZ-metal dual-phase membrane preparation procedure. To prepare the suspensions, 8 mol % yttria-doped zirconia powders (TZ-8YS (D50: 0.6 m), Tosoh Corporation, Japan) were dispersed in distilled water with 2 wt% ammonium polyacrylate as a dispersant (Alon-A6114, Toagosei, Japan). The metal foams were cut into a 15-mm diameter disk shape. The prepared metal foams were placed in the YSZ suspension then evacuated for 30 minutes to remove all the gas inside the porous structure. The YSZ impregnated metal foams then had the distilled water removed by the vacuum filtration process to obtain the green composite compact. The green sample was polished by sandpaper. A cold isostatic press process (350 MPa, 10 minutes) was

used to achieving the uniform packing of the YSZ particles inside the porous structure. A spark plasma sintering (SPS, LaboxTM-325 Sinter Land, Inc., Japan) process was used to sinter the green sample in a vacuum atmosphere. Depending on the melting point of the metal foams, the YSZ-metal dual-phase membranes were sintered at 1200 ºC. The SPS was performed at the pressure of 80 MPa for 10 minutes.

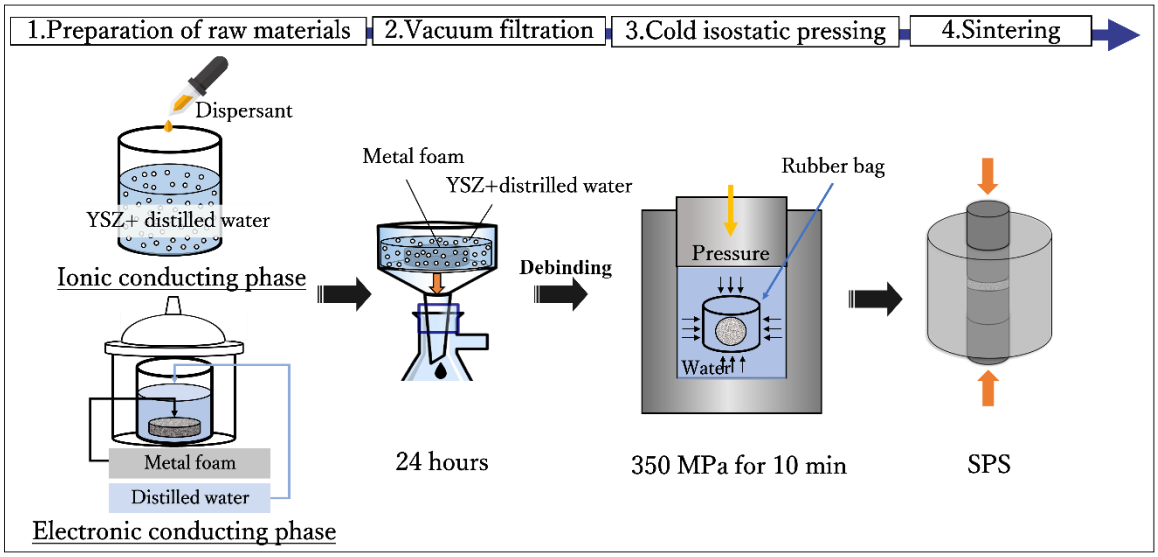

Fig. 3-2 Schematic showing the preparation process of the YSZ-based dual-phase membranes.

The Archimedes' method was used to determine the relative density of the sintered dual-phase membrane using kerosene. The phase stability and chemical

compatibility of the dual-phase membranes fabricated at the various sintering temperatures were studied. An X-ray diffraction analysis was performed on the sintered samples that were ground in an agate mortar (XRD, Miniflex 600, Rigaku Corporation, Japan). Using a scanning electron microscope (JSM-5600LV, JEOL Ltd., Japan), the microstructure of the dual-phase membranes was observed. For the oxygen permeability test of the fabricated dual-phase membrane, the air flow rate on the feed side and the Ar flow rate on the permeation side were both set to 250 ml/min. Prior to the measurement process, a 14-mm-diameter silver ring was placed on the membrane and sealed at 900 °C. An oxygen galvanic analyzer was used to measure the amount of oxygen in the permeate gas (MC-8G-L, Iijima Electronics Corporation, Japan). The temperature range for this experiment was 500 to 900 °C. The air leak behavior was analyzed using a gas chromatograph (GC-8A, Shimadzu Corporation, Japan).

3. Results and discussion

3.1 Characterization of the membranes

By using the vacuum filtration technique, it was possible to successfully produce the green YSZ-electronic conducting foam membrane compacts. During

the spark plasma sintering process, the high pulsed direct current was transferred from the punch to the green compact. Metals have a much higher thermal conductivity than graphite. As a result of the DC current applied to the specimen, the metallic phase rapidly heated up, and the temperature inside the die probably significantly exceeded the set temperature. At a temperature of 1200 °C, the relative density of the YSZ-metal foam composite membrane increased to more than 90%. However, the excessive SPS current caused both the Ni-Cr and SiC foam to melt. Therefore, a high-density YSZ-based dual-phase membranes cannot be produced with Ni-Cr and SiC. For the nickel and stainless-steel foam, the melting did not occur at 1200 °C. Figure 3-3 shows the XRD pattern of (a) YSZ-Ni foam membrane and (b) YSZ-SS foam membrane sintered by SPS in the temperature range of 900 to 1200 °C. The XRD patterns of the sintered samples at all temperatures indicated that the sintered sample consisted of YSZ and a metal (nickel or stainless steel), suggesting that there is no reaction of YSZ with either the nickel or stainless steel.

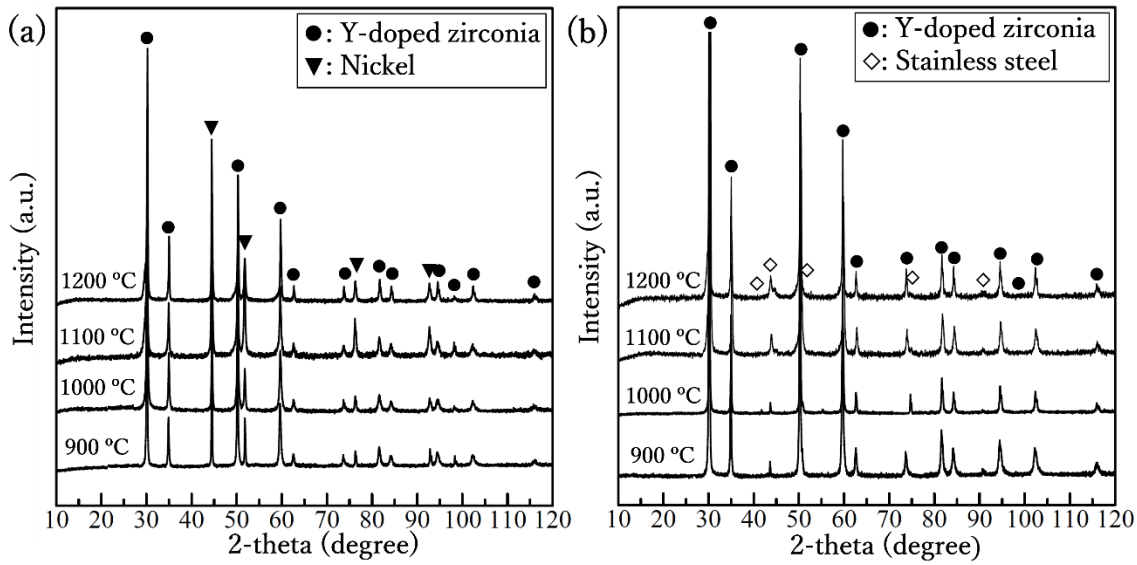

Fig. 3-3 XRD patterns of (a)YSZ-Ni foam membrane and (b) YSZ-SS foam membrane sintered at 900-1200 °C by SPS.

Figure 3-4 show the microstructure of the YSZ-Ni foam and YSZ-SS foam dual-phase membrane. At a sintering temperature greater than 1100 °C, a structure was observed in which the two phases were tightly bound.

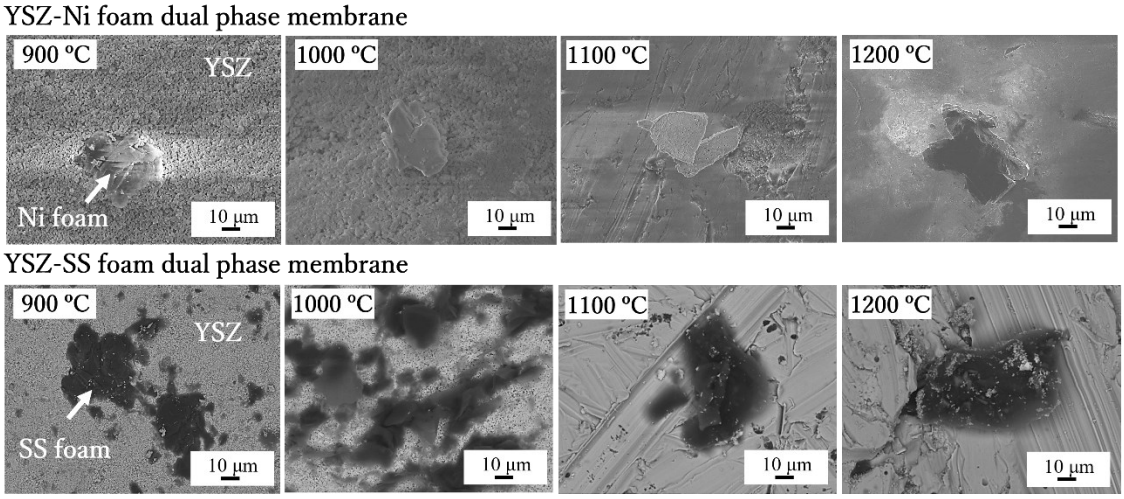

Fig. 3-4 Surface images of the microstructures of YSZ-Ni foam and YSZ-SS foam dual-phase membrane sintered at various temperatures.

3.2 Oxygen separation performance of the YSZ-metal foam dual-phase membrane

The oxygen permittivity of the YSZ-metal foam dual-phase membrane as a function of the temperature is indicated in Figure 3-5 As shown in the graph, the oxygen permeability of the YSZ-SS foam dual-phase membrane is greater than that of the YSZ-Ni foam dual-phase membrane at all operating temperatures. Typically, nickel has a higher electronic conductivity than stainless steel. However, nickel has a low oxidation resistance, so the oxidation of nickel readily occurs during operation, resulting in a decreased oxygen exchange activity. The YSZ-SS foam achieved the highest oxygen permeation flux of 0.32

ml(STP)/min·cm².

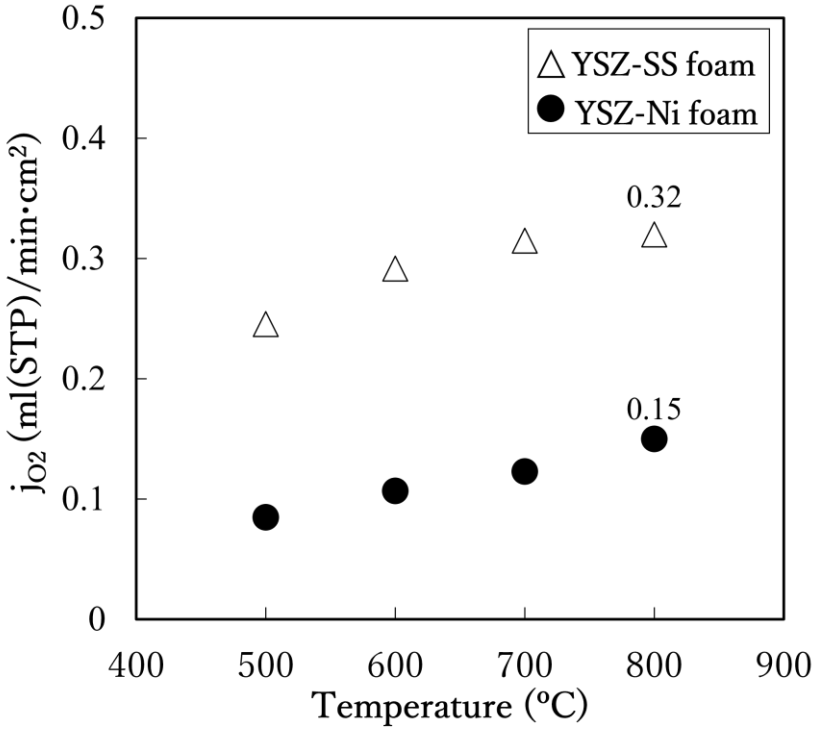

Fig. 3-5 Oxygen separation performance of the YSZ-Ni foam and YSZ-SS foam dual-phase membranes.

4. Conclusions

YSZ-metal foam dual-phase membranes were successfully fabricated by applying the SPS process. Due to the high thermal conductivity of the metal foam, a relative density of 90% could be achieved for a YSZ-metal foam dual-phase membrane when sintered at the set temperature of 1200 °C. Among all the types

of electronic conducting foams tested, only the nickel and stainless-steel foam did not melt during the sintering process. Both composite membranes can achieve a good phase stability and high chemical compatibility. The YSZ-Ni foam and YSZ-SS foam dual-phase membranes attained the highest oxygen permeation flux of 0.32 and 0.34 ml(STP)/min·cm², respectively. Due to nickel's low oxidation resistance, oxidation occurred during the measurement, resulting in a significant decrease in the oxygen permeation flux at high temperature. Therefore, it was concluded that stainless steel is an excellent candidate for composting with YSZ in order to create a dual-phase oxygen separation membrane.

References

1. Kim J., Lin Y.S., Synthesis and oxygen permeation properties of ceramic metal dual phase membrane. Journal of Membrane Science, (2000) 123-133.

2. Zhou J., Tang X., He D., Wu C., Zhang Y., Ding W., Jin Y., and Sun C., Oxygen permeability and CO_2-tolerance of $Ce_{0.9}Gd_{0.1}O_{2-\delta}$–$SrCo_{0.8}Fe_{0.1}Nb_{0.1}O_{3-\delta}$ dual-phase membrane. Journal of Alloys and Compounds, 646(2015) 204-210.

3. Fang W., Zhang Y., Gao J., and Chen C., Oxygen permeability of asymmetric membrane of functional $La_{0.8}Sr_{0.2}Cr_{0.5}Fe_{0.5}O_{3-\delta}$ (LSCrF)–$Zr_{0.8}Y_{0.2}O_{2-\delta}$ (YSZ) supported on porous YSZ. Ceramics International, 40(2014) 799-803.

4. Zhu X., Liu Y., Cong Y., and Yang W., $Ce_{0.85}Sm_{0.15}O_{1.925}$–$Sm_{0.6}Sr_{0.4}Al_{0.3}Fe_{0.7}O_3$ dual-phase membranes: One-pot synthesis and stability in a CO_2 atmosphere. Solid State Ionics, 253(2013) 57-63.

5. Cao Z., Zhu X., Li W., Xu B., Yang L., and Yang W., Asymmetric dual-phase membranes prepared via tape-casting and co-lamination for oxygen permeation. Materials Letters, 147(2015) 88-91.

6. Huang H., Cheng S., Gao J., Chen C., and Yi J., Phase-inversion tape-casting preparation and significant performance enhancement of $Ce_{0.9}Gd_{0.1}O_{1.95}$–$La_{0.6}Sr_{0.4}Co_{0.2}Fe_{0.8}O_{3-\delta}$ dual-phase asymmetric membrane for oxygen separation. Materials Letters, 137(2014) 245-248.

7. Gaudillere C., Garcia-Fayos J., Balaguer M., and Serra J.M., Enhanced oxygen separation through robust freeze-cast bilayered dual-phase membranes. ChemSusChem, 7(2014) 2554-2561.

8. Zhu W., Ding D., and Xia C., Enhancement in Three-Phase Boundary of SOFC Electrodes by an Ion Impregnation Method: A Modeling Comparison. Electrochemical and Solid-State Letters, 11(2008) B83.

9. Balaguer M., García-Fayos J., Solís C., and Serra J.M., Fast Oxygen Separation Through SO_{2-} and CO_{2-}Stable Dual-Phase Membrane Based on $NiFe_2O_4$–$Ce_{0.8}Tb_{0.2}O_{2-\delta}$. Chemistry of Materials, 25(2013) 4986-4993.

10. Luo H., Jiang H., Klande T., Cao Z., Liang F., Wang H., and Caro J., Novel Cobalt-Free, Noble Metal-Free Oxygen-Permeable $40Pr_{0.6}Sr_{0.4}FeO_{3-\delta}$–$60Ce_{0.9}Pr_{0.1}O_{2-\delta}$ Dual-Phase Membrane. Chemistry of Materials, 24(2012) 2148-2154.

11. Hendriksen P.V., Larsen P.H., Mogensen M., Poulsen F.W., and Wiik K.,

Prospects and problems of dense oxygen permeable membranes. Catalysis Today, 56(2000) 283-295.

12. Dyer P.N., Richards R.E., Russek S.L., and Taylor D.M., Ion transport membrane technology for oxygen separation and syngas production. Solid State Ionics, 134(2000) 21-33.

13. Zhang Z., Zhou W., Chen Y., Chen D., Chen J., Liu S., Jin W., and Shao Z., Novel Approach for Developing Dual-Phase Ceramic Membranes for Oxygen Separation through Beneficial Phase Reaction. ACS Applied Materials & Interfaces, 7(2015) 22918-26.

14. Li C., Song J., Zhang S., Tan X., Meng X., Sunarso J., and Liu S., SDC-SCFZ dual-phase ceramics: Structure, electrical conductivity, thermal expansion, and O_2 permeability. Journal of the American Ceramic Society, 104(2021) 2268-2284.

15. Zhang G., Liu Z., Zhu N., Jiang W., Dong X., and Jin W., A novel Nb_2O_5-doped $SrCo_{0.8}Fe_{0.2}O_{3-\delta}$ oxide with high permeability and stability for oxygen separation. Journal of Membrane Science, 405-406(2012) 300-309.

16. Weber A. and Ivers-Tiffée E., Materials and concepts for solid oxide fuel cells (SOFCs) in stationary and mobile applications. Journal of Power

Sources, 127(2004) 273-283.

Chapter 4 | Percolation structure design and surface modification of YSZ-stainless steel dual-phase membrane fabricated by powder mixing method

Preface

In the previous chapter, a dual-phase membrane composed of YSZ and electronic conducting foam was investigated. Among the utilized metal phases, the 316L stainless steel (SS) exhibited an excellent oxidation resistance and YSZ inertness. However, the dense packing of YSZ was difficult, and increasing the sintered density of YSZ was limited. In this chapter, an attempt was made to fabricate a dual-phase membrane with percolation structures by sintering the 316L SS and YSZ powders. The percolation structure was optimized by varying the SS concentrations in order to obtain a good oxygen transport activity. The catalyst surface coating was applied to increase the membrane's oxygen permeation flux.

1. Introduction

Oxygen production has been in high demand for use in numerous industries, including chemical synthesis, wastewater treatment, medical care, and metal production[1-4]. Generally, pure oxygen gas is produced by separating air.

There are various types of air separation procedures, including cryogenic separation [5], pressure swing adsorption [6] and membrane separation [7]. The oxygen separation membrane is one of the most energy-efficient and cost-effective air separation processes with a low oxygen production volume that is suitable for the development of household oxygen generators [7]. In a pandemic situation, portable oxygen generators for the household will be essential for medical care. Inorganic ceramic membranes are a type of membrane having a high mechanical strength, heat resistance, and chemical stability [8, 9]. The single-phase mixed ionic-electronic conducting (MIEC) membrane is typically used as an oxygen separation membrane [10]. The MIEC membrane enables selective oxygen transport via the following elementary processes: (i) adsorption and dissociation of oxygen in the atmosphere, (ii) diffusion of oxide ions and back diffusion of electrons in the membrane, and (iii) association and desorption of oxygen on the recovery side. The mechanism is driven by the oxygen partial pressure difference across the membrane at elevated temperatures. To develop oxygen separation membranes with an improved performance, there are many studies seeking a new kind of MIEC to enhance the performance of the membrane; however, the main limitations are the material's limited oxide diffusion rate. The

well-known MIEC material, $Ba_{0.5}Sr_{0.5}Co_{0.8}Fe_{0.2}O_{3-\delta}$ (BSCF), a single-phase perovskite oxide (ABO_3), is currently the most promising material for use in an oxygen separation membrane [11-13]. However, practical applications require a higher oxygen diffusion. Typically, MIEC materials have an insufficient oxide ion conductivity, which is the current challenge for a single-phase oxygen separation membrane [14]. Due to the demand for new materials that exceed the oxide diffusion rate limit, dual-phase membranes are gaining attention. The dual-phase membrane is a composite membrane made up of an oxide ion conductive phase (transporting oxide ions) and an electronic conductive phase (transporting electrons). The dual-phase membrane has an advantage over a single-phase membrane in which the best characteristics of the used compounds are combined to achieve both a high oxygen permeability with good chemical and mechanical stabilities at elevated temperatures and under harsh conditions. Ceramic oxide ion conductors, such as the yttria-stabilized zirconia (YSZ) and gadolinium-doped ceria (GDC) mixed with noble metal electronic conductors (Pd, Ag, Pt, etc.), have been initially reported as dual-phase membranes. Since the noble metal influences the oxygen permeability with a high stability under harsh conditions, however, the noble metals are expensive, which makes them unsuitable for industrial

applications. Therefore, there is more interest in ceramic-ceramic dual-phase membranes [15]. These composites consist of an ionic conductor and a pure electronic conductor or mixed ionic electronic conductor (MIEC). Ceramic-ceramic dual-phase membranes are currently the most studied, but there are many concerns such as phase stability, chemical compatibility, and sintering behavior between the two phases [16]. Moreover, each of the two phases requires a percolation structure. As shown in Figure 4-1, the oxygen exchange reaction takes place at the triple phase boundary (TPB) of the dual-phase membrane where air, an oxide ion conductor and an electronic conductor are in contact. However, simultaneously controlling the percolation structure and TPB in the ceramic-ceramic membranes is very difficult. For these reasons, the study of a dual-phase membrane for oxygen separation applications is limited. It is of great significance to establish a process for fabricating dual-phase membranes consisting of a combination of ceramics and inexpensive metals.

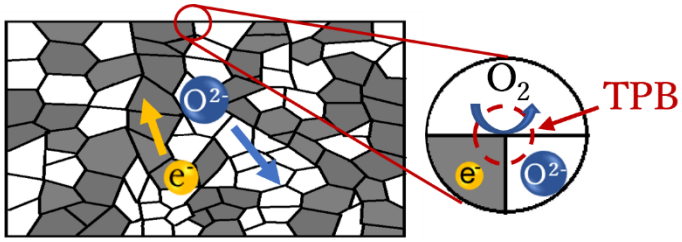

Fig. 4-1 Schematic overview of triple phase boundary (TPB) in a dual-phase membrane material. The white and grey regions indicate the oxide ion and electron-conducting phases, respectively.

Yttrium stabilized zirconia (YSZ) is commonly used as an oxide ion conductor for intermediate to high temperature reactions due to its high oxide ion conductivity, mechanical strength, and chemical stability [17]. Stainless steel (SS) is a metal alloy mainly containing iron, chromium, nickel, and small amounts of other elements. SS, as an electronic conductor with a high oxidation resistance, strength, and melting point [18], is suitable to mix with YSZ in order to achieve a high-density sintering. The solid-state reaction process is one of the most widely used methods for the preparation of a dual-phase membrane [15, 19]. The spark plasma sintering (SPS) process is a rapid sintering technique in which a pulsed DC current and uniaxial pressure are applied during the sintering process [20]. This sintering technique is useful for producing composites in which both metals

and ceramics are densified at low temperatures and in a short period of time [21]. Research on the fabrication of a dual-phase oxygen separation membrane using SPS is limited by various the concerns and obstacles, such as damage caused by thermal shrinkage during the rapid sintering. The difference in densification temperatures between different materials and the reduction in the membrane thickness to improve the oxygen separation capability also make crack prevention difficult. In this study, the fabrication of YSZ-SS dual-phase membranes by the SPS process was investigated with the aim of pursuing new possibilities for oxygen separation membranes. Basically, the oxygen permeation rate is controlled by two different mechanisms, i.e., the surface exchange reaction and bulk diffusion [22]. When the permeation process is controlled by bulk diffusion at a high operating temperature, reducing the membrane thickness is necessary [23]. However, it was difficult to form an extremely thin self-supporting film by SPS sintering. In this study, an attempt was made to improve the oxygen separation performance from the viewpoint of increasing the TPB by changing the content of the SS powder. In addition, silver paste was used as a catalyst to improve the surface exchange reaction.

2. Experimental methods

Commercially-available 8 mol% yttria-doped zirconia (TZ-8YS (ρ = 5.9 g/cm^3, D_{50}: 0.6 μm), Tosoh Corporation, Japan) and 316L SS ((ρ = 8.0 g/cm^3, -100 mesh) Nilaco Co., Tokyo, Japan) powders were used as the raw materials. The 316L SS powder in the amount of 15-55 vol% to the YSZ powder was mixed in a mortar. The powder mixture was then put in a graphite die with an inner diameter of 15 mm and sintered by the SPS process. The melting point of the 316L SS and the densification temperature of the YSZ by conventional pressureless sintering are around 1400 ºC and 1500 ºC, respectively. The SPS process enables a temperature reduction of approximately 200 ºC compared to the pressureless sintering process. Thus, in this study, the powder mixtures were sintered by SPS (SPS, LaboxTM-325 Sinter Land, Inc., Japan) in a vacuum atmosphere at 1200 ºC and an applied pressure of 80 MPa for 10 minutes.

Figure 4-2 shows the spark plasma sintering program optimized by the preliminary experiments in this study. In order to fabricate dense membranes with a thickness of 0.5 mm by a fast-sintering process like SPS, it was necessary to control the sintering rate step by step. First, for the heating process, a heating rate of 100 ºC/min was applied to rapidly remove the moisture and adsorbed gases on

the particles to prevent gas blockage which affects the subsequent densification of the membrane. After increasing the temperature to 800 ºC, the heating rate was changed to 50 ºC/min to avoid high thermal shrinkage leading to crack formation. When the temperature reached 900 ºC, a pressure of 80 MPa was applied. The heating rate decreased to 25 ºC/min during the subsequent heating from 1000 ºC to the maximum temperature. After reaching the maximum temperature, the pressure was maintained for 10 minutes. The cooling process was then carried out without applying any pressure. It was important to control the cooling rate at 10 ºC/min for crack prevention during the cooling process. By using this program, no cracks were detected despite the differential sintering program. The selected membrane was then coated with silver paste on both sides of the membrane surface; silver was used as a catalyst to enhance the oxygen permeation flux by improving the oxygen exchange rate.

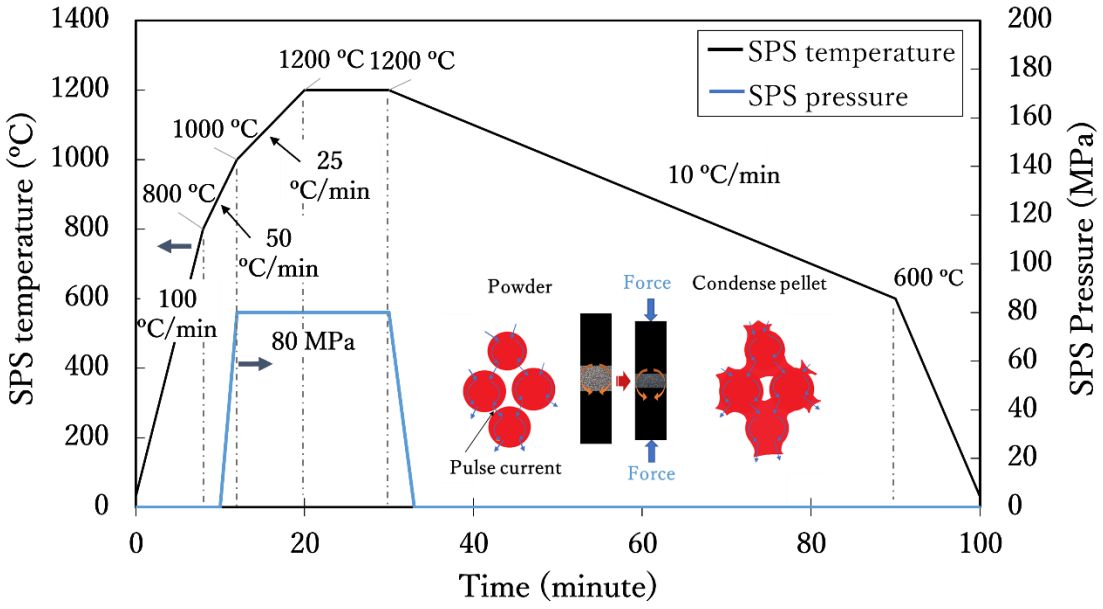

Fig. 4-2 Spark plasma sintering temperature and pressure cycle.

For the prepared specimens, their relative densities were measured by Archimedes' method. The stability of the YSZ and SS phases during the sintering process was characterized by X-ray diffraction (XRD, Miniflex 600, Rigaku Corporation, Japan). A scanning electron microscope (SEM, JSM-5600LV, JEOL Ltd., Japan) with an energy dispersive spectrometer (EDS) (JEOL Ltd., Japan) was used to determine the microstructure and composition of the dual-phase membrane. The microstructure inside the sintered body was observed by a non-destructive method using high-resolution 3D X-ray microscopy and computed tomography (Xradia 520 Versa, Carl Zeiss Co.,Ltd., Tokyo, Japan). In order to

confirm the percolation structure of the SS inside the sintered body, the cross-sectional slice images were three-dimensionally visualized by image processing software (Avizo, Thermo Fisher Scientific, Inc., USA). The total conductivity was measured by the direct current two-probe method at room temperature. A schematic of the experimental set-up for the oxygen permeation test has been described in Chapter 2. The sealing of the 15-mm-diameter membrane disk and the aluminum tube was performed using a silver ring at 900 ºC. Air was flowed on the feed side at the rate of 250 ml/min. On the permeation side, Ar sweep gas was flowed at the rate of 250 ml/min, and the amount of oxygen in the permeate gas was monitored by an oxygen galvanic analyzer (MC-8G-L, Iijima Electronics Corporation, Japan). This experimental setup was operated at temperatures between 500 to 900 ºC. A gas chromatograph (GC-8A, Shimadzu Corporation, Japan) was used to monitor the air leak behavior.

3. Results and discussion

3.1 Membrane characterization

During conventional pressureless sintering, densification of the YSZ requires temperatures in excess of 1500 ºC, which is higher than the melting point

of SS. However, by using SPS, the YSZ-SS dual-phase membrane was densified to a relative density of 98% at the temperature of 1200 ºC, resulting in a gas-tight YSZ-SS two-phase film with a diameter of 15 mm and a thickness of 0.5 mm. A membrane was successfully fabricated. Figure 4-3 shows the XRD patterns of the YSZ-SS membranes sintered by SPS. No phases other than YSZ and SS were identified at the sintering temperatures up to 1200 ºC regardless of the SS content, indicating that no reaction occurred between them.

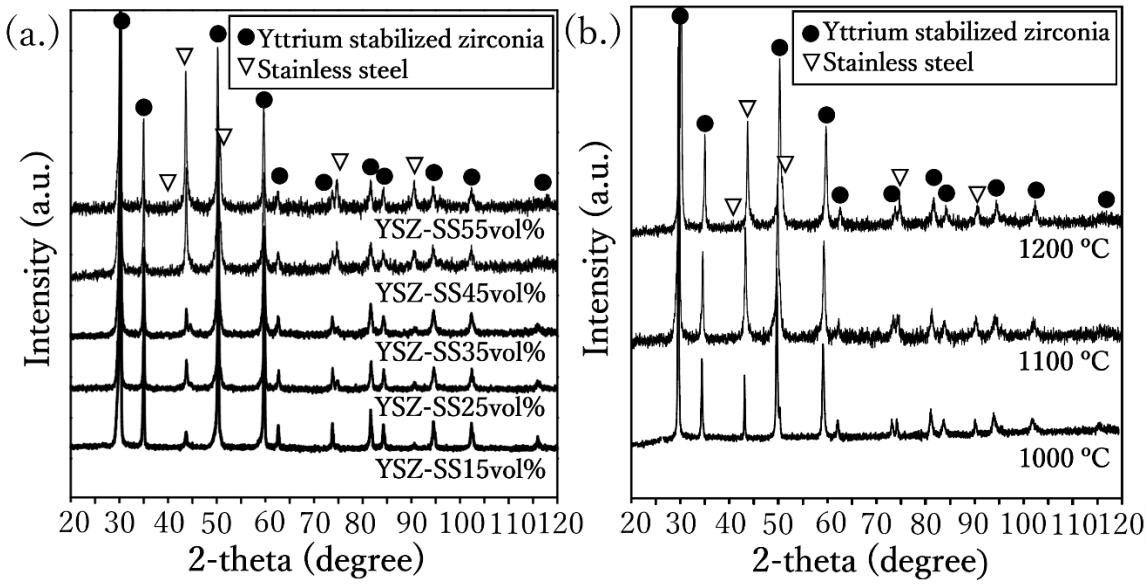

Fig. 4-3 XRD patterns of the YSZ-SS membranes sintered by SPS. (a) 15-55% SS content, 1200 ºC sintering temperature; (b) 45% SS content, 1000-1200 ºC sintering.

The microstructures of the YSZ-SS dual-phase membrane prepared with varying amounts of SS are shown in Figure 4-4. The surface images of the membranes sintered by SPS showed that SS was tightly attached to the YSZ, which confirms the gas-tight structure. Increasing the SS content enhanced the triple phase boundary point which is the ion exchange site and raised the surrounding temperature inside the die. With an increase in the SS contents to 45 vol%, YSZ achieved a full densification. However, when the SS was increased to 55 vol%, there was an outflow of molten SS. Therefore, it was determined that the 45 vol% SS addition amount is suitable for forming a dual-phase membrane with a percolation structure under the conditions of this experiment. The EDS mappings of the backscattered electron (BSE) images of the membrane surfaces in Figure 4-5 indicated that the YSZ and SS are homogeneously distributed.

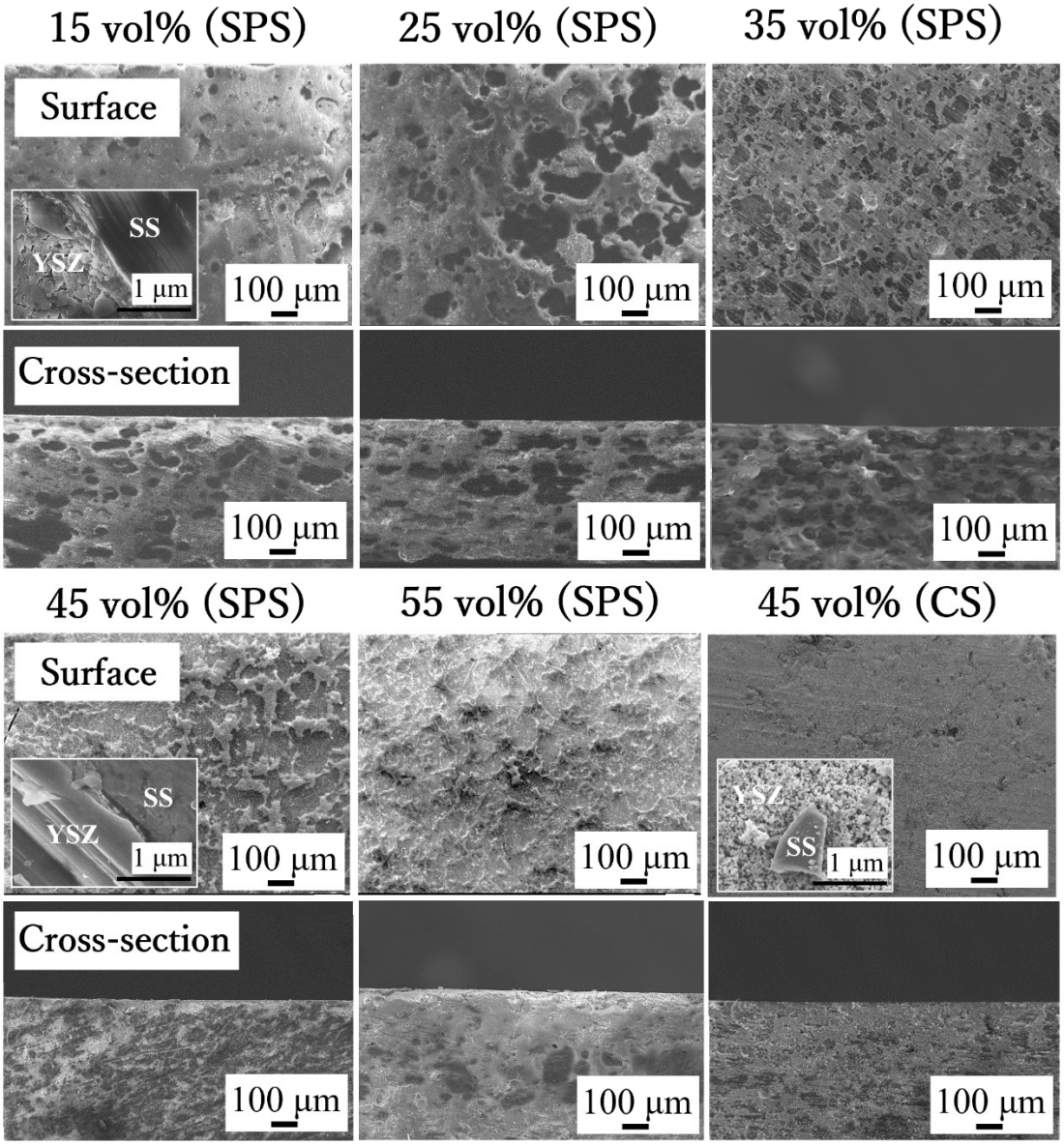

Fig. 4-4 Surface and cross-section images of the microstructures of the YSZ-SS dual-phase membranes with various additions of SS by SPS and conventional sintering (CS) at 1200 ºC for comparison.

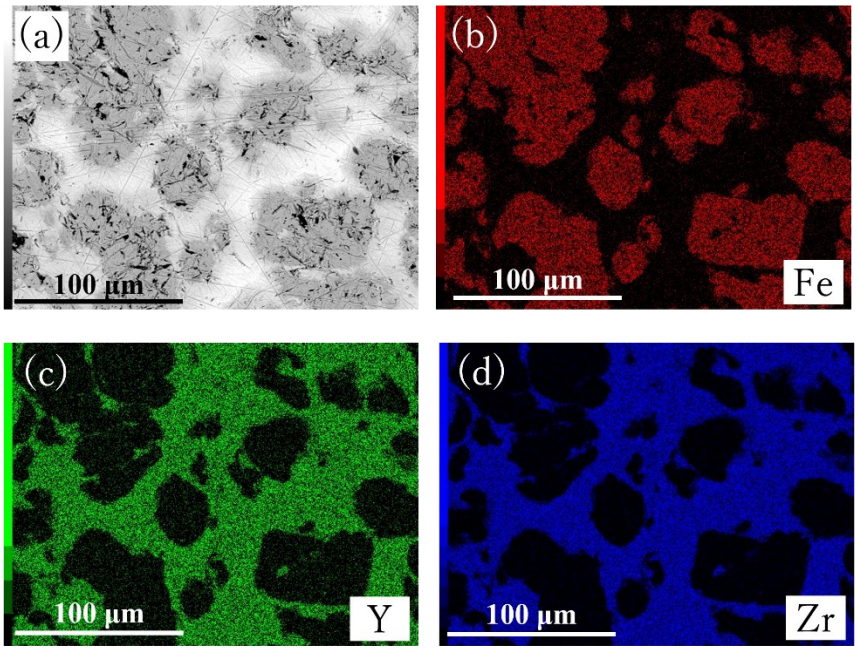

Fig. 4-5 Back scattered electron image of the YSZ-SS45vol% dual-phase membrane: (a) Surface (b-d) EDS element mapping images.

The percolation structures in both the YSZ and SS phases are necessary to achieve oxygen and electron transportation pathways through the dual-phase membrane. Figure 4-6 shows the internal structure images of the YSZ-SS45vol% dual-phase membrane observed by X-ray CT. The YSZ and SS phases are shown as the white and black parts, respectively. The 3D images of the YSZ and SS phases suggested that both phases have percolation structures. The volume ratio of YSZ and SS calculated from the 3D image was 55:45, which is in good agreement with the actual ratio.

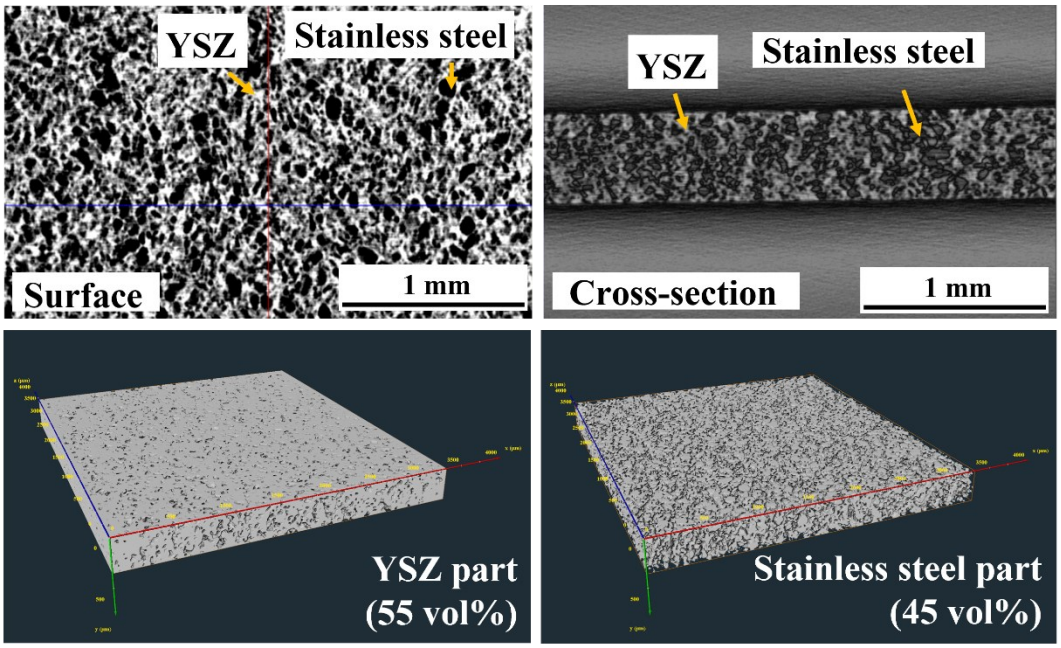

Fig. 4-6 X-ray CT image of YSZ-SS45vol% dual-phase membrane. The white and black regions indicate the YSZ and SS phases, respectively.

The total conductivity of the YSZ-SS dual-phase membrane with different amounts of SS measured in air at room temperature is shown in Figure 4-7. Typically, the electric conductivity of the electronic conducting phase (SS) is much higher than that of the oxide-ionic conducting phase (YSZ). As a result, the total conductivity of a dual-phase membrane was dominated by the electronic conducting SS part. Enhancing the SS contents tends to increase the total conductivity of the dual-phase membrane. The YSZ-SS45vol% dual-phase membrane showed a high conductivity of 7.93 S/cm^2, indicating that the

electronic conduction path of the SS phase was achieved. However, increasing the SS content to 55 vol% significantly decreased the electronic conductivity to 0.0143 S/cm^2. This is probably because the percolation structure of the SS phase was destroyed due to the melting of the SS as will be described later.

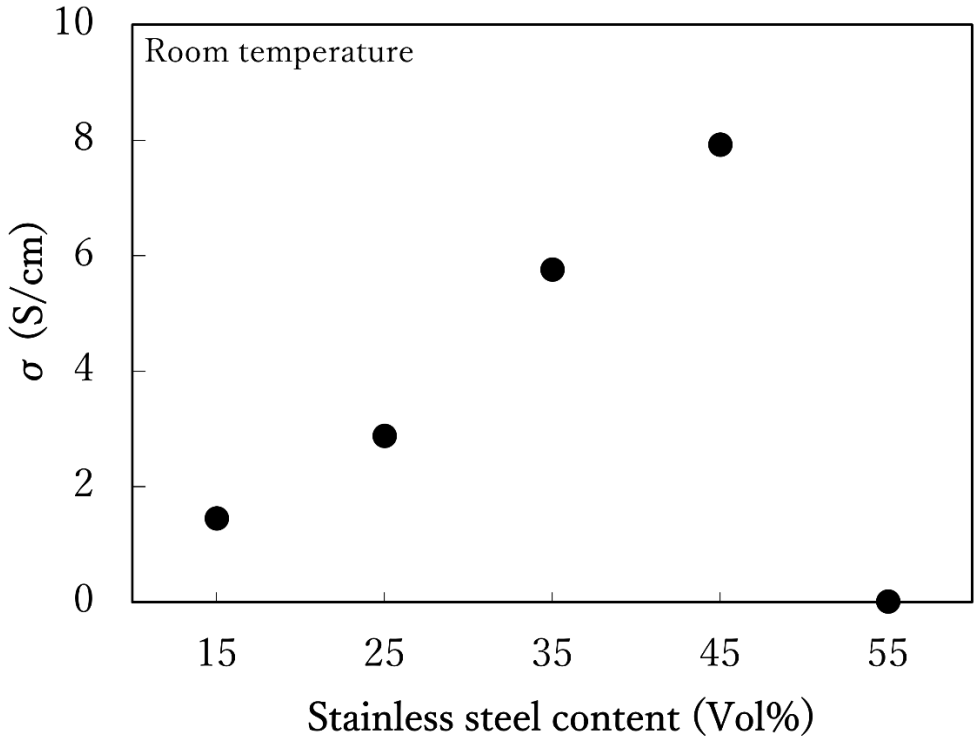

Fig. 4-7 Total electric conductivity of the YSZ-SS45vol% dual-phase membrane.

3.2 Oxygen separation performance of the YSZ-SS dual-phase membrane

Figure 4-8 shows the oxygen permittivity of the YSZ-SS dual-phase membrane with the different SS contents from 15 to 45 vol% as a function of the temperature. As show in the graph, increasing the contained SS phase improved the oxygen permeation of the composite membrane due to increasing the triple phase boundaries on the membrane surface which act as the sites for oxygen exchange. However, when SS was added up to 55 vol%, the membrane almost lost its ability to permeate oxygen. This is probably due to the sudden rise in the amount of current flowing through the SS part during the SPS process. This led to an abnormal rise in temperature, which caused molten SS to flow out of the graphite die and be lost. Also, molten SS may have interfered with the formation of the percolation structures in the YSZ, the oxide ion conducting phase. The highest oxygen permeation flux (j_{O2}) of 0.83 ml(STP)/min·cm^2 was obtained at 900 °C for the YSZ-SS45vol% self-standing dual-phase membrane without surface modification. For the silver paste coating on both sides of the membrane surfaces, a YSZ-SS45vol% dual-phase membrane was selected. The improvement of the oxygen permeation flux (j_{O2}) of 1.38 ml(STP)/min·cm^2 was achieved at 900 °C.

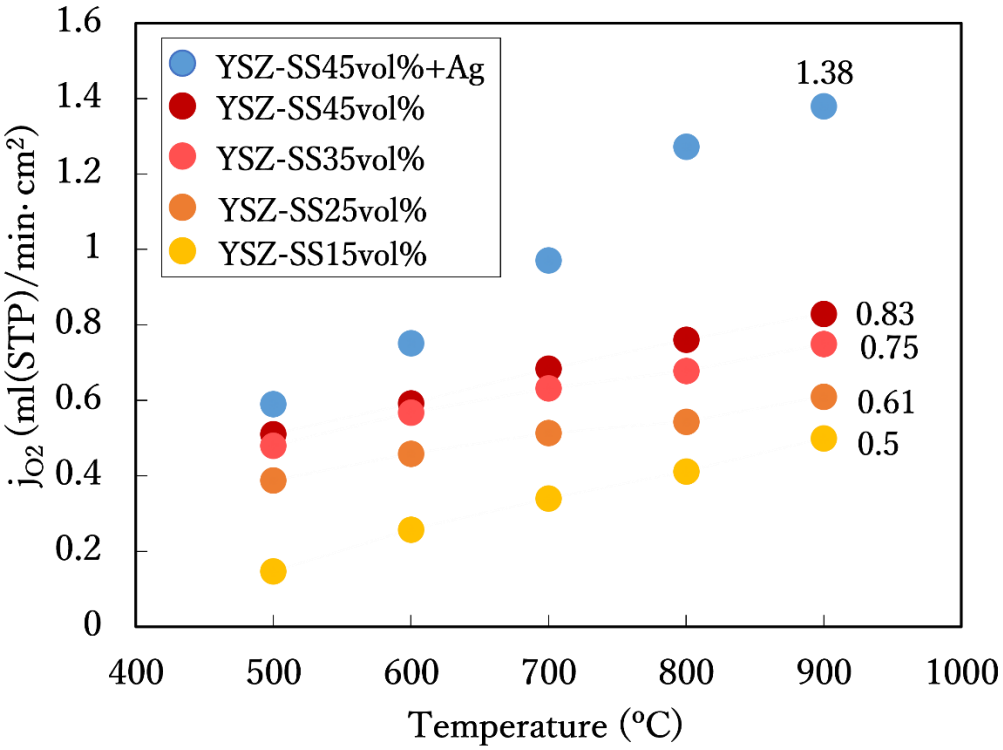

Fig. 4-8. Oxygen separation performance of the YSZ-SS dual-phase membrane.

Figure 4-9 shows the XRD patterns of the YSZ-SS dual-phase membrane before and after the permeation measurement. The composition of both the feed and permeate sides remained unchanged during the measurement. The secondary phase and metal oxide phase did not appear after the permeation test.

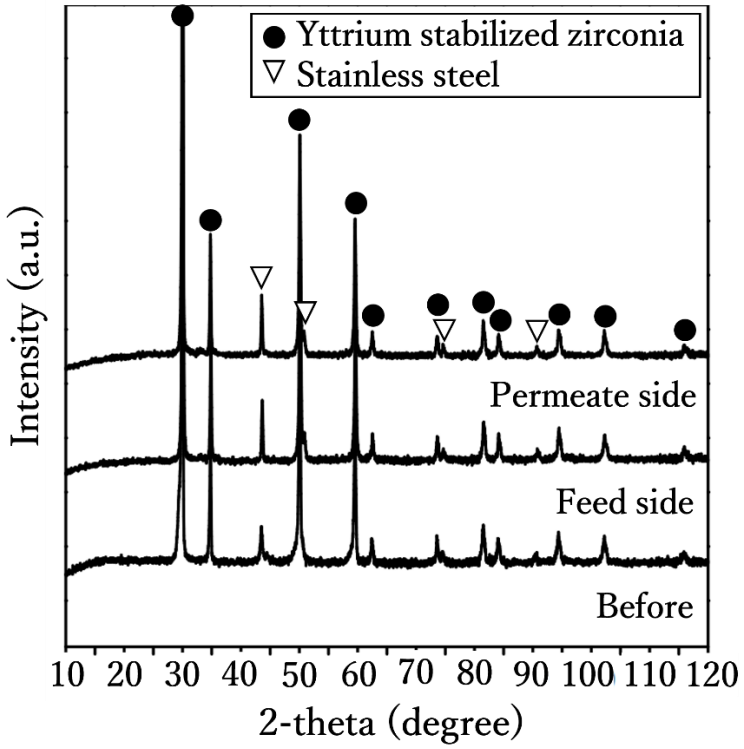

Fig. 4-9. XRD patterns of the YSZ-SS membrane before and after the oxygen separation performance test.

Based on the performance of the zirconia-based dual-phase membranes, $Zr_{0.79}Sc_{0.2}Ce_{0.01}O_{2-\delta}$-$La_{0.7}Sr_{0.3}MnO_{3-\delta}$, 10Sc1YSZ-$MnCo_2O_4$ and 10Sc1YSZ-$LaCr_{0.85}Cu_{0.10}Ni_{0.05}O_{3-\delta}$ (LCCN) composites have realized the high oxygen permeation rates of 1.65, 1.05 and 1.02 ml(STP)/min·cm^2, respectively [15]. All these membranes have either a porous support layer or a catalyst coating layer. Different membrane thicknesses, measurement equipment, and surface treatments also change their properties. Therefore, the properties of our YSZ-SS

free-standing membranes cannot be simply compared to them. Further performance improvement of the YSZ-SS membrane would be expected by a post-surface treatment such as the formation of porous layers.

4. Conclusions

Gas-tight YSZ-SS dual-phase membranes were successfully fabricated by a spark plasma sintering process. A high-volume percentage of SS addition affected the oxygen permeation flux of the membrane by enhancing the oxygen exchange rate. The YSZ-SS45vol% dual-phase membrane demonstrated a good percolation structure with the high oxygen permeation flux of 0.83 ml(STP)/min·cm^2 at 900 °C. A coating of silver paste significantly enhanced the oxygen permeability of the dual-phase membrane which exhibited the highest oxygen permeation flux of 1.38 ml(STP)/min·cm^2 at 900 °C.

References

1. Van Haandel A. and Van der Lubbe J., Handbook of Biological Wastewater Treatment: IWA Publishing, (2012).
2. Dal Negro R.W. and Hodder R., Long-term oxygen therapy: Springer Milano, (2012).
3. Blostein P., Devaux M., and Grant M., Use of industrial gases in blast-furnace operation. Metallurgist, 55(2011) 552-557.
4. Badwal S.P.S. and Ciacchi F.T., Ceramic Membrane Technologies for Oxygen Separation. Advanced Materials, 13(2001) 993-996.
5. Santos J.C., Cruz P., Regala T., Magalhães F.D., and Mendes A., High-Purity Oxygen Production by Pressure Swing Adsorption. Industrial & Engineering Chemistry Research, 46(2007) 591-599.
6. Sircar S., Pressure Swing Adsorption. Industrial & Engineering Chemistry Research, 41(2002) 1389-1392.
7. Phair J.W. and Badwal S.P.S., Materials for separation membranes in hydrogen and oxygen production and future power generation. Science and Technology of Advanced Materials, 7(2006) 792-805.
8. Amin S.K., Hassan M., El-Sherbiny S., and Abdallah H., An Overview of

Production and Development of Ceramic Membranes. International Journal of Applied Engineering Research, 11(2016) 7708-7721.

9. Sahini M.G., Mwankemwa B.S., and Kanas N., $Ba_xSr_{1-x}Co_yFe_{1-y}O_{3-\delta}$ (BSCF) mixed ionic-electronic conducting (MIEC) materials for oxygen separation membrane and SOFC applications: Insights into processing, stability, and functional properties. Ceramics International, 48(2022) 2948-2964.

10. Sunarso J., Baumann S., Serra J.M., Meulenberg W.A., Liu S., Lin Y.S., and Diniz da Costa J.C., Mixed ionic–electronic conducting (MIEC) ceramic-based membranes for oxygen separation. Journal of Membrane Science, 320(2008) 13-41.

11. Ishii K., Matsunaga C., Kobayashi K., Stevenson A.J., Tardivat C., and Uchikoshi T., Fabrication of BSCF-based mixed ionic-electronic conducting membrane by electrophoretic deposition for oxygen separation application. Journal of the European Ceramic Society, 39(2019) 5292-5297.

12. Ishii K., Matsunaga C., Kobayashi K., Stevenson A.J., Tardivat C., and Uchikoshi T., Fabrication of BSCF-based mixed oxide ionic-electronic

conducting multi-layered membrane by sequential electrophoretic deposition process. Journal of the European Ceramic Society, 41(2021) 2709-2715.

13. Shao Z.P., Yang W.S., Cong Y., Dong H., Tong J.H., and Xiong G.X., Investigation of the permeation behavior and stability of a $Ba_{0.5}Sr_{0.5}Co_{0.8}Fe_{0.2}O_{3-\delta}$ oxygen membrane. Journal of Membrane Science, 172(2000) 177-188.

14. Jiang Y., Wang S., Zhang Y., Yan J., and Li W., Kinetic Study of the Formation of Oxygen Vacancy on Lanthanum Manganite Electrodes. Journal of The Electrochemical Society, 145(1998) 373.

15. Kiebach R., Pirou S., Martinez Aguilera L., Haugen A.B., Kaiser A., Hendriksen P.V., Balaguer M., García-Fayos J., Serra J.M., Schulze-Küppers F., Christie M., Fischer L., Meulenberg W.A., and Baumann S., A review on dual-phase oxygen transport membranes: from fundamentals to commercial deployment. Journal of Materials Chemistry A, 10(2022) 2152-2195.

16. Zeng F., Malzbender J., Baumann S., Zhou W., Ziegner M., Nijmeijer A., Guillon O., Schwaiger R., and Albert Meulenberg W., Mechanical

reliability of $Ce_{0.8}Gd_{0.2}O_{2-\delta}$-$FeCo_2O_4$ dual phase membranes synthesized by one-step solid-state reaction. Journal of the American Ceramic Society, 104(2021) 1814-1830.

17. Yun K.S., Yoo C.Y., Yoon S.G., Yu J.H., and Joo J.H., Chemically and thermo-mechanically stable LSM–YSZ segmented oxygen permeable ceramic membrane. Journal of Membrane Science, 486(2015) 222-228.

18. Huang X., Xiao K., Fang X., Xiong Z., Wei L., Zhu P., and Li X., Oxidation behavior of 316L austenitic stainless steel in high temperature air with long-term exposure. Materials Research Express, 7(2020) 066517.

19. Zhu X., Wang H., and Yang W., Relationship between homogeneity and oxygen permeability of composite membranes. Journal of Membrane Science, 309(2008) 120-127.

20. Chen X.J., Khor K.A., Chan S.H., and Yu L.G., Overcoming the effect of contaminant in solid oxide fuel cell (SOFC) electrolyte: spark plasma sintering (SPS) of 0.5wt.% silica-doped yttria-stabilized zirconia (YSZ). Materials Science and Engineering: A, 374(2004) 64-71.

21. Guillon O., Gonzalez-Julian J., Dargatz B., Kessel T., Schierning G., Räthel J., and Herrmann M., Field-Assisted Sintering Technology/Spark Plasma

Sintering: Mechanisms, Materials, and Technology Developments. Advanced Engineering Materials, 16(2014) 830-849.

22. Manning P.S., Sirman J.D., and Kilner J.A., Oxygen self-diffusion and surface exchange studies of oxide electrolytes having the fluorite structure. Solid State Ionics, 93(1996) 125-132.

23. Hong W.K. and Choi G.M., Oxygen permeation of BSCF membrane with varying thickness and surface coating. Journal of Membrane Science, 346(2010) 353-360.

Chapter 5 | Formation of porous MIEC layer on dense dual-phase oxygen separation membranes

Preface

In the previous chapter, a YSZ-SS45vol% dual-phase membrane with a good percolation structure was successfully fabricated resulting in a high oxygen permeation flux. In this chapter, a method to further enhance the oxygen separation performance of the 8YSZ-45% SS dual-phase membrane was investigated. To increase the oxygen flux by increasing the oxygen exchange rate, the formation of porous layers of the mixed oxide ionic electronic conductor (MIEC) was applied to both sides of the YSZ-SS dual-phase membrane surface. In order to prevent the reaction between the two phases, a thin buffer layer was created prior to the MIEC coating. The MIEC layer was deposited using electrophoretic deposition (EPD). In this study, an attempt was made to produce a membrane with a five-layer sandwich structure as a prototype for the fabrication process of a multilayered membrane.

1. Introduction

The current challenge of the dual-phase membrane for oxygen separation application is to increase the oxygen permeability. The surface exchange reaction involving the adsorption/dissociation and association/desorption mechanisms of oxygen and oxide ions on both sides of the membrane is also an important factor for improving the oxygen separation efficiency [1-3]. The limitation of the surface exchange can be overcome by increasing the membrane surface area or by coating the membrane surface with a porous layer with superior oxygen and electron exchange properties [4]. Mixed ionic–electronic conductors (MIEC) are the most popular material for the oxygen separation membrane. In the MIEC membrane, both oxide ions and electrons transport through the material which can be a single-phase membrane [5, 6]. $Ba_{0.5}Sr_{0.5}Co_{0.8}Fe_{0.2}O_{3-\delta}$ (BSCF) is one of the most promising mixed ionic-electronic conductors [7-9]. However, BSCF has a poor chemical stability with YSZ during the fabrication and operation process [10, 11]. Direct formation of a porous BSCF layer on a YSZ-SS dual-phase membrane may generate a highly resistant secondary phase at the interface between them during the heat treatment process for bonding. Therefore, BSCF cannot be directly applied to the YSZ. Gadolinium-doped ceria (GDC) is known to be chemically

compatible with BSCF, which has an oxide ion conductivity significantly higher than that of YSZ [12-15], particularly at lower temperatures (500–700 ºC). In addition, the reduction of Ce^{4+} results in the simultaneous formation of oxide ion vacancies and Ce^{3+} in the reducing atmosphere causing the development of an electronic conductivity and thus being a mixed conductor [16, 17]. The inserting of GDC on YSZ as a buffer layer to prevent interaction between the BSCF and YSZ has attracted attention. This research aims to improve the oxygen separation performance of the YSZ-SS dual-phase membrane by coating BSCF on both sides of the membrane surface to increase the oxygen exchange activity on the membrane surface. Electrophoretic deposition (EPD) is a coating technique that uses the electrochemical effect of an electric current to deposit charged particles on a conductive substrate in a solvent. In this study, EPD was selected to deposit BSCF onto the multilayered membrane.

2. Experimental methods

In Figure 5-1, Process (1) shows a schematic illustration of the preparation of the dense layer. Commercially-available 8 mol% yttria-doped zirconia (TZ-8YS (ρ = 5.9 g/cm3, D50: 0.6 μm), Tosoh Corporation, Japan), gadolinium-doped ceria (CGO10, grade UHSA, Solvay Special Chem Japan)), and 316L stainless steel ((ρ = 8.0 g/cm3, -100 mesh) Nilaco Co., Tokyo, Japan) powders were used as the raw materials. The 316L stainless steel powder was combined with the oxide ion conductor powder (YSZ and GDC) in a mortar at the ratio of 45 vol%. The powder mixture was then placed in a graphite mold with the internal diameter of 15 mm, layer by layer (GDC-SS/YSZ-SS/GDC-SS) and sintered by the SPS process in a vacuum atmosphere at 1200 ºC and the applied pressure of 80 MPa for 10 minutes. In Figure 5-1, Process (2) shows the preparation of the EPD suspension. The most important factor for an efficient deposit is a high zeta potential of the particles, which determines the direction and mobility of the particles and provides repulsion forces to stabilize the suspension by an electrostatic repulsion mechanism. Therefore, the zeta potential of the suspension measured by laser doppler velocimetry (Zetasizer Nano-ZS, Malvern Panalytical Ltd., UK) was used to evaluate the stability of the BSCF suspension.

$Ba_{0.5}Sr_{0.5}Co_{0.8}Fe_{0.2}O_{3-\delta}$ (BSCF) was dispersed in reagent-grade ethanol after being prepared by the citrate precursor method with a D50 particle size of 0.55 m (Kusaka Rare Metal Products Co., Ltd., Japan). 1 M acetic acid or sodium hydroxide was used to adjust the pH of the suspension. The actual pH measurement of a nonaqueous solvent using a calibrated meter differs from the pH of aqueous solvents as shown in the following equation.

$$\mathrm{pH} - \mathrm{p}a_H = \frac{\Delta E_j}{\left(\frac{\mathrm{RT}\ln 10}{F}\right)} \text{ or } \mathrm{pH} - \mathrm{p}a_H = \frac{\Delta E_j}{0.05916} \text{ (at 25 °C)} \qquad (5\text{-}1)$$

where $\mathrm{p}a_H$ (=loga_H) is the negative logarithm of the proton activity in a nonaqueous solvent and $\Delta \mathrm{E_j}$ is the residual liquid junction potential encountered during the calibration and testing phase of a standard pH meter. (ΔE_j/0.05916) =1.23 was calculated for an ethanol suspension [18]. Thus, in this research study, the operational pH was utilized. The zeta potential of the BSCF suspension as a function of pH is illustrated in Figure 5-2. The maximum zeta potential of BSCF is +36 mV at pH 7, indicating the suspension is stable at this pH.

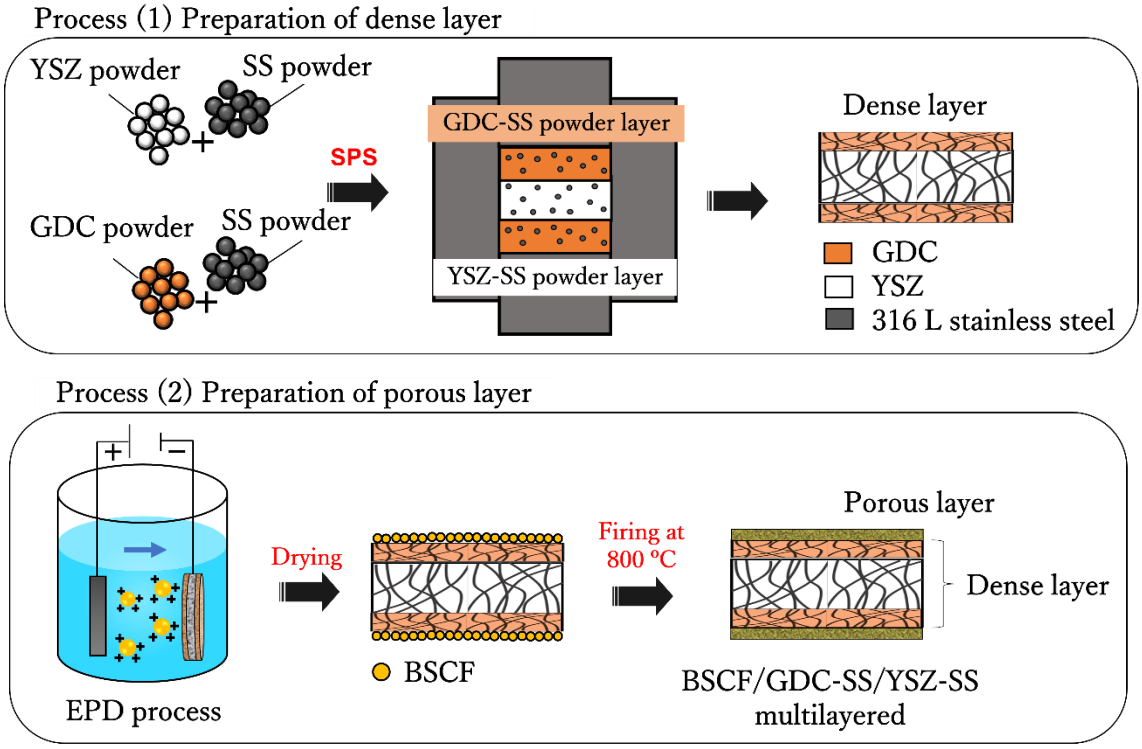

Fig.5-1 Schematic showing the preparation process of multilayered dual-phase membranes.

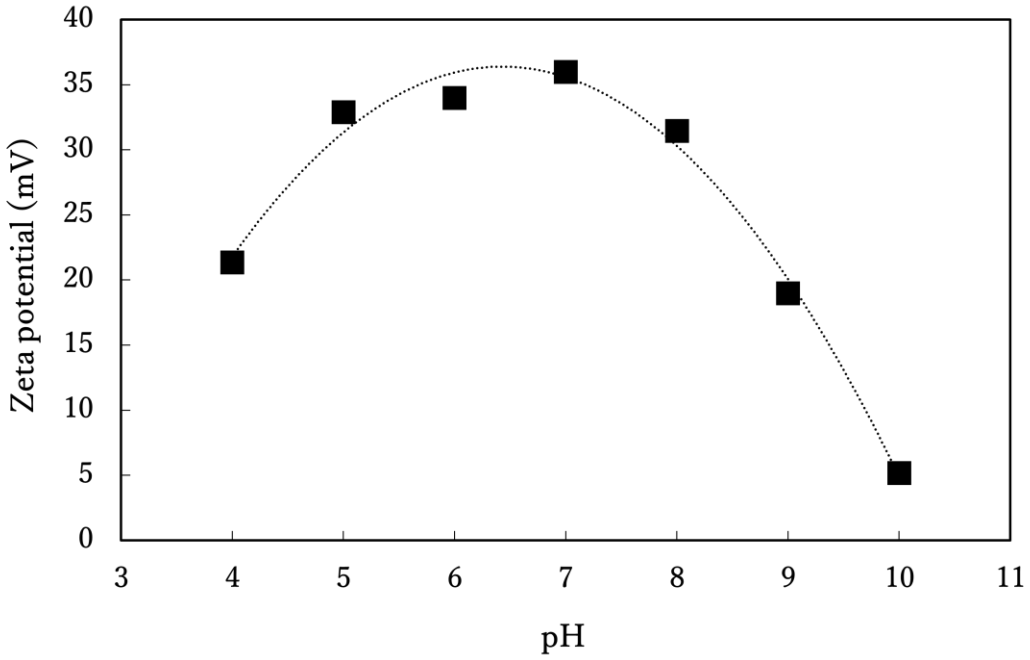

Fig. 5-2 Zeta potential of BSCF in ethanol as a function of the operational pH.

After measuring the zeta potential, 10 g of BSCF powder was mixed with 100 ml of ethanol to make a suspension. The pH was then adjusted to 7. The electrode distance was fixed at 10 mm. To determine the optimal EPD conditions, the applied voltage was varied at 25, 50, 100 and 150 V with a variation in the deposition time of 5, 10 and 15 minutes. After the EPD process, the coated membrane was dried, then fired at 800 °C for 3 hours in an Ar atmosphere. X-ray diffraction (XRD, Miniflex 600, Rigaku Corporation, Japan) was used to characterize the stability of each layer following the sintering process. The microstructure of the multilayered membranes was observed using a scanning electron microscope (SEM, JSM-5600LV, JEOL Ltd., Japan).

3. Results and Discussion

Electrophoretic deposition of the BSCF particles was successfully performed, and a five-layer sandwich structure membrane with a thickness of 0.5 mm was successfully fabricated. Figure 5-3 shows the surface image of the BSCF deposits on a multilayer dual-phase membrane by EPD. It was found that uniform BSCF coatings were made with higher voltages. In terms of the deposit time, BSCF was unable to be coated on the entire surface of the membrane if the deposit

time was less than it should have been. Nevertheless, increasing the deposition time to 15 minutes produces a nonuniform coating on the membrane surface. Based on the result, the voltage and deposition time of 150 V and 10 minutes produced the most uniform coating.

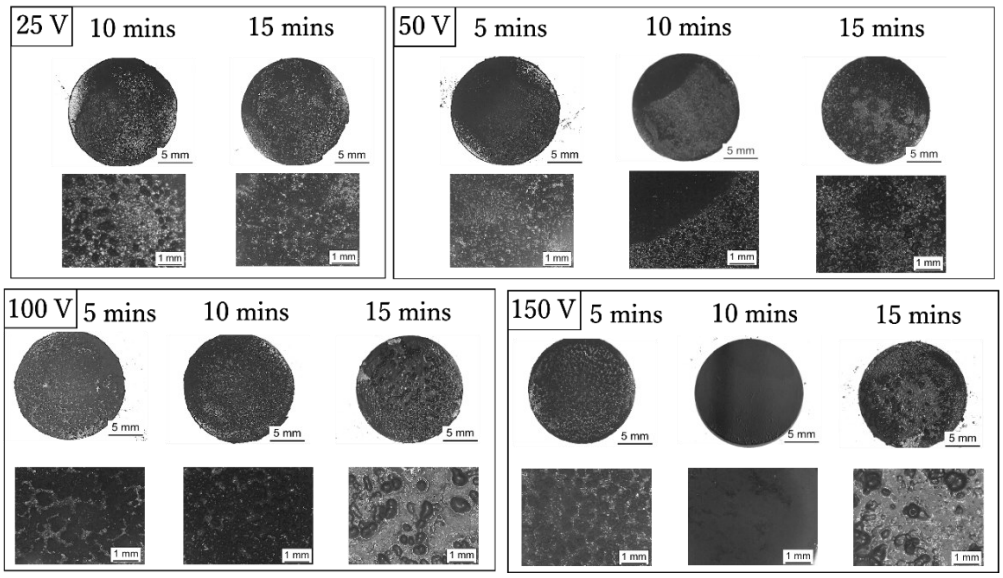

Fig. 5-3 The deposit BSCF with variation of the EPD voltage and deposition time.

Figure 5-4 shows the microstructures of the BSCF porous layers of both the YSZ-GDC-BSCF and YSZ-BSCF multilayered membranes after cofiring at 800 ºC. The BSCF porous layer was well-bonded to the membrane. The thickness of the BSCF coatings that were deposited on the membrane was approximately 20 μm.

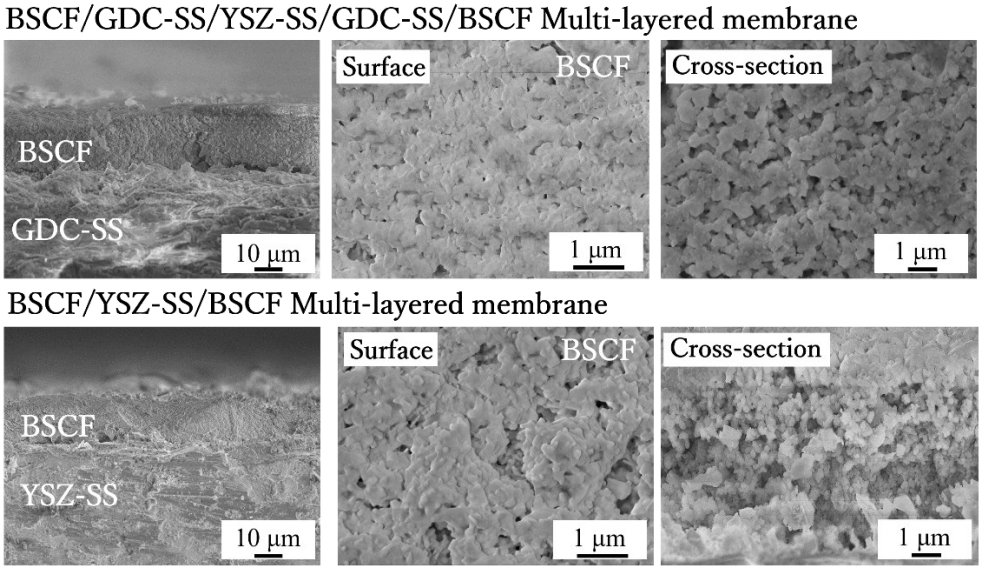

Fig. 5-4 Cross section and surface images of the microstructures of the multilayered membrane.

Figure 5-5 shows the cross-sectional microstructure of the multilayered membrane of the GDC-SS/YSZ-SS/GDC-SS dense layer with BSCF porous layers on both sides of the membrane surface. To compare the reactivity of each layer, a similar membrane was created by sandwiching the YSZ-SS dense layer compact between two BSCF porous layers. Good adhesion between the layers was achieved. Since there are no voids at the bonding interface between the GDC-SS and YSZ-SS layers, gas leakage will probably not occur during the process of air separation.

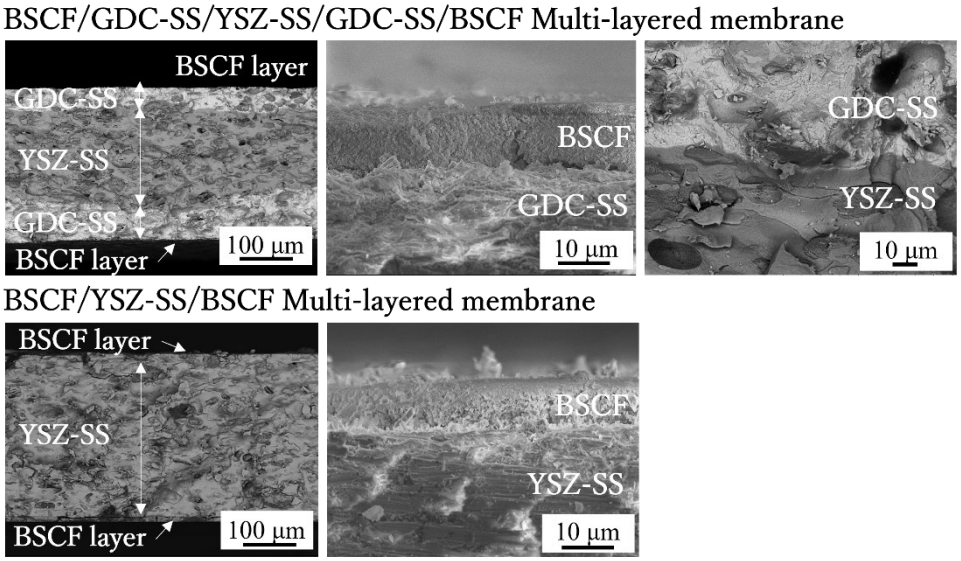

Fig. 5-5 Cross section images of the microstructures of multilayered membrane.

An X-ray diffraction analysis was performed on the raw powder mixtures after heat treatment to evaluate the presence or absence of the secondary phase formation at the interfaces of GDC-SS/YSZ-SS, YSZ-SS/BSCF, and GDC-SS/BSCF. The results are shown in Fig. 5-6. Figure 5-6(a) suggested that there is no reaction taking place between the GDC and the YSZ phases. In Figure 5-6 (b), the formation of perovskite zirconate was confirmed for the YSZ-SS/BSCF mixture. The occurrence of the secondary phase may restrict the membrane's oxygen diffusion performance. Figure 5-6(c) demonstrates that the reaction between BSCF and GDC did not occur, indicating that the insertion of the GDC layer has a high chemical compatibility with both YSZ and BSCF, allowing it to

serve as a buffer layer to prevent any reaction between YSZ and BSCF.

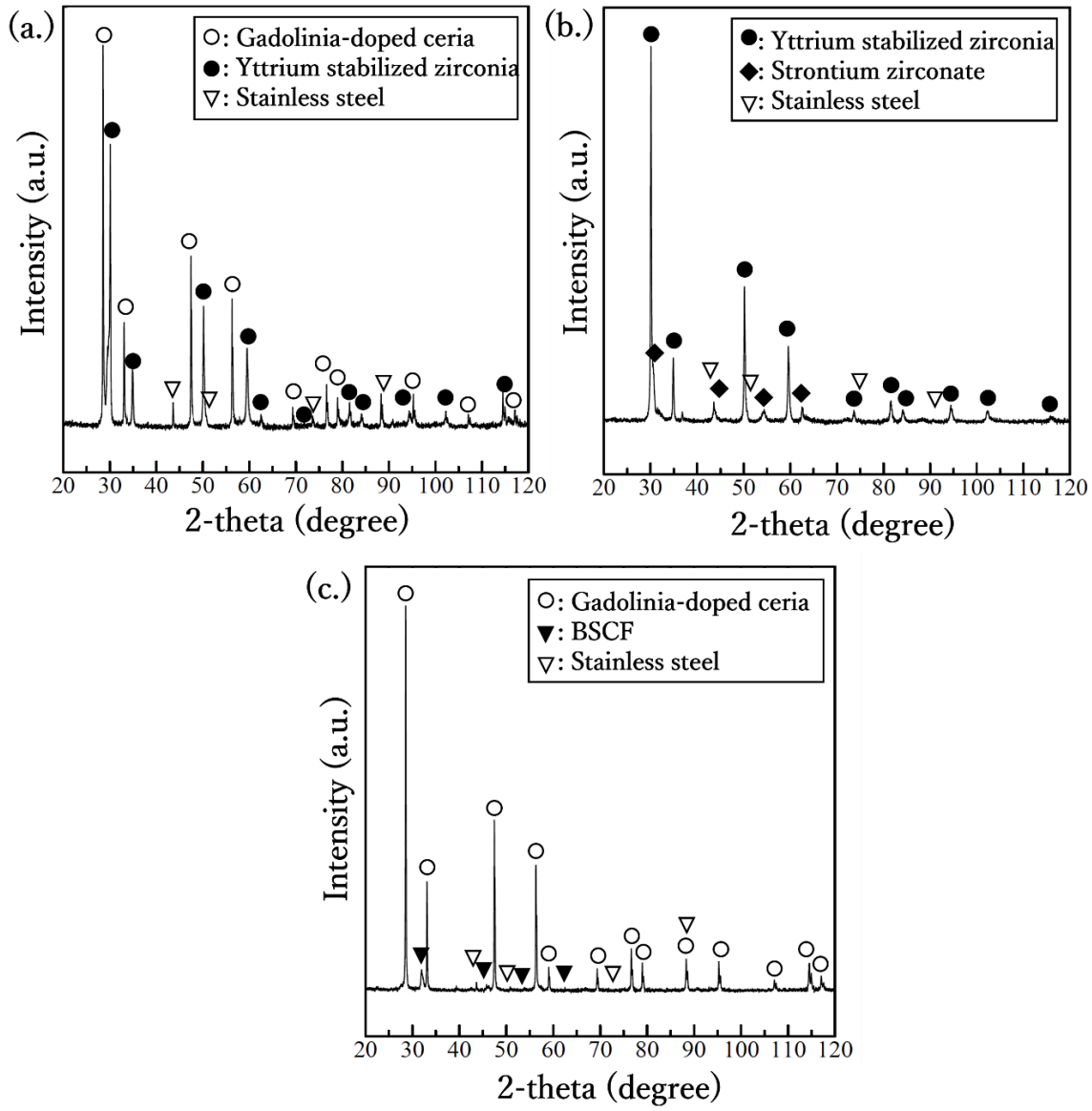

Fig. 5-6 XRD patterns of each layer of the multilayered membranes (a) GDC-SS/YSZ-SS, (b) YSZ-SS/BSCF and (c) GDC-SS/BSCF interface.

4. Conclusions

In this research study, a GDC-SS/YSZ-SS/GDC-SS dense multilayer membrane was fabricated using SPS. It was clarified that the two layers are firmly attached. The EPD process was applied to deposit a BSCF layer on the multilayered composite membrane. Since the substrate was a dual-phase membrane composed of a high electronic conducting phase (SS) and a low or non-electronic conducting phase (YSZ and GDC), the coating process was adjusted by varying the voltage and deposition time. The homogeneous coating was achieved with an applied voltage of 150 V for 10 minutes. In addition, it has been confirmed that the GDC buffur layer can inhibit the formation of zirconate, a byproduct of the BSCF and YSZ reactions. As a result, a five-layer composite membrane was successfully fabricated. Although it was not possible to investigate the oxygen separation characteristics of this multilayered membrane, this structure would further improve the oxygen separation performance.

References

1. Sunarso J., Hashim S.S., Zhu N., and Zhou W., Perovskite oxides applications in high temperature oxygen separation, solid oxide fuel cell and membrane reactor: A review. Progress in Energy and Combustion Science, 61(2017) 57-77.

2. Hunt A., Dimitrakopoulos G., and Ghoniem A.F., Surface oxygen vacancy and oxygen permeation flux limits of perovskite ion transport membranes. Journal of Membrane Science, 489(2015) 248-257.

3. Habib M.A., Nemitallah M., and Ben-Mansour R., Recent Development in Oxy-Combustion Technology and Its Applications to Gas Turbine Combustors and ITM Reactors. Energy & Fuels, 27(2013) 2-19.

4. Etchegoyen G., Chartier T., and Del-Gallo P., An architectural approach to the oxygen permeability of a $La_{0.6}Sr_{0.4}Fe_{0.9}Ga_{0.1}O_{3-\delta}$ perovskite membrane. Journal of the European Ceramic Society, 26(2006) 2807-2815.

5. Sunarso J., Baumann S., Serra J.M., Meulenberg W.A., Liu S., Lin Y.S., and Diniz da Costa J.C., Mixed ionic–electronic conducting (MIEC) ceramic-based membranes for oxygen separation. Journal of Membrane Science,

320(2008) 13-41.

6. Engels S., Markus T., Modigell M., and Singheiser L., Oxygen permeation and stability investigations on MIEC membrane materials under operating conditions for power plant processes. Journal of Membrane Science, 370(2011) 58-69.

7. Leo A., Smart S., Liu S., and Da Costa J.C.D., High performance perovskite hollow fibres for oxygen separation. Journal of Membrane Science, 368(2011) 64-68.

8. Hong W.K. and Choi G.M., Oxygen permeation of BSCF membrane with varying thickness and surface coating. Journal of Membrane Science, 346(2010) 353-360.

9. Brisotto M., Cernuschi F., Drago F., Lenardi C., Rosa P., Meneghini C., Merlini M., and Rinaldi C., High temperature stability of $Ba_{0.5}Sr_{0.5}Co_{0.8}Fe_{0.2}O_{3-\delta}$ and $La_{0.6}Sr_{0.4}Co_{1-y}Fe_yO_{3-\delta}$ oxygen separation perovskite membranes. Journal of the European Ceramic Society, 36(2016) 1679-1690.

10. Sumi H., Ohshiro T., Nakayama M., Suzuki T., and Fujishiro Y., Prevention of Reaction between (Ba,Sr)(Co,Fe)O_3 Cathodes and Yttria-

stabilized Zirconica Electrolytes for Intermediate-temperature Solid Oxide Fuel Cells. Electrochimica Acta, 184(2015) 403-409.

11. Ai N., Jiang S.P., Lü Z., Chen K., and Su W., Nanostructured (Ba, Sr)(Co, Fe)$O_{3-\delta}$ Impregnated (La, Sr)MnO_3 Cathode for Intermediate-Temperature Solid Oxide Fuel Cells. Journal of The Electrochemical Society, 157(2010) B1033.

12. Yang H., Lee H., Lim Y., and Kim Y.B., Atomic layer deposition of GDC cathodic functional thin films for oxide ion incorporation enhancement. Journal of the American Ceramic Society, 104(2021) 86-95.

13. Azad S., Marina O.A., Wang C.M., Saraf L., Shutthanandan V., McCready D.E., El-Azab A., Jaffe J.E., Engelhard M.H., Peden C.H.F., and Thevuthasan S., Nanoscale effects on ion conductance of layer-by-layer structures of gadolinia-doped ceria and zirconia. Applied Physics Letters, 86(2005) 131906.

14. Bae J., Lim Y., Park J.S., Lee D., Hong S., An J., and Kim Y.B., Thermally-Induced Dopant Segregation Effects on the Space Charge Layer and Ionic Conductivity of Nanocrystalline Gadolinia-Doped Ceria. Journal of The Electrochemical Society, 163(2016) 919-926.

15. Develos-Bagarinao K., Yokokawa H., Kishimoto H., Ishiyama T., Yamaji K., and Horita T., Elucidating the origin of oxide ion blocking effects at GDC/SrZr(Y)O_3/YSZ interfaces. Journal of Materials Chemistry A, 5(2017) 8733-8743.

16. Inaba H., Sagawa R., Hayashi H., and Kawamura K., Molecular dynamics simulation of gadolinia-doped ceria. Solid State Ionics, 122(1999) 95-103.

17. Lin T.N., Lee M.C., Yang R.J., Chang J.C., Kao W.X., and Lee L.S., Chemical state identification of Ce^{3+}/Ce^{4+} in the $Sm_{0.2}Ce_{0.8}O_{2-\delta}$ electrolyte for an anode-supported solid oxide fuel cell after long-term operation. Materials Letters, 81(2012) 185-188.

18. Uchikoshi T. and Sakka Y., Phosphate Esters as Dispersants for the Cathodic Electrophoretic Deposition of Alumina Suspensions. Journal of the American Ceramic Society, 91(2008) 1923-1926.

Chapter 6 Summary

Oxygen separation membranes are expected to be used for small-scale oxygen production. However, the oxygen separation properties have not yet reached the level of practical use. A mixed ionic electronic conductor (MIEC) membrane is the most widely used membrane for oxygen separation. The oxygen partial pressure difference across the membrane acts as the driving force that selectively separates high-purity oxygen through this single-phase membrane. However, the main challenge with the MIEC is that it has a restricted oxide diffusion rate. Dual-phase membranes are attracting attention to improving the oxygen separation performance. The dual-phase membrane has an advantage over a single-phase membrane in that it separates both the oxide ion conductor and the electronic conductor, so it is possible to overcome the limitation of the MIEC through the selection of the appropriate materials. In this thesis, an attempt was made to fabricate a dual-phase membrane with a percolation structure. The spark plasma sintering (SPS) technique, which is a high pulse direct current and pressure-assisted sintering method, was utilized to sinter the dual-phase membrane. This thesis explored various materials and fabrication processes as well as the possibility of enhancing the membrane's performance through surface

modification. To achieve a high oxygen permeability, the microstructure, phase stability, and chemical compatibility of a sintered dual-phase membrane were all discussed. Each chapter's contents are as follows:

Chapter 1

The background and essential information for understanding the basics of oxygen separation membranes are explained, and the current status of this research field is described.

Chapter 2

A new facile fabrication method for a dual-phase oxygen separation membrane has been presented. This method allows us to form a co-continuous microstructure of the two phases, realizing the ideal structure of a dual-phase membrane with highly-efficient conducting paths for both carriers. A slurry of oxide ion-conducting materials (8 mol% yttria-stabilized zirconia, 8YSZ) was filled in the void of a porous body of electron-conducting materials (carbon felt) by a vacuum infiltration process. The spark plasma sintering (SPS) process was adopted as a sintering method. As a result, the YSZ-based dual-phase membrane

with gas-tight and continuous structures, high chemical compatibility, and good phase stability was successfully fabricated. YSZ-carbon felt felt that is a dual-phase membrane has the ability to separate the oxygen at 550 ºC, suggesting that this new processing route can be used to fabricate oxygen separation membranes.

Chapter 3

Several electronic conducting phases were investigated to determine suitable materials to be used with 8YSZ for an oxygen separation application. 8YSZ was filled into the voids of the metal foam by a vacuum filtration process. For metals with a low oxidation resistance, a platinum coating was applied to the foam before the 8YSZ filling process and applied to the sample surface after SPS sintering. Among the metal phases used, 316L stainless steel (SS) showed a good oxidation resistance and non-reactivity with YSZ. The presence of the platinum coating prevented the oxidation of the metal phase during oxygen separation characterization and promoted gas exchange reactions at the membrane surface.

Chapter 4

An 8YSZ-316L SS dual-phase membrane was fabricated with a variation in the stainless-steel powder contents. The SS content was varied from 15 vol% to 55 vol% to achieve a percolation structure for obtaining the oxygen transport activity. The surface modification was done by applying silver paste to both sides of the membrane surface. A free-standing dense 8YSZ-SS dual-phase membrane with a thickness of 0.5 mm was successfully fabricated by SPS. The 8YSZ-SS45vol% dual-phase membrane achieved a good percolation structure in the 8YSZ and SS phases. With a silver coating, the oxygen permeability of the dual-phase membrane was successfully improved.

Chapter 5

Further improvement of the oxygen separation performance of the 8YSZ-45vol% SS dual-phase membrane was studied. To improve the oxygen flux by increasing the oxygen exchange rate, both sides of the YSZ-SS two-phase membrane surface were coated with $Ba_{0.5}Sr_{0.5}Co_{0.8}Fe_{0.2}O_{3-\delta}$ (BSCF), an excellent mixed oxide ionic electronic conductor (MIEC).To prevent any reaction between YSZ and BSCF, a thin GDC-SS buffer layer was fabricated on both sides of the YSZ-SS dual-phase

membrane before coating of the BSCF. In this study, electrophoretic deposition (EPD) was selected as a method to deposit BSCF on the multilayered membrane surface. The membrane with a five-layer sandwich structure was achieved.

Appendix

Publications:

1. EKSATIT Aunsaya, ISHII Kento, UEMATSU Masako, LIU Lihong, UCHIKOSHI Tetsuo, Fabrication of YSZ-Carbon Felt Composite Materials by Spark Plasma Sintering Process. Key Engineering Materials, **904** 339-343 (2021). https://doi.org/10.4028/www.scientific.net/KEM.904.339

2. EKSATIT Aunsaya, ISHII Kento, UEMATSU Masako, LIU Lihong, SUZUKI. S. Tohru, UCHIKOSHI Tetsuo, Microstructural and Interfacial Designs of Dual-Phase Oxygen Permeable Membranes for Oxygen Separation Application. Science and Innovation of Advanced Materials, **1** 64006 (2021)

3. EKSATIT Aunsaya, ISHII Kento, KOBAYASHI Kiyoshi, Thi Kim Ngan NGUYEN, SUZUKI. S. Tohru, UCHIKOSHI Tetsuo Dual-phase oxygen separation membrane composed of Y_2O_3-doped ZrO_2 and stainless steel. Journal of the Ceramic Society of Japan, **131**(2)22-26(2023). http://doi.org/10.2109/jcersj2.22142

Presentations at international conferences:

1. EKSATIT Aunsaya, ISHII Kento, UEMATSU Masako, LIU Lihong, UCHIKOSHI Tetsuo, Fabrication of YSZ-Carbon Felt Composite Materials by Spark Plasma Sintering Process, Oral presentation, 2021 10th International Conference on Advanced Materials and Engineering Materials, Bangkok, Thailand (On-Line) (May 29-30, 2021)

2. EKSATIT Aunsaya, ISHII Kento, UEMATSU Masako, LIU Lihong, UCHIKOSHI Tetsuo, Fabrication of YSZ-Carbon felt dual-phase membrane by using spark plasma sintering process, Poster presentation, 10th JACI/GSC

Symposium, Japan (On-Line) (June 28-29, 2021)

3. EKSATIT Aunsaya, ISHII Kento, UEMATSU Masako, LIU Lihong, UCHIKOSHI Tetsuo, Microstructural and Interfacial Designs of Dual-Phase Oxygen Permeable Membranes for Oxygen Separation Application, Poster presentation, The 12th Asian Meeting on Electroceramics (AMEC 2021), Thailand (On-Line) (July 7-9, 2021)

4. EKSATIT Aunsaya, ISHII Kento, UEMATSU Masako, KOBAYASHI Kiyoshi, SUZUKI. S. Tohru, UCHIKOSHI Tetsuo, A novel technique for fabrication of dual phase oxygen separation membrane using spark plasma sintering process", Oral presentation, The 60th Symposium on Basic Science of Ceramics, Kumamoto, Japan (January 8-9,2022)

5. EKSATIT Aunsaya, ISHII Kento, KOBAYASHI Kiyoshi, SUZUKI. S. Tohru, UCHIKOSHI Tetsuo, Fabrication of ceramic-metal dual phase oxygen separation membrane by spark plasma sintering process, Oral presentation, The 7th International Conference on the Characterization and Control of Interfaces for High Quality Advanced Materials, Fujiyoshida, Japan (November 15-18,2022)

Award:

Best Poster Presentation Award in Functional Ceramic Materials and Applications, The Asian Meeting on Ferroelectricity - The Asian Meeting on Electroceramics (AMF-AMEC 2021)

Grant:

International Collaborative Chemical Science Program (Scholarship for short term visit), grant from Graduate School of Chemical Science and Engineering hosted by Friedrich Alexander university of Erlangen-Nuremberg, Germany (1 month) (2022)

Acknowledgments

First of all, I would like to express my sincere gratitude to my supervisor, Professor Tetsuo Uchikoshi. He consistently advised me on how to become a good researcher in the future. I am grateful for all the time he has invested in my development. I would like to thank the thesis committee members, Professor Kiyoharu Tadanaga, Associate Professor Akira Miura, and Professor Naoto Shirahata, for taking the time to make suggestions on my research work. The Hokkaido University-NIMS Joint Graduate School Program provided me the opportunity to do my research at the National Institute for Materials Science (NIMS). I had a great time sharing with the members of the Fine Particles Engineering Group and also appreciate the great support from the NIMS staff. My experimental research would not have been possible without the help of Dr. Kiyoshi Kobayashi, Dr. Tohru S. Suzuki, Dr. Kento Ishii, Dr. Thi Kim Ngan Nguyen, and Dr. Lihong Liu. It was my pleasure to get so many great comments and suggestions from them. Lastly, I would like to thank my family for their great support and encouragement throughout this strenuous. Every moment of my PhD life has been surrounded by great companions, for which I am extremely grateful.

Aunsaya Eksatit